

Aus dem Institut für Transfusionsmedizin und Immunologie  
der Medizinischen Fakultät Mannheim  
(Direktor: Prof. Dr. med. Harald Klüter)

# **Analysis of macrophage responses to titanium nanoparticles in hyperglycemic conditions**

Inauguraldissertation  
zur Erlangung des Doctor scientiarum humanarum (Dr. sc. hum.)  
der  
Medizinischen Fakultät Mannheim  
der Ruprecht-Karls-Universität  
zu  
Heidelberg

vorgelegt von  
Tatyana N. Sevastyanova

aus  
Korolev, Russia

2021

Dekan: Prof. Dr. Sergij Goerd  
Referentin: Prof. Dr. Julia Kzhyshkowska

## TABLE OF CONTENTS

<b>TABLE OF CONTENTS</b> .....	3
<b>ABBREVIATION LIST</b> .....	5
<b>1 INTRODUCTION</b> .....	9
1.1 Titanium implant materials and toxicity .....	9
1.2 Implant complications in diabetic patients.....	12
1.3 Major sources of non-implant related exposure to titanium materials.....	13
1.4 Role of macrophages in human immune system .....	14
1.5 Glucocorticoids for alleviation of inflammation .....	21
1.6 Reactive oxygen species in macrophage responses .....	22
1.7 Aims and objectives .....	23
<b>2 MATERIALS AND METHODS</b> .....	24
2.1 Chemicals, reagents and kits .....	24
2.2 Consumables .....	25
2.3 Equipment .....	26
2.4 Buffers and solutions .....	27
2.5 Molecular biology techniques .....	27
2.6 Cell culture techniques .....	33
2.7 Immunological methods.....	37
2.8 Protein-related techniques .....	40
2.9 Statistical analysis .....	42
<b>3 RESULTS</b> .....	44
3.1 Experimental design .....	44
3.2 Analysis of titanium surfaces and nanoparticles on macrophage viability .....	45
3.3 Effect of Ti NPs on gene expression of CHI3L1, chitotriosidase and CC18 under normal glucose conditions .....	47

3.4 Effect of Ti NPs on macrophage secretion of TNF- $\alpha$ , CHI3L1, CC18 and chitotriosidase activity in normal glucose.....	49
3.5 Effect of hyperglycemia on Ti NPs-induced changes in of TNF- $\alpha$ , CHI3L1, CHIT1 and CCL18 production .....	52
3.6 Effect of dexamethasone on CHI3L1 and CHIT1 expression in normal and hyperglycemic M1 exposed to Ti NPs .....	62
3.7 Effect of Ti NPs on CHIT1 intracellular localization.....	66
3.8 Effect of Ti NPs on mitochondrial ROS release .....	69
3.9 Affymetrix gene expression analysis of transcriptome in macrophages exposed to Ti NPs in normal and hyperglycemic conditions .....	73
3.10 RT-PCR analysis and validation of selected Ti NPs-induced biomarkers .....	76
<b>4 DISCUSSION .....</b>	<b>79</b>
4.1 Interaction of Ti NPs with macrophages .....	79
4.2 Impact of hyperglycemia on Ti NPs-induced macrophage responses.....	83
4.3 Role of dexamethasone in Ti NPs-induced CHIT1 and CHI3L1 responses .....	85
4.4 Effect of Ti NPs on mitochondrial ROS release .....	86
4.5 Affymetrix gene expression analysis and validation of Ti NPs-induced biomarkers .....	87
<b>5 SUMMARY .....</b>	<b>91</b>
<b>6 REFERENCES .....</b>	<b>93</b>
<b>7 CURRICULUM .....</b>	<b>109</b>
<b>8 ACKNOWLEDGEMENTS .....</b>	<b>111</b>

## ABBREVIATION LIST

°C	celcius
µg	microgram
µl	microliter
µm	micrometer
µM	micromolar
Ab	antibody
AGEs	advanced glycation products
Akt	protein Kinase B
ANOVA	analysis of variance
APMA	4-aminophenylmercuric acetate
APS	amonium persulfate
BHQ1	black hole quencher-1
BMDM	bone-marrow-derived macrophage
bp	base pairs
BSA	bovine serum albumin
CCL	chemokine (C-C motif) ligand
CCR	C-C chemokine receptor
CD	cluster of differentiation
CD14	CD14 positive macrophages
cDNA	complementary deoxyribonucleic acid
CHI3L1	chitinase-3-like protein 1
CHIT1	chitotriosidase
CLSM	confocal laser scanning microscopy
COPD	chronic obstructive pulmonary disease
COX	cytochrome c oxidase
Cp Ti	commercially pure titanium
CR	complement receptor
CSF1/M-CSF	colony stimulating factor
Ct	threshold cycle
CXCL	C-X-C motif chemokine ligand
DAMP	damage-associated molecular pattern
DAPI	4',6-diamidino-2-phenylindole
DCF	dichlorofluorescein
DCs	dendritic cells
DCSTAMP	dendritic cell-specific transmembrane protein
ddH <sub>2</sub> O	double distilled water
ddNTP	dideoxynucleotide triphosphate
DEPC	diethyl pyrocarbonate
Dex	dexamethasone
DM	diabetes mellitus
DMEM	dulbecco's modified eagle's medium
DMSO	dimethylsulfoxide
DNA	deoxyribonucleic acid
dNTPs	deoxyribonucleotides
E171	food-grade titanium dioxide (mixture of nanoparticles)
ECM	extracellular matrix

## Abbreviation list

---

$E_{corr}$	corrosion potential
EDTA	ethylene diamine tetra acetic acid
EGF	epidermal growth factor
ELISA	enzyme-linked immunosorbent assay
EM	emission
EMEM	eagle's minimal essential medium
ER	endoplasmatic reticulum
ERK	extracellular-signal-regulated kinase
FACS	fluorescent activated cell sorting
FBR	foreign body response
FBRC	foreign body giant cells
Fc	fragment crystallisable
FCS	fetal calf serum
Fc $\gamma$ R	Fc gamma receptor
FDOJ	fatty degenerative osteonecrosis of the jaw
FDR	false discovery rate
FI	fluorescent intensity
FITC	fluorescein
g	gram / relative centrifugal force
GAPDH	glyceraldehyde 3-phosphate dehydrogenase
GM-CSF	granulocyte-macrophage colony-stimulating factor
GPa	gigapascal
GSK	glycogen synthase kinase
h	hour(s)
HG	hyperglycemic conditions (25mM glucose)
HIF	hypoxia-inducible factor
HLA	human leukocyte antigens
HLA-DR	major histocompatibility complex (MHC) II cell surface receptor
HMGB1	high mobility group box 1 protein
HRP	horseradish peroxidase
HSCs	hematopoietic stem cells
HSP	heat shock protein
IF	immunofluorescence
IFN $\gamma$	interferon gamma
IgG	immunoglobulin G
IKK	I $\kappa$ B kinase
IL	interleukin
IL-1Ra	Interleukin 1 receptor antagonist
iNOS	inducible nitric oxide synthase
kD	kilodalton
KEGG	kyoto encyclopedia of genes and genomes
L	liter
LDL	low-density lipoprotein
LOX-1	lectin-type oxidized LDL receptor 1
LPS	lipopolysaccharide
LTA	lymphotoxin-alpha
M	molar concentration
M(Control)/M0	non-stimulated macrophages
M(IFN $\gamma$ )/M1	macrophages activated with IFN $\gamma$

## Abbreviation list

---

M(IL-4)/M2	macrophages activated with IL-4
mA	milliamp
MACS	magnetic-activated cell sorting
MAPK	mitogen-activated protein kinase
MARCO	macrophage receptor with collagenous structure
MCP-1	monocyte chemoattractant protein 1
M-CSF	macrophage colony-stimulating factor
MDSC	myeloid-derived suppressor cells
MEM	minimal essential medium
mg	milligram
MHC	major histocompatibility complex
MIF	macrophage migration inhibitory factor
min	minute(s)
MIP-1alpha	macrophage inflammatory protein 1 alpha
miRNA	microRNA
mitoSOX	mitochondrial superoxide indicator
ml	milliliter
mM	millimolar concentration
mm	millimeter
MME	membrane metalloendopeptidase
MMP	matrix metalloproteinase
MPa	megapascal
mPGES	PGE synthase
MPs	microparticles
MRI	magnetic resonance imaging
mRNA	messenger RNA
MTs	metallothioneins
N	equivalent concentration
NADPH	nicotinamide adenine dinucleotide phosphate
NF-kB	nuclear factor kappa-light-chain-enhancer of activated B cells
ng	nanogram
NG	normal glucose conditions (5mM glucose)
NLRP3	NLR family pyrin domain containing 3
nm	nanometer
NOS	nitric oxide synthase
OLR1	oxidized low density lipoprotein receptor 1
OPG	osteoprotegerin
ORM1	orosomuroid 1
OXPPOS	oxidative phosphorylation
PAI-1	plasminogen activator inhibitor 1
PAR/HA	polyarginine-hyaluronic acid-based coating
PBMC	peripheral blood mononuclear cell
PBMC-CD14	PBMC depleted of the CD14 positive monocytes
PBS	phosphate buffered saline
PCR	polymerase chain reaction
PDGF	platelet-derived growth factor
PE	R-phycoerythrin
PEG	poly(ethylene-glycol)
PELA	ethylene oxide/lactic acid copolymer

## Abbreviation list

---

PET	polyethylene terephthalate
PFA	paraformaldehyde
pg	picogram
PGE	prostaglandin E
PI3K	phosphatidylinositol 3-kinase
PKC	protein kinase C
PLA	polylactic acid
pM	picomolar
PMFI	paracrine macrophage-fibroblast interaction
PMMA	polymethylmethacrylate
pmol	picomolar
PPAR	proliferator-activated receptor
ppm	parts per million
PRR	pattern-recognition receptor
PVA	poly(vinyl-alcohol)
RAGE	receptor for Advanced Glycation End Products
RANK	receptor activator of nuclear factor kappa B
RBC	red blood cells
RNA	ribonucleic acid
RNS	reactive nitrogen species
ROS	reactive oxygen species
rpm	revolutions per minute
RT	room temperature
RT-qPCR/RT-PCR	reverse transcription real-time polymerase chain reaction
s	second(s)
SDS	sodium dodecyl sulfate
SFM	serum free medium
SOD	superoxide dismutase
SR	scavenger receptor
STAT	signal transducer and activator of transcription
TAE	tris/Acetate/EDTA-buffer
TAM	tumor-associated macrophages
TGF	transforming growth factor
TGF $\beta$ R1	transforming growth factor, beta receptor I
TGN	trans-Golgi network
THP-1	human acute monocytic leukemia cell line
Ti NPs/TiO <sub>2</sub> NPs	titanium nanoparticles
TLR	toll-like receptor
TNF	tumor necrosis factor
TNFRSF	tumor necrosis factor receptor superfamily, member
TNFSF	tumor necrosis factor (ligand) superfamily, member
UV	ultraviolet
V	volt(s)
VEGF	vascular endothelial growth factor
Vs	versus
wt%	percentage by mass
$\Delta\psi_m$	mitochondrial membrane potential



# 1 INTRODUCTION

## 1.1 Titanium implant materials and toxicity

### 1.1.1 Titanium materials in human implantation and complications

Human implantation of artificial materials and devices are of crucial importance to modern society, providing the most optimal solutions to regenerative medicine. Some examples of medical conditions which utilize implantation are tooth loss, rheumatoid arthritis, inflammatory arthritis, scoliosis, spinal deformity, osteoporosis, osteonecrosis and end-stage heart failure<sup>1-5</sup>. Titanium materials are considered the most popular, amongst other metals, due to good mechanical properties, strong resistance to corrosion and high biocompatibility<sup>6-8</sup>. Upon contact with air, titanium composites form a protective TiO<sub>2</sub> layer, which helps to prevent metal degradation<sup>8,9</sup>. Today, titanium composites are utilized for medical solutions to treat loss or damage of bone tissue in various body parts such as the hips, shoulders, knees, spine and skull<sup>6,10,11</sup>. Moreover, application of titanium materials in dentistry is probably the most common and practical. Titanium is used in the composition of dental implants, and dental cast metal frameworks<sup>4,11</sup>.

Metal implants often trigger adverse immune responses, which lead to health complications associated with a diverse range of medical conditions. Table 1 provides some examples of metal implant materials with the corresponding complications and inflammatory mediators involved<sup>1,8,10,12-14</sup>.

**Table 1. Examples of metal implant composition materials, implant-related health complications and corresponding inflammatory factors**<sup>1,8,10,12-14</sup>.

Metal Implant Material	Implant Type	Body Part	Type of Complication	Inflammatory Mediators
Co-Cr alloys, Ti alloys and pure Ti	Femoral hip stands, metal backed acetabular shells	Hip, knee	Microbial infection, aseptic loosening, osteolysis, and metal-induced adverse periprosthetic inflammation	Interferons, TNF-alpha, IL1-beta, CHIT1, IL6, IL8
Stainless steel, Co-Cr alloys, Ti alloys and pure Ti	Left ventricular assist devices, pacemakers and defibrillators, vascular stents	Heart	Infections, multi organ failure, coagulation disorders, wound, stroke	IL-6, IL-8, neopterin, TNF-alpha, IL1-beta, PAI-1, MCP-1
Gold alloys, Cr-Ni alloys, Ti alloys and pure Ti	Dental implants, dental cast metal frameworks	Jaw, mouth	Microbial infections, peri-implantitis, chronic dental pain, gum recession, bone graft failure, fibrosis at the implant-bone interface, osteolysis	IL-10, MMP2, nuclear factor kappa-B ligand (RANKL), TNF-alpha, IL1-beta

These post-surgical complications in implantation are typically divided into two major groups: mechanical and biological. Mechanical complications correspond to the physical quality of the implant itself, which is associated with mechanical breakage of metal surfaces<sup>15</sup>. For example, metal corrosion caused by high frictional force between the sub-parts of an implant. This can be a problem for orthopedic implants because they often have many accessory components. However, corrosion of the implant

surfaces induced by the electrochemical properties of the local microenvironment would be considered a biological complication.

Typical implant complication outcomes are associated with intensive pain, infection, and acute and chronic inflammation. Implant complications are provoked by adverse immune reactions and macrophages are the major players in this game, because they are in control of the responses to artificial materials<sup>13</sup>. Failure to resolve adverse inflammatory reactions at initial stages can essentially lead to chronic conditions and increase the risk of implant rejections. The primary causes of implant failure related to these conditions are: periprosthetic fracture, aseptic loosening, arthrofibrosis, fibrosis at the implant–bone interface, infections, peri-implantitis, osteolysis, pain, coagulation disorders, and stroke<sup>16–20</sup>. It is established that macrophages are key innate immune cells responsible for the recognition and primary reaction to foreign bodies, including implants<sup>8,21–23</sup>. Macrophage responses responsible for the adverse immune reactions that lead to the development of implant complications are sustained by persistent inflammatory signals produced upon their recognition of foreign biomaterials and the implant wear particles<sup>8,13</sup>. Most severe medical conditions happen to ascend during the interplay of both acute and chronic inflammatory responses. The inflammation responses associated with recognition of foreign particles are driven by a wide range of pro-inflammatory cytokines and growth factors: TNF- $\alpha$ , IL-1 $\alpha$ , IL-1 $\beta$ , IL-6, IL-8, IL-11, IL-15, TGF $\alpha$ , GM-CSF, M-CSF, PDGF, epidermal growth factor<sup>21,24</sup>. Chronic inflammation shares some inflammatory mediators with acute immune reactions. However, on top of classically activated macrophage responses, chronic responses also exhibit characteristics of alternatively activated macrophage responses. For example, rheumatoid arthritis, which is considered to be the consequences of chronic inflammation is associated with IL-1 $\alpha$ <sup>25</sup>, however IL-1 $\alpha$  is also secreted during acute lung inflammation upon exposure to silicon micro- and nanoparticles secreted in the acute phase<sup>26</sup>. On the other hand, development of fibrosis results from failed wound healing and anti-inflammatory responses, associated with a pathological change in production levels of TGF-b1, PDGF, MMPs, CCL7, CCL8, etc., which are responsible for proliferation, migration, and collagen synthesis in fibroblasts<sup>8,27</sup>.

### 1.1.2 Metal degradation and release of implant wear-off particles

Degradation of metal implant materials can also be defined as corrosion. Since all metals undergo corrosion, metal implants are susceptible to corrosion as well, which occurs upon interaction of implant surfaces with the surrounding bio-environment<sup>28</sup>. For instance, saliva is an electrolytic solution, which can make titanium dental implants corrode and release metal particles in the jawbone region<sup>29</sup>. Chronic inflammation of the jawbone induced by implant-related complications often leads to a disease called “fatty degenerative osteonecrosis of the jaw” (FDOJ). The samples from patients with FDOJ disorder were examined to determine the amount of dissolved Ti particles in the surrounding areas of the titanium-based dental implants. More than one third of the samples revealed a range from (3200 to 50600)  $\mu\text{g}/\text{kg}$  which is equivalent to (0.003 – 0.0050) wt%; it is known that the concentration of any heavy metal particles that exceeds 250  $\mu\text{g}/\text{kg}$  is considered to be toxic to the human body<sup>30</sup>.

Corrosion of implant materials is a significant variable in the response of bone and tissues to implant placement. Electrochemical techniques are used to measure corrosion properties in various biological environments. One study investigated endosseous implants to characterize corrosion in environments with blood, inflammatory cells and elevated glucose, which has revealed that implants undergo the inflammatory stress tend to corrode more by exhibiting greater negative  $E_{\text{corr}}$

values<sup>31</sup>. These findings also support a medical observation that in patients with Type I and Type II diabetes, the risk of implant failure is significantly increased<sup>31,32</sup>. There were other factors found and investigated, such as hydrogen peroxide, proteins, mechanical stress and cells, which also trigger implant corrosion and contribute to the release of wear-off particles into the local bio-environment<sup>33–35</sup>.

There are major types of implant-related corrosion: galvanic, fretting, pitting, crevice corrosion and environmentally induced cracking corrosions. Galvanic corrosion involves flow of ions and electrons induced by changes in the electrochemical gradient due to direct contact of two very dissimilar metal materials<sup>36</sup>. Fretting occurs due to physical friction between the implant and another material in result of excessive mechanical activity or micro-motion. Spontaneous breakdown of the protective surface layer of a flat implant area is associated with pitting corrosion<sup>28</sup>. While crevice corrosion is characterized by a localized corrosion, which occurs due to geometric confinement in the design and is generally associated with uneven surfaces<sup>37</sup>. Corrosion-triggered spontaneous loss of implant surface particles promotes physical degradation of the implant material, which disturbs the mechanical stability of an entire implant device leading to its aseptic loosening.

Titanium and its alloys are easily passivated metals. Titanium's high resistance to corrosion can be explained by its fast passivation, which is an immediate formation of a protective layer upon exposure to air. This layer is responsible for anti-corrosive qualities of titanium material and acts as a shield between the metal surface and the surrounding environment<sup>9</sup>. Nevertheless, titanium implants still undergo corrosion.

Overall, implant corrosion has two major unfavorable effects: 1) destruction of mechanical stability of an implant, which leads to aseptic loosening; 2) generation of small metal wear-off particles or implant debris typically composed of nanoparticles, micro particles and small ions (Figure 1).

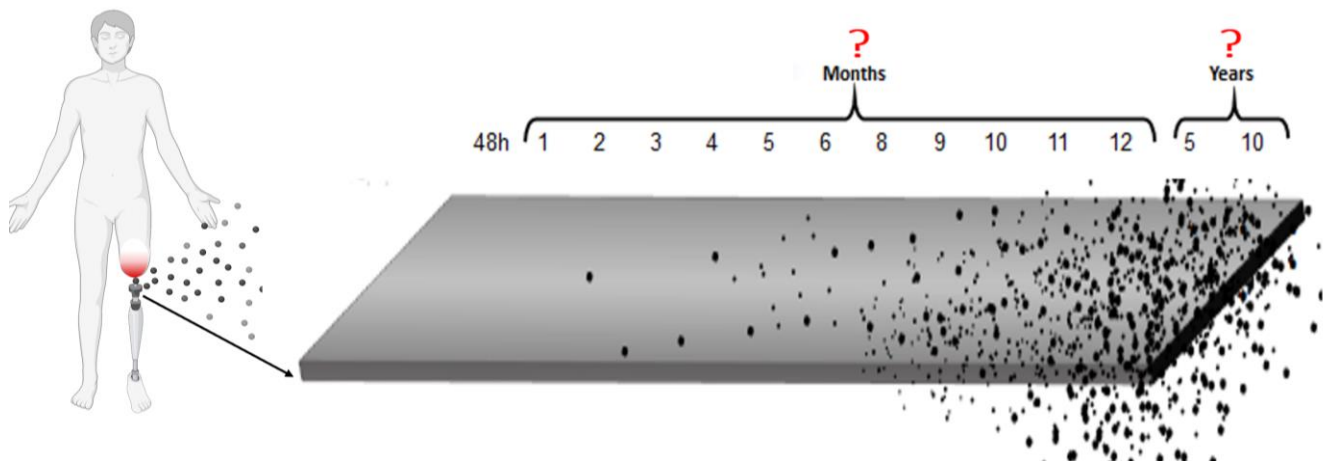


**Figure 1. Representation of implant degradation during corrosion** (created with Biorender.com).

Amongst the metal particles, which are released in result of corrosion, particles of a smaller diameter size, or nanoparticles, generate most biological toxicity<sup>12,38</sup>. Titanium nanoparticles can exist in three polymorphic forms: rutile, anatase, and brookite<sup>39</sup>. The forms come from the only naturally occurring oxide of titanium at atmospheric pressure. Rutile corresponds to a stable phase, while both anatase and brookite are metastable<sup>39,40</sup>. Rutile and anatase  $\text{TiO}_2$  are typically used in coatings of medical devices and implant materials<sup>41,42</sup>.

## 1.2 Implant complications in diabetic patients

Patients who suffer from diabetes mellitus (DM) often injure themselves and break bones<sup>43</sup>, which makes them very susceptible to medical solutions requiring implants. On top of that, DM patients have an increased probability of periodontitis and tooth loss<sup>44</sup>. The risk of implant failure is increased in diabetic patients<sup>31,32,45</sup>. Diabetic conditions are known to reduce osseointegration and the success rate of dental implants, because the success or failure of implants are dependent on how fast and efficient the local tissues grow in close apposition to the implant<sup>46,47</sup>. In the diabetic healing bone, the time point of cell proliferation and osteoblast differentiation are significantly delayed<sup>46,48</sup>.

Adverse foreign body response occurs adjacent to the implanted materials, and impairs the function of implant devices, which can be very critical for the implantable glucose or other biosensors. To completely understand the full spectra of these health risks, it is critical to consider all the potential negative interactions from the immune responses at the interface of diabetic pathology and implant complication responses. Figure 2 illustrates inflammatory mediators involved in the responses to biomaterials and hyperglycemia<sup>8,49–52</sup>.

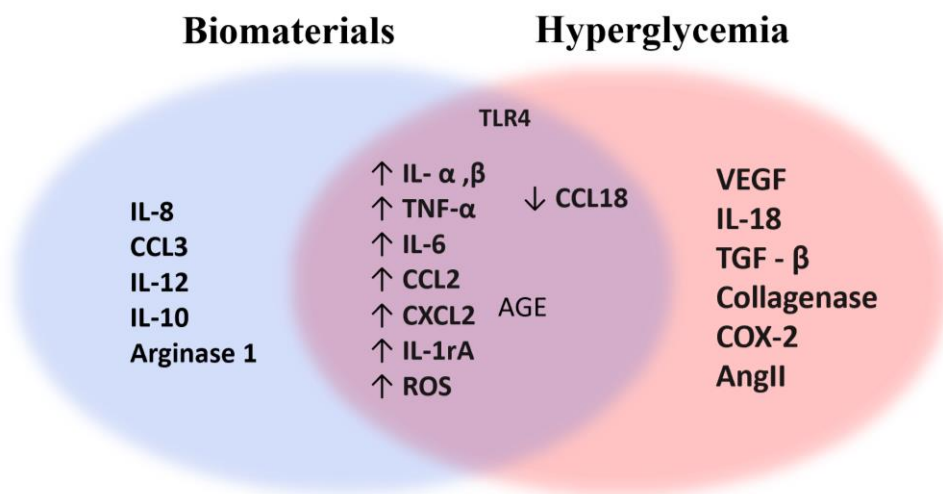


**Figure 2. Interface of inflammatory responses induced by biomaterials and hyperglycemia**<sup>8,49–52</sup>.

Hyperglycemia is a key element of the diabetic pathology. Elevated levels of glucose produce higher risks in the corrosion state of metal implants, which has been demonstrated by multiple studies in the investigation of electrochemical corrosion behavior of metal implants<sup>53,54</sup>. Also, hyperglycemia stimulates elevated levels of proinflammatory responses leading to overproduction of superoxide, delaying wound healing, which is a crucial factor for successful implantation. Implant material consisting of titanium is considered to be most stable due to extra features in the formation of titanium dioxide surface layers; however, hyperglycemic blood can directly interact with implant surfaces and also degrade those TiO<sub>2</sub> layers, releasing small toxic titanium particles<sup>53</sup>.

It was demonstrated by numerous dental studies, that patients in the condition with poorly controlled TD2, as also, with pre-diabetic conditions, characterized by obesity syndrome, undergo significantly higher risks of developing implant complications than healthy patients<sup>55–57</sup>. Delayed wound healing and compromised

immune responses responsible for the pathological defense are amongst key leading elements in unsuccessful implantation procedures. Diabetic conditions significantly increase production of the pro-inflammatory cytokines such as TNF- $\alpha$ , IL-1 $\beta$  and IL-6<sup>49,58</sup>, which interfere with anti-inflammatory responses necessary for post-implantation. The peri-implant inflammatory parameters are worse in patients with diabetes and prediabetic conditions<sup>55</sup>.

Hyperglycemia increases the expression of toll-like receptors (TLRs) at the periodontal tissue, which is consistent with the location of dental implants. An increase in TLR-mediated responses results in over-activation of pro-inflammatory macrophages<sup>59,60</sup>, hence facilitating a more extreme inflammatory state at the interfaces of implant material and tissue. High levels of advanced glycation products (AGEs) have been associated with hyperglycemia-induced pathogenesis of tissue destruction around dental implants in T2D<sup>57,61</sup>. In a study about orthopedic implant devices, it was demonstrated that the patients with obesity and T2D suffer worse from osteomyelitis, a type of a bone infection, in comparison to patients without obesity or T2D<sup>56</sup>. Hyperglycemic conditions increase the likelihood of infections, which is also supported by delayed or impaired wound healing processes. The mechanisms responsible for increased peri-implant damage may very well be explained by the implication of prolonged hyperglycemia or poor glycemic control, since chronic hyperglycemic exposure interrupts the synthesis, maturation and maintenance of collagen and extracellular matrix in the periodontal and peri-implant tissues<sup>61,62</sup>.

The detrimental effects of hyperglycemia and biomaterials have been studied independently; however, the interaction of these negative effects needs to be investigated further to understand the mechanisms which are responsible for implant failure in diabetic patients. It must be taken under consideration that hyperglycemic environment not only promotes the release of implant wear-off particles, such as Ti NPs, but also cooperates with their detrimental outcomes on the human immune system.

### **1.3 Major sources of non-implant related exposure to titanium material**

Titanium dioxide materials are one of the most commonly used nanomaterials<sup>63</sup>. Although metal implants are considered to be a well-known source of exposure to titanium nanoparticles, most exposure actually comes from industrial sources. These industrial sources include paints, plastic, rubber, paper-making, fiber etc.; these contribute to the route of exposure through inhalation, intranasal or intratracheal instillation<sup>63,64</sup>. The other sources, contribute to oral and dermal exposures, and they come from cosmetics, food additives, drug coatings, toothpaste etc.<sup>65</sup>. The common properties of various forms of titanium nanoparticles, which lead to detrimental health effects, include efficient penetration, poor elimination, and tissue accumulation, in addition to toxicity<sup>65-68</sup>.

#### **1.3.1 Airborne exposure to TiO<sub>2</sub>**

Metal nanoparticles are increasingly used in the manufacturing of industrial products, such as antibacterial surface coatings and semiconductors<sup>69</sup>. In addition, the ingredients of paint or the additives in different paint coatings and where they are used as a white pigment often contain Ti NPs<sup>70,71</sup>. These particles can be inhaled upon exposure to these reagents. The consequences of exposure result in immediate

transport of this material from the lungs to lymphatic drainage, which eventually reach blood circulation. It was reported that Ti NPs of 21nm diameter size trigger a more severe pulmonary inflammatory response than TiO<sub>2</sub> of the same mass, with greater amounts of Ti NPs entering the alveolar interstitium in the lungs<sup>72</sup>. Moreover, inhalation of rutile Ti NPs leads to pulmonary neutrophilia, increased expression of TNF- $\alpha$  and neutrophil attracting chemokine (CXCL1) in lung tissues<sup>73</sup>. Several studies have shown that the uptake of the nanoparticles worsen respiratory disorders such as pulmonary fibrosis or LPS-induced lung inflammation<sup>74–76</sup>.

### 1.3.2 Intestinal exposure to TiO<sub>2</sub>

Titanium dioxide, also referred to as E171, is widely used as part of food ingredients, drug coating, toothpaste, chewing gums and candy<sup>65,77,78</sup>. E171 is ingested daily as a combination of nanoparticles and microparticles in the human diet. Powdered donuts contain as high as 100mg Ti per serving<sup>65</sup>. Products such as sweets or candies including chocolate and white sugar toppings contain 0.01 to 1mg Ti per serving<sup>65</sup>. When white dairy products, such as, mayonnaise, whipped cream and yogurts, were tested for Ti content, most of them contained low concentrations. Cheeses were ranked highest amongst dairy products in the content of Ti (0.0069  $\mu$ g of Ti per mg)<sup>65</sup>. After being ingested, Ti NPs certainly interact with the gastrointestinal system. Ti NPs of sizes between 4 and 30nm are constantly found in sewage<sup>67</sup>. Dual flow cytometry analysis of human whole blood has shown that food grade anatase TiO<sub>2</sub> of non-toxic concentrations (10  $\mu$ g/ml (10,000 ppb)) are primarily taken up by neutrophils and CD14+ cells<sup>79</sup>. In vitro, E171-type Ti NPs ingested by human bone-marrow macrophages and intestinal epithelial cells induce assembly of NLRP3-ASC-caspase-1 and NLRP3-dependent release of IL-1 $\beta$  and IL-18<sup>80</sup>.

### 1.3.3 TiO<sub>2</sub> in cosmetics

Titanium dioxide is commonly found in cosmetic products and, in fact, they are the primary ingredient of sunscreen lotions<sup>81</sup>. Due to intensive application of cosmetic products, the danger of dermal exposure has been addressed by multiple studies, where there has been some contradiction. The Scientific Committee on Consumer Safety considers Ti NPs as a mild-irritant to skin<sup>82</sup> and some investigations claim that the nanoparticles do not penetrate the skin<sup>83,84</sup>, while others observed the opposite effect<sup>85</sup>. The use of TiO<sub>2</sub> in lip balm products contributes to oral exposure but the experts claim that the concentrations are not strong enough to harm the gastrointestinal system<sup>81</sup>. Cosmetic products in a form of sprays are not recommended due to the exposure through inhalation and risk of lung damage<sup>86</sup>.

## 1.4 Role of macrophages in the human immune system

Macrophages are innate immune cells that coordinate a diverse pool of immunological responses. These cells are evolutionarily designed for the resolution of inflammation by altering their phenotype and the phenotypes of the cells present in their microenvironment<sup>87</sup>. Macrophages are involved in, both processes, advancing inflammation and promoting tissue repair and regeneration<sup>88</sup>.

### 1.4.1 Macrophage phenotypes and plasticity

Macrophages are well-known for their regulatory function executed by secreting pro-inflammatory, anti-inflammatory and healing-supporting factors that control inflammation and its resolution<sup>89</sup>. By nature, macrophages are very dynamic and exhibit a large spectrum of heterogeneity. Macrophage plasticity is a remarkable ability of these cells to acquire different phenotypes in response to changes in the local microenvironment<sup>89,90</sup>.

Based on the expression of cell surface markers, production of specific factors and functional activity, macrophages can be classified into two major subtypes: classically activated macrophages (M1) and alternatively activated macrophages (M2). Originally, these terms were created in the 1990s when the differential effects of stimulation with interleukin-4 (IL-4) and interferon gamma (IFN $\gamma$ ) and/or lipopolysaccharide (LPS) on macrophage expression were described<sup>91,92</sup>. M1 macrophages are known to possess pro-inflammatory properties and M2 possess anti-inflammatory<sup>88,91</sup>. M0 macrophages are also used in the terminology, which are considered to be uncommitted macrophages, and possess neither pro-inflammatory nor anti-inflammatory characteristics. Stimulation with CSF-1 (M-CSF) of murine bone marrow and human peripheral-blood monocytes remain the predominant *in vitro* systems used for generating macrophages<sup>88</sup>.

Polarization to M1 in response to IFN $\gamma$  and/or LPS induces production of TNF- $\alpha$ , IL-1 $\beta$ , IL-10, IL-12, NO, H<sub>2</sub>O<sub>2</sub>, MCP2 and YKL-40 (CHI3L1) (Figure 3)<sup>93</sup>. The transcriptional profile of M1 is induced by activation of STAT1<sup>93</sup>. The mechanism for pathogen removal promoted by the pro-inflammatory mediators is relatively uniform and typically involves activation of the nicotinamide adenine dinucleotide phosphate (NADPH) oxidase system, which stimulates generation and release of reactive oxygen species (ROS)<sup>94</sup>.

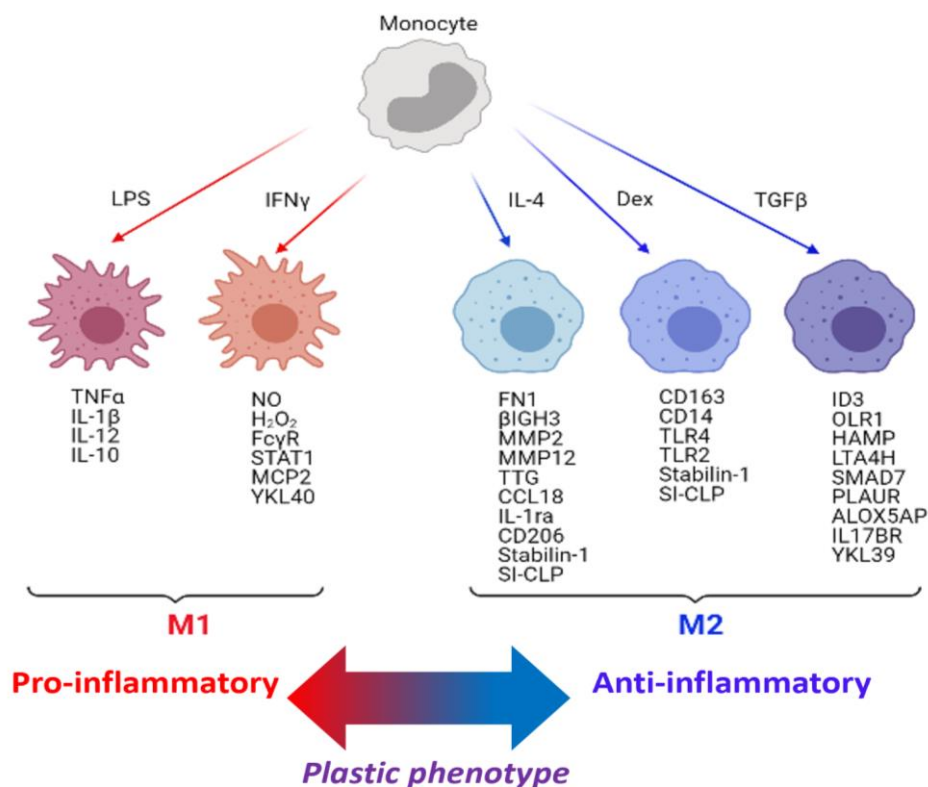


**Figure 3. Macrophage polarization schematic**<sup>93</sup> (Modified from Kzhyshkowska, J et al. 2016 using Biorender.com).



M2 macrophages are also defined as healing or anti-inflammatory macrophages. M2 do not possess an enhanced killing property towards pathogens but downregulate inflammation instead. Polarization to M2 is induced by IL-4, glucocorticoids (dexamethasone), TGF- $\beta$  and other factors<sup>88,95–97</sup>.

A major transcriptional factor of the M2 program is STAT6<sup>8</sup>. M2 in response to IL-4 can secrete a number of matrix remodeling factors including FN1,  $\beta$ IGH3, MMP2, and MMP12<sup>93</sup>. Glucocorticoids are responsible for the enhancement of scavenging potential of M2 mediated by elevated expression of CD206, stabilin-1 and other scavenger receptors. Chitinase-like proteins SI-CLP and YKL-39 are differentially regulated in M2, where SI-CLP is induced by IL-4 and dexamethasone, while YKL-39 is highly specifically induced by TGF- $\beta$ <sup>98,99</sup>. Most characteristic M2 cytokines include CCL18 and IL-1ra (Figure 3)<sup>93</sup>. Thus, stimulation with IL-4 is a major driver for the tissue remodeling activity of M2 via the production of matrix metalloproteinases (MMPs), tissue transglutaminase, and other extracellular matrix components<sup>95</sup>. Glucocorticoids have a major impact on the M2 macrophage profile through the enhancement of endocytic and phagocytic activity, which is crucial in the maintenance of homeostasis and resolution of inflammation<sup>95</sup>. During the differentiation process from monocytes to macrophages, the presence of glucocorticoids is necessary for TGF- $\beta$ RII expression on the macrophage plasma membrane, which allows them to react to activation by TGF- $\beta$ 1 via activation of Smad2/3-dependent signaling<sup>96</sup>. Activation of Smad1/5 by TGF- $\beta$ 1 upregulates expression of HAMP (coding for the antimicrobial peptide hepcidin) and PLAUR (urokinase activator), which is associated with susceptibility to atherosclerotic plaques<sup>97</sup>. Also, M2 exhibit elevated expression of arginase, which counteracts production of nitric oxide (NO). Additionally, expression of MHC class II molecules such as HLA-DR and HLA-DQ is upregulated in IL-4-induced M2, which is important in antigen presentation<sup>100</sup>.

### 1.4.2 Macrophages in foreign body response

Foreign body response (FBR) is often discussed in a context of macrophage behavior during their interaction with biomaterials<sup>8,101</sup>. Macrophages recognize implant material as a foreign body in the tissue, which encompasses recruitment, interaction with the surface, and release of chemokines to recruit additional macrophages and other immune cells that leads to acute inflammation<sup>8</sup>. Implant surfaces can adsorb proteins, such as fibrinogen, fibronectin, vitronectin, etc., which play a major role in implant recognition and initiation of FBR<sup>102</sup>. The absorbed proteins are recognized by macrophage integrins, which are involved in their initial adhesion to biomaterials and fibrotic encapsulation of implant surfaces<sup>103</sup>. The recognition of metal alloy particles involves a signaling pathway via transcription factors NF- $\kappa$ B, followed by production of TNF- $\alpha$  and IL-6<sup>104</sup>. TLRs play a significant role in the recognition of small titanium particles and certain types of biomaterial surfaces<sup>8,105,106</sup>. In addition, TLRs recognize endogenous DAMPs on the surface of biomaterials upon initial tissue injury<sup>105</sup>. Scavenger receptors on macrophages (SR-A, macrophage receptor with collagenous structure) can also recognize metal particles or implant debris, including titanium dioxide<sup>8,107</sup>. Known pathways of implant recognition by macrophages are illustrated in Figure 4A<sup>8</sup>.

The ineffective resolution of acute inflammation often leads to chronic inflammation, supported by fusion of macrophages<sup>8</sup>. In the events of fusion, macrophages form big giant cells in an effort to engulf bulky implant surfaces or the corresponding implant debris (Figure 4B). Foreign body giant cells (FBRCs) are

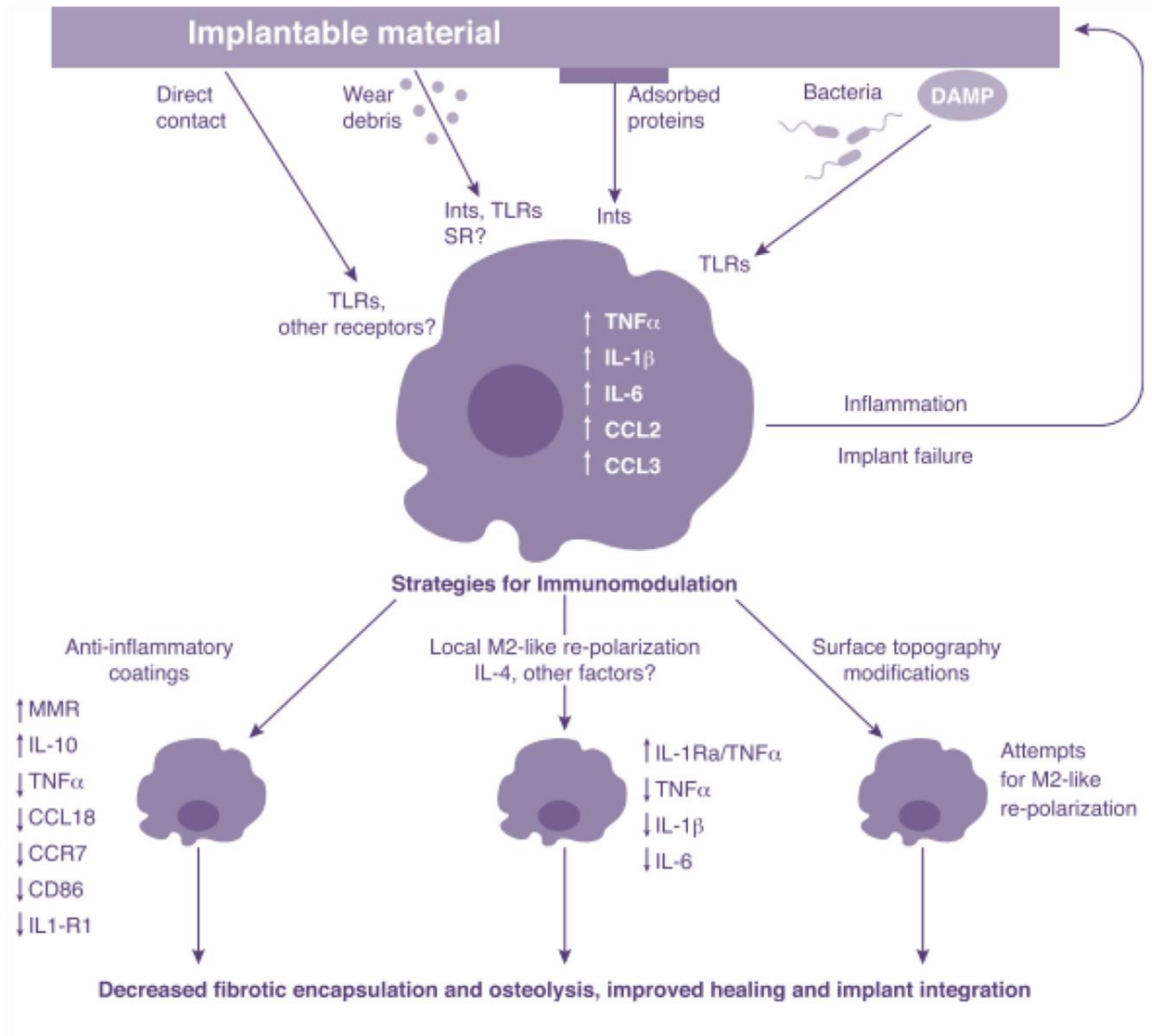


generated from the fusion of monocytes and macrophages and is a typical hallmark of the FBR, which involves direct degradation of implant materials that can lead to a defective implantation system.<sup>101</sup> FBRCs accumulate at the tissue/biomaterial interface, start secreting reactive oxygen species (ROS) and degradative enzymes, which generates a highly volatile molecular environment<sup>102</sup>. The acidic background favors the erosion of the implant accelerating the release of implant wear-off particles, which gives an additional level of cytotoxicity on top of the initial inflammatory reactions in response to bulky implant surfaces.

In the events of FBR and FBR-associated inflammation, monocyte/macrophage migration is necessary. The major chemokines and cytokines which are responsible for this migration have chemoattractive properties and are classified in 4 families: CXC, CC, C and CX3C<sup>108</sup>. Migration of the macrophage is supported by cytokine secretion, which guides the inflammatory responses and determines how successful the wound healing reactions will be in a state of implantation<sup>8,102</sup>. During recent years we have developed a human macrophage-based model system to identify and to predict individual patient responses to implant materials<sup>109–111</sup>.

Both, CD14+ monocytes and CD68+ macrophages are crucial components of the FBR<sup>22,112</sup>. A gene expression study of CD68+ macrophages during early FBR confirmed that macrophages are clearly responsible for FBR and myofibroblast deposition and differentiation<sup>113</sup>. The results of this study revealed a group of upregulated cytokine genes and genes responsible for inflammatory responses, such as TNF $\alpha$ , IL-1a, IL-1b, IL-6 and IL-10, which were clustered around macrophages. Amongst all 197 genes upregulated by FBR macrophages, there were also intercellular adhesion molecule 1 (ICAM-1), integrin  $\alpha$ 5 (ITGA5), integrin  $\alpha$ V (ITGAV), vascular cell adhesion molecule 1 (VCAM-1), syndecan 4 (SDC4), interleukin 4 receptor  $\alpha$  (IL-4RA), CD14 antigen (CD14), endothelial cell adhesion molecule (ESAM) and matrix metalloproteinase 13 (Mmp13). In the analysis of the corresponding gene expression, a switch was identified from monocytes and macrophages attracted by fibrinogen, to activated macrophages and eventually wound-healing macrophages. Moreover, the FBR tissue was found to be comprised of a subpopulation of CD34+ cells, which are known to differentiate into myofibroblasts, the main cell population in mature FBR-tissue<sup>113</sup>.

A



B

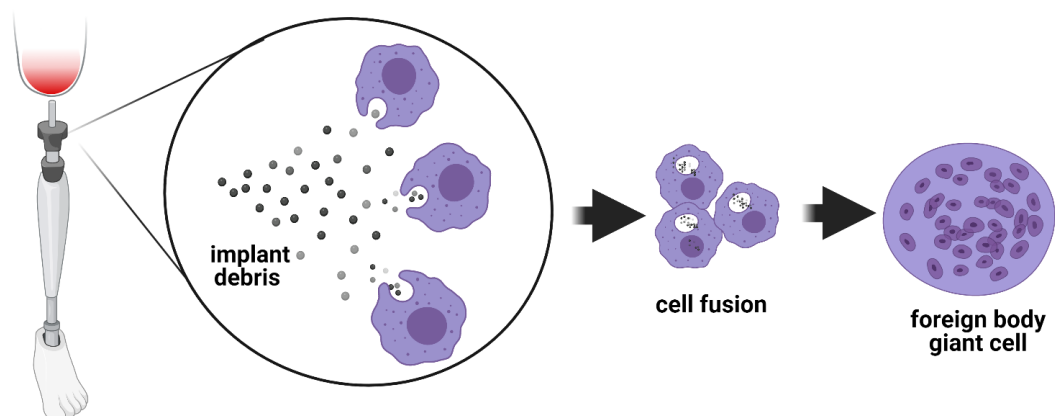


**Figure 4. Macrophages in foreign body response. A. Adverse reaction of macrophages to implantable materials<sup>8</sup>** (adopted from Kzhyshkowska, J et al. 2015). **B. Foreign body response to implant debris** (created with Biorender.com).

### 1.4.3 Macrophage function in normal healing

Macrophage function is necessary for wound healing and tissue regeneration. The actual “pro-healing” process is mainly supported by M2 phenotype macrophages, while M1 macrophages are rather associated with tissue damage, impaired tissue regeneration and slow wound healing<sup>89,114</sup>. The detrimental macrophage-mediated responses can lead to delayed wound healing after injury or development of dangerous immune disorders characterized by chronic inflammation.

On the other hand, it is important to consider that although M2 macrophages are predominantly involved in the healing event, the entire process requires the function of both M1 and M2 macrophages. At the initial stages of trauma, macrophages with pro-inflammatory characteristics infiltrate the wound and retain the M1 phenotype for some time. It takes up to few days for M2 macrophages to accumulate at the wound site and become active<sup>115</sup>.

Due to high plasticity potential, activation of macrophage M2 responses can be accomplished by direct polarization of M1 macrophages to M2 and by the recruitment of new macrophages. Excessive pro-inflammatory activity administered by M1 macrophages can become detrimental to wound healing. Consequently, the M2 phenotype is favorable to tissue regeneration, since it supports proliferation of somatic cells and extracellular matrix remodeling. M2 macrophages are the major source of ECM and collagen which are the necessary raw materials for healing<sup>115</sup>.

### 1.4.4 Macrophages in acute and chronic inflammation

Monocytes and macrophages are essential players in the clearance process of abnormal or dead cells and usually a high number of them are found at inflammatory sites and necrotic tissues. Monocytes in peripheral blood are precursors of adult tissue macrophages. Upon migration towards inflammatory sites, they undergo activation and polarization into distinct macrophage subtypes characterized by specific surface markers. Consequently, the process of inflammation itself is directed by macrophages, which is a critical and complex component of the response to biological, chemical and physical stimuli. Monocytosis is an increased number of monocytes in peripheral blood, which can happen in both acute and chronic inflammation<sup>116</sup>.

Acute inflammatory reactions are required as an initial line of protection against injury. Acute inflammatory mediators are short-lived and have a fast degradation period<sup>117</sup>. Upon the removal of stimuli, the inflammation is diminished, however, many inflammatory mediators are involved in both acute and chronic responses depending on the persistency of a stimulus (Table 2)<sup>8,26,118,119</sup>. During the acute phase of the inflammatory response, macrophages migrate to the injury site and participate in a sequence of events coordinated by cytokines, chemokines, and acute-phase proteins. An acute inflammatory response can be sufficient to cure the injury. However, depending on the injury type, if it is not resolved for a long time, the persistent inflammatory responses from macrophages often lead to chronic phase inflammation, followed by further tissue damage or fibrosis<sup>116</sup>.

**Table 2. Inflammatory cytokines in acute and chronic inflammation phases**<sup>8,26,118,119</sup>

Inflammatory Mediators	Acute	Chronic	Ref. Nr.
<b>TNF-<math>\alpha</math></b> <sup>8,118</sup>	+	+	<b>8, 118</b>
<b>IL-1<math>\alpha</math></b> <sup>26</sup> , <b>IL-1<math>\beta</math></b> <sup>8,118,119</sup>	+	+	<b>8, 26, 118, 119</b>
<b>IL-2</b> <sup>119</sup> , <b>IL-3</b> <sup>119</sup> , <b>IL-4</b> <sup>119</sup> , <b>IL-5</b> <sup>119</sup>		+	<b>119</b>
<b>IL-6</b> <sup>8,118,119</sup>	+	+	<b>8, 118, 119</b>
<b>IL-7</b> <sup>8,119</sup>		+	<b>8, 119</b>
<b>IL-8</b> <sup>8,118,119</sup>	+	+	<b>8, 118, 119</b>
<b>IL-10</b> <sup>8,118,119</sup>	+		<b>8, 118, 119</b>
<b>IL-11</b> <sup>119</sup>	+	+	<b>119</b>
<b>IL-12</b> <sup>8,118,119</sup>	+	+	<b>8, 118, 119</b>
<b>IL-13</b> <sup>8,118,119</sup> , <b>IL-14</b> <sup>119</sup> , <b>IL-15</b> <sup>8,119</sup>		+	<b>8, 118, 119</b>
<b>IL-16</b> <sup>119</sup>		+	<b>119</b>
<b>IL-17</b> <sup>119</sup>		+	<b>119</b>
<b>IL-18</b> <sup>8,119</sup> , <b>IL-19</b> <sup>8,119</sup> , <b>IL-20</b> <sup>8,119</sup> , <b>IL-23</b> <sup>118,119</sup> , <b>IL-24</b> <sup>8,119</sup> , <b>IL-32</b> <sup>8,119</sup>		+	<b>8, 118, 119</b>
<b>GM-CSF</b> <sup>8,118,119</sup>	+	+	<b>8, 118, 119</b>
<b>Eotaxin (CCL11)</b> <sup>8,119</sup>	+	+	<b>8, 119</b>

#### 1.4.5 Mechanisms of chronic inflammation

Chronic inflammation develops as a result of a sustained inflammatory signal, which can potentially spread and disturb the kinetics of metabolic reactions crucial for the maintenance of a healthy cell metabolism. There are numerous cellular and molecular mechanisms and inflammatory mediators (Table 2) associated with chronic inflammation. For instance, sustained activation of TLRs is a known factor that leads to chronic inflammatory diseases<sup>120</sup>. Prolonged inhibition of COX enzymes in macrophages leads to reduced production of PGE<sub>2</sub>, which drives activation of pro-inflammatory macrophages that contribute to prolongation of chronic inflammation during the resolution period<sup>121</sup>. A well-functioning system of clearance is very important in the removal of inflammatory macrophages that can eventually drive chronic inflammation and tissue fibrosis<sup>122</sup>. Disruption of the efficient clearance of apoptotic cells leads to their accumulation, release of necrotic cell debris and persistent inflammatory activation by consistent release of damage associated molecular patterns (DAMPs), which also leads to chronic inflammation<sup>123</sup>.

Various diseases correspond to chronic inflammatory disorders; these include arthritis, asthma, atherosclerosis, autoimmune diseases, diabetes and its complications, obesity, cancer, and implant-related inflammation<sup>124</sup>. During atherosclerosis, low density lipoproteins (LDL) accumulate in the vascular intima, which activates endothelial cells and resident macrophages that lead to expression of adhesion molecules and chemokines<sup>125</sup>. Monocytes migrate in response to activated chemokines and adhesion proteins, where they differentiate into macrophages. Macrophages become foam cells and after excessive accumulation they die through apoptosis, and if they are not effectively cleared it leads to the formation of a pro-inflammatory necrotic core. Further, macrophages form lesions in the arterial wall through the persistent secretion of cytokines and other inflammatory mediators<sup>125</sup>. In the case of obesity, there is a chronic response in adipose tissue, which is associated with persistent cytokine release that promotes accumulation and activity of M1-polarized macrophages<sup>114,126</sup>. The recruitment of M1 macrophages contributes to prolonged secretion of TNF $\alpha$  and an increased ratio of M1 to M2 macrophages, which

is a hallmark of inflammation in adipose tissue associated with metabolic syndrome and insulin resistance<sup>126</sup>. Hyperglycemia plays essential role in the mechanism of diabetic pathology. Prolonged hyperglycemic stimulus has been shown to affect the activation of circulating monocytes<sup>49,127</sup>. In pre-diabetic subjects, characterized by hyperglycemic episodes, peripheral blood cells were analyzed via flow cytometry<sup>128</sup>. The quantification of traditional monocyte subsets was based on CD14 and CD16 expression as well as novel monocyte–macrophage pro-inflammatory CD68+CCR2+ (M1) and anti-inflammatory CX3CR1+CD163+/CD206+ (M2) phenotypes<sup>128</sup>. The flow cytometry analysis revealed increases in pro-inflammatory M1 cells and percent expression of oxLDL scavenger receptor CD68 with a direct correlation to HbA1c<sup>128</sup>. In animal studies, glucose itself promoted diabetes-induced atherosclerosis by increasing monocyte production and macrophage infiltration in atherosclerotic plaques, as well as significantly larger necrotic cores in diabetics than in nondiabetics<sup>129</sup>. Infiltrating macrophages release ROS, NO, lysosomal enzymes and cytokines, which contribute to direct podocyte injury and/or an abnormal podocyte niche leading to diabetic nephropathy<sup>130,131</sup>. Wound healing is impaired in diabetic patients partially due to alterations in kinetic and functional differences in wound monocytes/macrophages<sup>132</sup>.

Periprosthetic osteolysis is a condition, which results from chronic inflammation and local bone disruption triggered by the reaction of immune cells, especially macrophages, to biomaterials<sup>133</sup>. After insertion of implants, implant wear off particles are continuously released into surrounding tissues. The interaction between periprosthetic cells and implant wear-off particles is a critical aspect in the development of osteolysis and aseptic loosening<sup>30</sup>. These particles induce a sustained inflammatory signal, which results in low-grade chronic inflammation eventually leading to periprosthetic osteolysis often followed by implant failure<sup>133</sup>.

## 1.5 Glucocorticoids for alleviation of inflammation

Macrophages are ideal targets for anti-inflammatory drugs, and glucocorticoids are very common treatments for numerous inflammatory disorders such as rheumatoid arthritis, contact allergy and pulmonary diseases<sup>134</sup>. Glucocorticoids have been characterized as immunosuppressants, due to their ability to attenuate or inhibit macrophage activation responses to various cytokines<sup>135,136</sup>. The inhibition of these responses can happen on several mechanistic levels: transcription, mRNA stability, translation and/or post translational processing<sup>135,137</sup>. The anti-inflammatory and cytokine-inhibiting effects of glucocorticoids require binding to glucocorticoid receptors. The glucocorticoid receptors (GRs) are constitutively expressed transcriptional regulatory factors (TRF), which are located in the nucleus and control many distinct gene networks that are associated with particular cellular and physiological processes<sup>138,139</sup>.

Dexamethasone is a synthetic analog of natural glucocorticoids, and widely used for induction of the M2 phenotype *in vitro*<sup>93,95</sup>. Glucocorticoids stimulate phagocytosis of opsonized and non-opsonized particles in macrophages<sup>134</sup>. In addition, glucocorticoids have an anti-apoptotic effect on macrophages, since it has been demonstrated that upon treatment with dexamethasone macrophages are more resistant to lipopolysaccharide (LPS)-induced apoptosis<sup>140–142</sup>. Similar effects were observed with other types of apoptotic stimuli, such as, staurosporine, actinomycin D and cyclohexine, where glucocorticoid action was achieved through ERK1/2 phosphorylation in an adenosine receptor A3-dependent-manner<sup>143,144</sup>. Also

dexamethasone suppresses the migratory capacity of macrophages, which is likely by promoting macrophages to take a smaller form with less cytoplasmic extensions<sup>145,146</sup>. Macrophages treated with cortisol exhibit a lower capacity of migration *in vitro*<sup>146,147</sup>. *In vivo*, it has been demonstrated that glucocorticoids can inhibit infiltration of macrophages into the lung during treatment of lung injury with bleomycin<sup>148</sup>.

Glucocorticoids, depending on their pharmacological potency, efficacy and concentration, can suppress the secretion of the pro-inflammatory cytokines, such as TNF- $\alpha$ , IL-1 and IL6 in macrophages exposed to IFN $\gamma$ <sup>95,148,149</sup>. On the other hand, monocytes exposed to glucocorticoids tend to secrete higher levels of IL-10 and TGF $\beta$ , and have an increased secretion of anti-inflammatory markers, such as CD206, CD163 and CD169<sup>143,150–153</sup>.

The therapeutic effects of dexamethasone in the context of potential attenuation of the inflammatory responses induced by implant wear debris has been studied in RAW 264.7 cells<sup>154</sup>. The results of the same study concluded that dexamethasone released from amino-functionalized titanium can potentially be applied in the prevention of aseptic loosening of joint replacement devices<sup>154</sup>. The precise mechanisms by which dexamethasone exerts its therapeutic function by alleviation of inflammatory reactions induced by implant wear off particles is a remaining research question.

## 1.6 Reactive oxygen species in macrophage responses

Reactive oxygen species (ROS) contribute to antimicrobial properties and are part of normal cell activity. ROS is a short-lived second messenger, it plays important role in cell signaling and is responsible for oxidation of the thiol group in cysteine residues of the proteins; this protein oxidation is tightly regulated by reducing systems such as peroxiredoxin (PRX) and thiopredoxin (TRX)<sup>155,156</sup>. ROS is essential in inducing and sustaining pro-inflammatory macrophage responses in host defense against infection<sup>116,157</sup>. Numerous studies revealed the function of ROS as a secondary messenger implicated in both M1 and M2 macrophage polarization states<sup>157,158</sup>. It has been reported that ROS has a role in the activation of the NF $\kappa$ B and p38 MAPK signaling pathways, which induce pro-inflammatory gene expression in macrophages, and the mechanism involves stimulation of TLR4 followed by activation of NOX and SOD and generation of H<sub>2</sub>O<sub>2</sub><sup>157,159</sup>.

Overproduction of ROS promotes oxidative stress, which occurs if the generation of ROS exceeds the capacity of the antioxidant defense. At this state the cells start undergoing severe cellular dysfunction and cell death by apoptosis via upregulation of proapoptotic PUMA and BIM followed by recruitment of BAX on the mitochondrial membrane, which triggers release of apoptotic factors such as caspases and cytochrome c<sup>160</sup>. Release of the apoptotic factors eventually lowers mitochondrial membrane potential (MMP,  $\Delta\psi$ m) and sends out a signal of self-destruction to the cells<sup>106,160</sup>.

Oxidative stress is associated with the development of various human disorders, such as cancer, cardiovascular, neurodegenerative, and metabolic disorders, inflammation, and aging<sup>161,162</sup>. Multiple studies are investigating oxidative stress in vascular complications by assessing levels of ROS in endothelial and epithelial cells and tissues<sup>163,164</sup>. The role of macrophage-generated ROS in diabetic complications has been frequently addressed<sup>164</sup>. Moreover, induction of apoptosis in murine macrophages in response to titanium dioxide materials has been revealed to occur through ROS-dependent SAPK/JNK and p38MAPK activation<sup>106</sup>. Production of ROS

induced by Ti NPs and silicon nanoparticles induce an inflammatory response in macrophages, which is suspected to drive lung inflammation<sup>165</sup>.

The unfavorable effects of ROS overproduction in the diabetes-induced impaired osteogenesis of titanium implants have been studied before<sup>166</sup>. It has been shown that ROS production associated with osteolysis can be inhibited by the stable coatings in biomaterials<sup>167</sup>. Mechanisms of implant debris-dependent ROS induction in the context of diabetic pathology needs to be studied separately.

### 1.7 Aims and objectives

Titanium biomaterials are typically used for human implantation. As a consequence of metal corrosion, all metal implants, including titanium, degrade over time, which triggers a release of titanium nanoparticles (Ti NPs), known as implant debris or metal wear-off particles. Patients with Diabetes Mellitus (DM) have elevated blood sugar levels and can suffer from consequences triggered by compromised immune responses. Amongst those consequences are the complications produced by metal implants. Hyperglycemia, which is a major factor of diabetic pathology, also promotes implant corrosion contributing to the release of metal wear-off particles, such as Ti NPs. Ti NPs are amongst the driving forces that contribute to the disruption of the mechanical stability of implant devices causing aseptic loosening and triggering adverse immune reactions that lead to chronic health complications. Macrophages are the vital immune cells, which are responsible for clearance and elimination of foreign materials and have a high influence on the acceptance or failure of implants. Although potential failure or acceptance of titanium implants in diabetic patients have been previously addressed, the cooperation of Ti NPs and hyperglycemia as major driving forces of implant failure in diabetic individuals require investigation.

The goal of the current study was to analyze the effect of titanium wear-off particles (nanoparticles) on primary human macrophages exposed to a hyperglycemic environment.

Specific aims:

1. To analyze cell viability of titanium surfaces and different concentrations of Ti NPs via the Alamar Blue assay.
2. To identify the effects of Ti NPs on macrophage responses and membrane transport via ELISA, RT-qPCR and confocal microscopy.
3. To identify the effects of hyperglycemia on Ti NPs–induced changes of macrophage pro-inflammatory and healing responses via ELISA and RT-qPCR.
4. To analyze the anti-inflammatory role of dexamethasone in suppression of Ti NPs-induced macrophage reactions cultured in a hyperglycemic environment via ELISA and RT-qPCR.
5. To identify the effects of Ti NPs and hyperglycemia on the release of mitochondrial ROS via FACS.
6. To identify the complete transcriptional program induced by Ti NPs in macrophages in hyperglycemic conditions using Affymetrix microarray analysis, and to validate selected differentially expressed genes and RT-qPCR.

## 2 MATERIALS AND METHODS

### 2.1 Chemicals, reagents and kits

**Table 3. Chemicals and reagents**

<b>Product</b>	<b>Company</b>
0.05% Trypsin/EDTA solution	Biochrom
10x Earle's Balanced Salt Solution (EBSS)	Sigma Aldrich
10x Incomplete PCR buffer	BIORON
30% Acrylamide/Bis Solution	Bio-rad
4',6-diamidino-2-phenylindole (DAPI)	Roche Diagnostics
Acetic Acid	Merck
Agarose	Roth
AlamarBlue®	Invitrogen
Biocoll solution	Biochrom
Ficoll solution	Cytiva
Bovine Serum Albumin (BSA)	Sigma Aldrich
CD14 MicroBeads	Miltenyi Biotec
D-(+)-Glucose solution 10%	Sigma Aldrich
DCF (fluorescent 2', 7'-dichlorodihydrofluorescein )	Thermo Fisher Scientific
Deoxyribonucleotides (dNTPs) 10M	Fermentas
DEPC Water	Thermo Fisher Scientific
Dexamethasone	Sigma Aldrich
Dimethylsulfoxide (DMSO)	Sigma Aldrich
DNA ladder	Thermo Fisher Scientific
DNA Loading Dye (6x)	Thermo Fisher Scientific
DNase Buffer(10x)	Thermo Fisher Scientific
DNase I RNase free 1U/μl solution	Fermentas
EDTA	Invitrogen
Ethanol	Roth
FcR Blocking Reagent, human	Miltenyi Biotec
Fetal calf serum (FCS)	Biochrom
GelRed Nucleic Acid Gel Stain, 10,000x	Biotium
GeneRuler DNA ladder	Fermentas
Glycerol	Sigma Aldrich
Loading dye 6x	Fermentas
Macrophage-SFM (serum-free medium)	Life Technologies
MEM Spinner modification	Sigma Aldrich
MgCl <sub>2</sub>	Sigma Aldrich
MitoSox™	Invitrogen
MitoTracker	Invitrogen
Oligo(dT) primer	Thermo Fisher Scientific
PBS Dulbecco, w/o Ca <sup>2+</sup> , Mg <sup>2+</sup>	Biochrom
PCR primers (designed in the lab)	Eurofins MWG Operon



<b>Product</b>	<b>Company</b>
PCR probes (designed in the lab)	Eurofins MWG Operon
PCR ready-made mixes	Life Technologies
Percoll	GE Healthcare Life Sciences
Phosphate buffered saline (D-PBS), sterile 1x	Invitrogen
Recombinant Human IFN- $\gamma$	Peprotech
Recombinant Human IL-4	Peprotech
Recombinant Human M-CSF	Peprotech
Sensimix II Probe kit	Bioline
Sodium Azide	Alfa Aesar
SytoxRed	Invitrogen
Triton X-100	Sigma Aldrich
Trypan blue solution	Sigma Aldrich
Tween 20	Sigma Aldrich

**Table 4. Kits.**

<b>Product</b>	<b>Company</b>
E.Z.N.A. total RNA kit I	Omega bio-tek
Human CCL18 DuoSet ELISA kit	R&D systems
Human Chitinase 3-like 1 DuoSet ELISA kit	R&D systems
Human CXCL10 DuoSet ELISA kit	R&D systems
Human IL-1 $\beta$ DuoSet ELISA kit	R&D systems
Human IL-6 DuoSet ELISA kit	R&D systems
Human IL-8(CXCL8) DuoSet ELISA kit	R&D systems
Human MMP-7 activity assay	Quickzyme Biosciences
Human TNF- $\alpha$ DuoSet ELISA kit	R&D systems
Human Total MMP-7 DuoSet ELISA kit	R&D systems
RevertAid H Minus First Strand Synthesis Kit	Fermentas
RNeasy mini kit	Qiagen
SensiFAST cDNA Synthesis Kit	Bioline

## 2.2 Consumables

**Table 5. Consumables.**

<b>Product</b>	<b>Company</b>
22 $\mu$ m filters	Fisherbrand
CASY cups	Omni Life Sciences
Cell culture plates	Greiner
Elisa plate sealers	R&D systems
Elisa Plates	R&D systems
LS columns	Miltenyi Biotec
Parafilm	American National Can
PCR tubes	Star Labs
Petri dishes	Nunc

<b>Product</b>	<b>Company</b>
Pipette tips	Eppendorf
Pipettes	Gilson, Eppendorf
Plastic wrap	Toppits
qPCR plate sealers	Axon Labortechnik
qPCR plates	Axon Labortechnik
Safe-Lock Eppendorf Tubes, 1.5ml	Eppendorf
Scalpel	Feather
Sterile pipette tips	Avantguard, Star Labs, Nerbeplus
TiO <sub>2</sub> 15nm nanoparticles	NanoAmor Europe
Tubes	Falcon
Ultra-low cell attachment surface culture plates	Corning

## 2.3 Equipment

**Table 6. Equipment.**

<b>Product</b>	<b>Company</b>
Autoclave VX-95	Systec
BD FACSCanto II	BD Biosciences
CASY Cell counter	Schärfe System
Centrifugal vacuum concentrator 5301	Eppendorf
Centrifuge 5415 D	Eppendorf
Centrifuge 5804R	Eppendorf
Centrifuge Rotina 420	Hettich
Centrifuge Rotina 420R	Hettich
Centrifuge Universal 320	Hettich
Cryo freezing container	Nalgene
Confocal software	Leica
Deep freezer (-80°C)	Sanyo
ENDURO Electrophoresis comb	Labnet
ENDURO Electrophoresis power supply	Labnet
Freezer (-20°C)	Liebherr
Fridge (4°C)	Liebherr
ACCU-Chek (Glucose Meter)	Roche
HydroFlex ELISA microplate washer	Tecan
Ice machine	Scotsman AF100
Incubator 37°C	Thermo
Inverted microscope	Leica
Laminar flow hood	Thermo
LightCycler 480	Roche
MACS MultiStand	Miltenyi
Magnetic stirrer MR3000	Heidolph
Microwave oven	Sharp
Micropipettes Set (10ul, 20ul, 100ul and 1000ul)	Eppendorf
Multichannel pipet (10 row)	Brand
MultiDoc-It™ Imaging System	UVP
Pipette Controller	Accu Jet Pro, Brand

Product	Company
Roller shaker	Ortho Diagnostic Systems
Rotator	Neolab
Shaker KS 260 basic	IKA
TCS SP2 laser scanning spectral confocal microscope	Leica
Tecan Infinite 200 PRO	Tecan
Tecan Nano Quant Plate	Tecan
Thermocycler DNA Engine	Bio-Rad
Thermomixer 5436	Eppendorf
Thermomixer comfort	Eppendorf
Tweezers	Neolab
Vortex Genie 2	Scientific Industries
Water bath	Memmert

## 2.4 Buffers and Solutions

### 2.4.1 Solutions for immunological methods

*Wash buffer for ELISA (0.05% Tween 20 in PBS)*

500 µl of Tween 20 was pipetted into 1 L of PBS. The beaker was stirred on a magnetic stirrer for 30 min and the solution was stored at RT.

*FACS buffer (0.4% BSA, 0.02% Sodium Azide):*

4 g of BSA and 2 ml of 10% Sodium Azide solution were dissolved in 1 L of PBS. The solution was adjusted to pH 7.4 and sterile filtered with a 0.22 µm filter.

### 2.4.2 Solutions for monocyte isolation

*Percoll gradient:*

Every 30 ml of Percoll gradient solution was prepared in a 50 ml Falcon tube with 13.5 ml Percoll, 15 ml Minimal Essential Medium Eagle Spinner modification and 1.5 ml of 10xEarle's Balanced Salt Solution.

*MACS buffer (0.5% BSA, 2mM EDTA):*

2.5 g of BSA was dissolved in 500 ml PBS. 2 ml of 0,5M EDTA was added and the mixture was filtered to a sterile flask.

## 2.5 Molecular biology techniques

### 2.5.1 Primers

**Table 7. List of primers designed in the lab.** F: forward, R: reverse, Pr: probe. All primers and probes were ordered from Eurofins MWG Operon.

Primer name	Target gene	Sequence (5'-3' direction)
FP2242	18SrRNA	CCATTTCGAACGTCTGCCCTAT
FP2242	18SrRNA	TCACCCGTGGTCACCATG
Pr2242	18SrRNA	ACTTTTCGATGGTAGTCGCCGTGCCT
FP2150	IL1beta	ACAGATGAAGTGCTCCTTCCA

RP2150	IL1beta	GTCGGAGATTCGTAGCTGGAT
Pr2150	IL1beta	CTCTGCCCTCTGGATGGCGG
F2020	CCL18	ATACCTCCTGGCAGATTCCAC
R2020	CCL18	GCTGATGTATTTCTGGACCCAC
Pr2020	CCL18	CAAGCCAGGTGTCATCCTCCTAACCAAGAGAG
F896	TNF- $\alpha$	TCTTCTCGAACCCCGAGTGA
F896	TNF- $\alpha$	AGCTGCCCTCAGCTTGA
Pr896	TNF- $\alpha$	AAGCCTGTAGCCCATGTTGTAGCAAACC

**Table 8. List of ready-made mixes.** All ready-made mixes were ordered from Life Technologies.

<b>Assay code</b>	<b>Target Gene</b>
Hs00609691_m1	CHI3L1
Hs00185753_m1	CHIT1
Hs00174164_m1	CSF1
Hs00174103_m1	CXCL8
Hs00171065_m1	CXCL9
Hs00171042_m1	CXCL10
Hs00153510_m1	MME
Hs01590790_g1	ORM1
Hs02578922_gH	MT1G
Hs00745167_sH	MT1X

### 2.5.2 Isolation of total RNA

E.Z.N.A. total RNA kit I from Omega was used for RNA isolation.

- 1) 350  $\mu$ l of lysis(TRK) buffer was added to  $3-5 \times 10^6$  cells, which were completely disrupted by passing through a needle fitted to a syringe for 10-15 times.
- 2) 350  $\mu$ l of 70% ethanol were added to the lysate and vortexed briefly. The sample was added to a HiBind RNA spin column placed into a 2 ml collection tube.
- 3) After centrifuging for 1 min at 10000 g the flow-through was discarded. The column was washed once with 500  $\mu$ l wash buffer I.
- 4) The column was centrifuged at 10000 g followed by washing twice in 500  $\mu$ l wash buffer II (each wash was followed by a centrifugation step at 10000 g).
- 5) The final flow-through was discarded and a new 2 ml collection tube was placed under the column which was centrifuged for 2 min at maximum speed.
- 6) The column was placed in a fresh 1.5 ml RNase free Eppendorf tube and RNA was eluted with 30  $\mu$ l of DEPC-treated water and incubated for 5min. Samples were centrifuged at maximum speed for 1 min.
- 7) The RNA concentration was determined by measuring the absorption peak at 260 nm wavelength with Tecan Infinite 200 PRO.
- 8) The quality of RNA samples was identified by gel electrophoresis using 1% agarose. RNA samples were stored at  $-80^\circ\text{C}$  for later application.

### 2.5.3 First strand cDNA synthesis

cDNA synthesis was performed using two different kits: RevertAid H Minus First Strand Synthesis Kit and SensiFAST cDNA Synthesis Kit.

#### 1. cDNA synthesis using with RevertAid H Minus First Strand Synthesis Kit

For the experiments that addressed the effect of HG on macrophages (M0, M1 and M2) exposed to polished titanium disks and different concentration of TiO<sub>2</sub>NPs, RevertAid H Minus First Strand Synthesis Kit from Fermentas was used.

- a. RNA samples were digested with DNase I to remove possible contamination of isolated RNA with fragments of genomic DNA.
- b. For this the following components were used:

Total RNA	5µl (up to 1µg)
10x DNase I buffer with MgCl <sub>2</sub>	1µl
RNase free DNase I	1µl
DEPC H <sub>2</sub> O	Up to 10µl

(If the RNA yield of a sample was below 50 ng/µl , 8 µl of RNA was used and no DEPC water was added. For samples with RNA yield above 60 ng/µl, 4 µl of RNA was used and 4 µl of DEPC water; for samples with RNA of 100 ng/µl, only 2 µl of RNA was used and 6 µl of water)

- c. The samples were incubated at 37°C for 40 min (DNA digestion step) in a Thermomixer followed by enzyme inactivation at 70°C for 10min.
- d. For primer annealing 1 µl of Oligo (dT) primer and 1 µl of water was added to each sample and incubated at 70°C for 5 min. The samples were placed on ice.
- e. For cDNA synthesis the following components were added and mixed well:

5x Reaction Buffer	4µl
RiboLock RNase inhibitor	1µl
10M dNTP mix	2µl
RevertAid H minus reverse transcriptase	1µl

- f. The samples were incubated at 42°C for 1 h in a Thermomixer. Afterwards, the enzymatic activity was stopped by incubation at 70°C for 10 min.
- g. The cDNA samples were diluted 10 times with ddH<sub>2</sub>O and stored at -20°C for later use.

#### 2. cDNA synthesis using SensiFAST cDNA Synthesis Kit.

For the experiments that addressed the effect of Dexamethasone presence and HG on M1 exposed TiO<sub>2</sub>NPs, Sensi FAST cDNA Synthesis Kit from Bioline was used:

- a. RNA of the samples was gently mixed with the master mix and DEPC water reagents. The following components were used:

<b>Total Amount of RNA for 500ng</b>	<b>(n)<math>\mu</math>l</b>
5x TransAmp Buffer	4 $\mu$ l
Reverse Transcriptase	1 $\mu$ l
DEPC H <sub>2</sub> O	Up to 20 $\mu$ l

- b. The core master mix was prepared from 5 x TransAmp Buffer and Reverse Transcriptase, which was made for total amount of RNA in  $\mu$ l calculated from addition of volume of all the samples required to make 500 ng.
- c. All the components including correct proportions of RNA, master mix and DEPC water were mixed in a single tube, which were first kept at 25 °C for 10 min for primer annealing.
- d. Samples were transferred to preheated thermal cycler with 42 °C and left to incubate for 15 min (reverse transcription), followed by 15 min at 48 °C
- e. For inactivation step, the samples were placed at 85 °C for 5 min

#### **2.5.4 RNA preparation for Affymetrix microarray analysis**

Total RNA was prepared using E.Z.N.A. total RNA kit I as described above.

- 1) The volume of RNA sample was adjusted with DEPC-treated water to 100  $\mu$ l. 12  $\mu$ l of 10 x DNase I buffer with MgCl<sub>2</sub> and 10  $\mu$ l of RNase free DNase I were added to sample and mixed well by pipetting.
- 2) DNA digestion was done at 37°C for 40 min in a Thermomixer.
- 3) For RNA cleanup procedure RNeasy kit from Qiagen was used. 350  $\mu$ l of RLT buffer were added to the samples and the samples were vortexed.
- 4) 250  $\mu$ l of 100% ethanol were added to the samples and mixed by pipetting.
- 5) The samples were added to RNeasy mini column, placed in a 2 ml collection tube and centrifuged at 10000 g for 1 min.
- 6) The flow through was discarded and columns were washed two times with 500  $\mu$ l of RPE buffer (each wash was followed by a centrifugation step at 10000 g).
- 7) The collection tubes were changed and the samples were centrifuged at maximum speed for 2 min.
- 8) The columns were placed in fresh 1.5 ml RNase free Eppendorf tube and RNA was eluted with 40  $\mu$ l of DEPC-treated water and incubated for 5 min. Samples were centrifuged at maximum speed for 1 min.
- 9) The elution step was repeated with the eluate to increase RNA concentration as recommended by the manufacturer.
- 10) The RNA concentration was determined by measuring the absorption peak at 260 nm wavelength with Tecan Infinite 200 PRO
- 11) The quality of RNA samples was determined by running the RNA on 1% agarose gel. RNA samples were stored at -80°C for later application.

#### **2.5.5 Hybridization of gene chip microarray data**

The extracted samples, which revealed RNA yield above 100 ng were selected for microarray analysis. The samples with sufficient yield were further tested for RNA integrity by the services of the core Affymetrix facility. RNA samples which revealed RIN below 7 were used in microarray analysis. Based on RNA integrity number and concentration, RNA from 6 of them was chosen for microarray analysis. RNA was tested by capillary electrophoresis on an Agilent 2100 bioanalyzer (Agilent) and high quality was confirmed. Hybridization of probes was done using arrays of human

HuGene-1\_0-st-type from Affymetrix. Biotinylated antisense cRNA was then prepared according to the Affymetrix standard labelling protocol with the GeneChip® WT Plus Reagent Kit and the GeneChip® Hybridization, Wash and Stain Kit (both from Affymetrix, Santa Clara, USA). Afterwards, the hybridization on the chip was performed on a GeneChip Hybridization oven 640, then dyed in the GeneChip Fluidics Station 450 and thereafter scanned with a GeneChip Scanner 3000. All of the equipment used was from the Affymetrix-Company (Affymetrix, High Wycombe, UK). All the necessary procedures needed for hybridization and scanning of chips were performed by Dr. Carolina De La Torre, Affymetrix Core Facility, Medical Research Center, Medical Faculty Mannheim, University of Heidelberg, Mannheim, Germany.

### **2.5.6 Polymerase chain reaction (PCR)**

Genes were amplified from cDNA templates using primers specific to the gene of interest.

1. The following reagents were added to a 1.5 ml Eppendorf tube to make a master mix for the number of samples:

<b>Reagent</b>	<b>Amount/sample (µl)</b>
<b>DEPC ddH<sub>2</sub>O</b>	18.3
<b>Buffer (w/o +Mg<sup>2+</sup>) 10x</b>	2.5
<b>dNTPs (10 mM)</b>	0.5
<b>MgCl<sub>2</sub> (100 mM)</b>	0.4
<b>Taq polymerase (5 U/µl)</b>	0.3
<b>Forward primer (10 pmol/µl)</b>	1.0
<b>Reverse primer (10 pmol/µl)</b>	1.0

2. The master mix was divided amongst PCR tubes and 1 µl of cDNA template was added to each tube and mixed by pipetting.
3. Amplification was performed using Thermocycler DNA Engine from Biorad and the following program was used:

95°C 3min	}	35 cycles
95°C 30s		
60°C 30s		
72°C 1min		
72°C 10min		
12°C forever		

\*PCR products were visualized using agarose gel electrophoresis.

### **2.5.7 Real-time PCR with Taqman probe**

Genes were amplified from cDNA templates using primers specific to the gene of interest.

- ❖ Method I: with two separate master mixes (separated reference and target primers)

- Two master mixes were prepared in two separate 1.5 ml Eppendorf tubes:

**Master Mix I**

Reagent	per well	per duplicate
Sensi Mix II (Taqman®)	5 µL	10 µl
Assay Primer Mix (Target Gene)	0.5 µL	1.0 µl
Nuclease-free ddH2O	3.5 µL	7.0 µl
Total	9 µL	18 µl

**Master Mix II**

Reagent	per well	per duplicate
Sensi Mix II (Taqman®)	5 µL	10 µl
Primer (Reference Gene)	0.5 µL	1.0 µl
Nuclease-free ddH2O	3.5 µL	7.0 µl
Total	9 µL	18 µl

- The master mix was divided amongst 1.5 ml Eppendorf tubes. As each sample was run in duplicates, 2 µl of cDNA template was added to each tube and mixed by pipetting.

❖ **Method II: with a single master mix (combined reference and target primers)**

- A master mix for all the samples was prepared in a 1.5 ml Eppendorf tube containing:

Reagent	per well	per triplicate
Sensi Mix II (Taqman®)	5 µL	15 µl
Primer (Reference Gene)	0.5 µL	1.5 µl
Assay Primer Mix (Target Gene)	0.5 µl	1.5 µl
Nuclease-free ddH2O	3 µL	9 µl
Total	9 µL	27 µl

- The master mix was divided amongst 1.5 ml Eppendorf tubes. As each sample was run in triplicates, 3 µl of cDNA template was added to each tube and mixed by pipetting.

Amplification for both cases (Method I and II) was performed using LightCycler 480 from Roche and the following program was used:

95°C 10min	} 50 cycles
95°C 15s	
60°C 1min	
37°C 2min	



Dual-labeled probes for target genes contained FAM on 5' end and BHQ1 quencher at 3' end of sequence. In all experiments 18S was used as the reference gene. The probe for 18srRNA contained JOE on 5' end and BHQ1 quencher at 3' end of sequence.

### 2.5.8 Agarose gel electrophoresis

- 1) 1% agarose gel was used for detection of the RNA. To prepare the electrophoresis buffer. 1 g of agarose was dissolved in 100 ml of 1xTAE, which was heated in a microwave until the solution started boiling.
- 2) After the solution was cooled down to about 50°C, 10 µl of GelRed Nucleic Acid Gel Stain (10000x) was added.
- 3) The solution was poured into a gel tray equipped with a comb and left 20 min to allow gel polymerization.
- 4) The comb was removed from the gel, which was placed into the electrophoresis unit, followed by pouring the 1xTEA buffer until the marks in the unit. 2 µl of GeneRuler DNA Ladder was added to the first lane in the gel.
- 5) The samples were prepared as follows: 1 µl of sample (for RNA above 100 ng), 2 µl (for RNA below 100 ng) and 3 µl (for RNA below 50 ng). The RNA was mixed with 2 µl of 6x Loading dye.
- 6) Electrophoresis was carried out at 110 V for 1 hour. The results were visualized by UV illumination and captured using E-BOX VX5 Gel Documentation System.

## 2.6 Cell culture techniques

### 2.6.1 Cultivation of cell lines and primary cells

Isolation of CD14+ monocytes from human peripheral blood (buffy coats), obtained from Deutsches Rotes Kreuz (DRK), Friedrich-Ebert-Straße 107, 68167 Mannheim.

- 1) Buffy coats with 20-50 ml of blood were received from A unique donor number was given to each Buffy Coat.
- 2) Buffy coats were transferred from the plastic bag to a T75 flask, diluted 1:1 with PBS (without Ca<sup>2+</sup> and Mg<sup>2+</sup>) and mixed by pipetting up and down.
- 3) For each 30 ml of diluted blood a 50 ml Falcon tube with 15 ml Biocoll separating solution was prepared.
- 4) 30 ml of diluted blood was carefully layered (against the tube wall) on top of Biocoll solution. The tubes were centrifuged at 420 g, for 30 min without break.
- 5) PBMC (the second layer) were collected with a sterile Pasteur pipet and transferred into a new 50 ml Falcon tube (cells from each tube were transferred into a new one).
- 6) The mixture was added up to 50 ml with PBS and the tubes were centrifuged at 420 g for 10 min with break.
- 7) New set of 50 ml tubes were labelled accordingly and used to spin the supernatants by pouring slowly about 45 ml of supernatant from after 10min spinning performed in step 6.
- 8) The cell pellets from each donor were resuspended with 5 ml PBS and collected in one 50 ml Falcon tube for each donor (tubes from the same donor were combined in this step).

- 9) The cells were washed with 50 ml PBS and centrifuged at 420 g for 10 min with break. The supernatant was discarded.
- 10) Percoll gradient (30 ml) was prepared with 13.5 ml Percoll, 15 ml of MEM Spinner modification and 1.5 ml 10x Earle's Balanced Salt Solution.
- 11) The cells were resuspended with 3 ml PBS and carefully layered (against the tube wall) on top of the Percoll gradient.
- 12) The old tube was washed with 4 ml of PBS and the content was added to the Percoll gradient tube. Cells were centrifuged at 420 g, for 30 min without break.
- 13) The upper phase (PBS) and second phase (cells enriched for monocytes) were collected into a 50 ml Falcon tube.
- 14) The solution was mixed well, filled up to 50 ml with PBS and centrifuged at 420 g, for 10 min with break. The supernatant was discarded.
- 15) The cell pellets were resuspended with 3 ml PBS and transferred into a 15 ml Falcon tube. The 50 ml tube was washed with 4 ml of PBS. The solution was added into the 15 ml tube and filled up to 10 ml.
- 16) Cells were counted and the rest of them were centrifuged at 420 g, for 10 min with break. Cell counting was performed on CASY Cell counter.
- 17) The cell pellet was resuspended in CD14+ microbeads and MACS buffer according to the formula: 5  $\mu$ l CD14 beads and 95  $\mu$ l MACS buffer per  $1 \times 10^7$  cells.
- 18) The cells were incubated for 20 min on a rotator at 4°C.
- 19) The tubes were filled up to 10 ml with MACS buffer and centrifuged at 420 g, for 10 min.
- 20) During this time, LS columns were attached to the magnetic stand (One column is maximal for  $1 \times 10^8$  cells) and 15 ml Falcon tubes were placed under columns. The columns were washed with 3 ml of MACS buffer.
- 21) The cell pellet was resuspended in 1 ml MACS buffer and then added to each column. The column was washed 3 times with MACS buffer, each time 3 ml.
- 22) The column was removed from the magnetic separation unit and placed on top of a fresh 15 ml Falcon tube. CD14+ monocytes were eluted from the column with 10 ml MACS buffer.
- 23) Cells were counted and centrifuged at 420 g, for 10 min. The cell pellet was resuspended in 1 ml of Macrophage-SFM medium and cultured according to the experimental plan.

### 2.6.2 Cell counting

*Monocyte and PBMC cell counting was performed on a CASY cell counter from Schärfe System.*

- 1) 10  $\mu$ l of sample was added to 10 ml of CASYton solution in a CASYcup.
- 2) The CASYcup was placed under the CASY capillary and the appropriate program for PBMC was chosen.
- 3) After each measurement 3 cycles of cleaning procedure were performed.
- 4) Only the viable cell number was used for further calculations.

### 2.6.3 Specific conditions used for primary human monocytes

- 1) Isolated primary human monocytes were separately cultured in 5 mM or 25 mM Glucose concentrations using Macrophage-SFM medium (prepared in advance for those glucose concentration using glucose meter).

- 2) All the medium contained  $10^{-8}$  M Dexamethasone and 5 ng/ml M-CSF, which were prepared fresh after the cells were counted for each donor upon the completion of monocyte isolation experiment.
- 3) The concentration of cells in experiments with polished titanium disks was maintained at  $2 \times 10^6$ /ml and the experiments with titanium nanoparticles were performed at  $1 \times 10^6$ /ml and  $2 \times 10^6$ /ml.
- 4) All the cells with  $1 \times 10^6$  concentration were cultured in 24-well plates (1.5 ml/well), except all ROS experiments performed with FACS which were done with the cells cultured in 6-well plates.
- 5) Nanoparticle experiments with cells of double concentration were performed in 12-well or 6-well plates.
- 6) Three subtypes of monocytes were obtained by stimulation: M0(Control) - no additional stimulation; M1(pro-inflammatory state) - stimulation with 100 ng/ml IFN $\gamma$ ; M(anti-inflammatory state) - stimulation with 10 ng/ml IL-4.
- 7) The cells were cultured for 6 days to allow sufficient time for macrophage differentiation. An exception were the cells used in experiments for TNF alpha production, which incubation time was strictly limited 6 hours.

#### **2.6.4 Analysis of macrophage cell viability with Alamar Blue**

##### *2.6.4.1 Cell Viability Test with Polished Titanium Disks:*

- 1) 0.5 ml of supernatants from each well was removed, leaving 1 ml of supernatant inside.
- 2) 100  $\mu$ l of Alamar Blue was added to each well, and the plate was incubated at 37°C for 3 h.
- 3) Three times 100  $\mu$ l of supernatant from each well (triplicates) was collected and transferred into a 96-well plate for measuring.

Measurement was done on with Tecan Infinite 200 PRO using 560EX nm/590EM nm filter settings.

##### *2.6.4.2 Cell Viability Test with Titanium Nanoparticle:*

260  $\mu$ l of cells resuspended in glucose-treated SFM-medium that already contained dexamethasone and M-SCF without any cytokine stimulation (M0), or pre-stimulated with IFN $\gamma$  (M1) and IL-4 (M2).

180  $\mu$ l of cells were pipetted in duplicates for each of the following conditions: in absence of titanium nanoparticles or Ti = 0 ppm, also used as control, and in presence of four different nanoparticle concentrations, which were 25 ppm, 50 ppm, 100 ppm and 200 ppm.

	<b>M0</b>		<b>M1</b>		<b>M2</b>	
<b>Concentration of Ti NPs</b>	0 ppm	0 ppm	0 ppm	0 ppm	0 ppm	0 ppm
	25 ppm	25 ppm	25 ppm	25 ppm	25 ppm	25 ppm
	50 ppm	50 ppm	50 ppm	50 ppm	50 ppm	50 ppm
	100 ppm	100 ppm	100 ppm	100 ppm	100 ppm	100 ppm
	200 ppm	200 ppm	200 ppm	200 ppm	200 ppm	200 ppm

Alamar Blue was added after 24 hours or 6 days at 1/10<sup>th</sup> of final volume in a well, followed by 3 hour incubation at 37°C and protected from light.

20 ul of Alamar Blue® reagent was added into each well, which already contained 180 ul of cells in the medium solution.

Immediately after 3 hours, the absorbance values in each well were detected by Tecan after selecting the correct protocol template called (Alamar Blue® Test)e and choosing appropriate settings for the plate type (number of wells, and the plate material).

## **2.6.5 Preparation of biomaterials for cell culture**

### *2.6.5.1 Preparation of titanium disks*

Medical grade polished titanium discs of 13.7x2 mm size were provided by our collaborators from Protip Medical in the frames of EU FP7 IMMODGEL project. The discs were autoclaved at 121°C for 20 min at 18 psi.

### *2.6 5.2 Preparation of TiO<sub>2</sub> nanoparticles*

TiO<sub>2</sub> nanoparticles of 15 nm size were purchased from NanoAmor Europe. The properties of the TiO<sub>2</sub> nanoparticles are described in the table below:

**Table 9. Characteristics of purchased Ti NPs.**

Formula and Mineral state	TiO <sub>2</sub> (rutile)
Atomic number	22
Molecular Weight	79.87 g/mol
Composition	15%wt of TiO <sub>2</sub> (rutile) and 85 wt% water
Average Particle size	15 nm
Form and Appearance	Dispersion state / a transparent white liquid
Company	NanoAmor Europe.

The TiO<sub>2</sub> nanoparticles were sterilized via UV. The stock solution was initially diluted to 1:4 in DPBS in one of the wells in a 6 well plate, followed by transferring 200 ul of the solution from the corresponding dilution to another well of the same plate containing 1800 ul of 5 mM glucose (NG) media to make the final dilution (1:40) for performing UV sterilization.

Table 10 describes dilution calculations from stock solution with nanoparticles required for preparation of different TiO<sub>2</sub> NPs concentrations used in stimulation of macrophages.

**Table 10. Dilution guide of Ti NPs concentrations.**

Target Concentrations in the Wells	Final dilution factor	Required Amount of (1:40) diluted stock solution containing nanoparticles after UV sterilization			
		96 well-plate (200ul/well)	24 well-plate (1.5ml/well)	12-well plate (2.0ml/well)	6-well plate (3.0ml/well)
0,0025% = 25ppm	1 : 6000	1.3 ul	10 ul	13 ul	20 ul
0,0050% =50ppm	1: 3000	2.6 ul	20 ul	26 ul	40 ul
0,0100% = 100ppm	1 :1500	5.2 ul	40 ul	52 ul	80 ul

## 2.7 Immunological methods

### 2.7.1 Antibodies

**Table 11. Primary antibodies.**

Antibody	Species	Company	Catalog number	Concentration in stock	Application	Dilution
Chitotriosidase	rabbit	ThermoFisher	PA582395	0.3 mg/ml	IF	1:40
TGN46	mouse	Serotec	MCA4333Z	0.5 mg/ml	IF	1:100
Rabbit IgG	rabbit	Millipore	PP64B	0.5 mg/ml	IF	1:24
Mouse IgG2b	mouse	Pharmingen	557351	0.5 mg/ml	IF	1:100

**Table 12. Secondary antibodies and labelling agents.**

Antibody/labelling agent	Species	Company	Catalog number	Concentration in stock	Application	Dilution
anti-Mouse IgG (H+L)-Alexa Fluor 488	donkey	Dianova	715-545-151	1.5 mg/ml	IF	1:400
anti-Rabbit IgG (H+L)-Cy3	donkey	Dianova	711-161-152	1.5 mg/ml	IF	1:400
DAPI	N/A	Roche	10236276001	2 mg/ml	IF	1:1,000
DRAQ5	N/A	Cell Signaling	4084s	5mM	IF	1:1,000

## 2.7.2 Indirect immunofluorescence and confocal microscopy

### 2.7.2.1 Preparation of cells for immunofluorescence

The cells used for immunofluorescence were seeded into 24-well plates on top of the round coverslips. (1.5 million cells per well). were cultured in presence or absence of titanium nanoparticles for 6 days. On day 6 the cells were PFA fixed and either stored or subjected to immunofluorescence staining.

### 2.7.2.2 Paraformaldehyde (PFA) fixation of cells

- 1) 1.4 ml of cell medium was aspirated away from each well.
- 2) 1.5 ml of 2% PFA was pipetted into each well and the samples were incubated for 10 min at RT.
- 3) The PFA was aspirated away. 1 ml of 0.5% Triton-X 100 in 1xPBS was added to each well followed by 10 min incubation at RT.
- 4) The Triton-X 100 solution was aspirated away followed by addition of 1 ml of 4% PFA and incubation for 10 min at RT.
- 5) The samples were washed 4 times with 1xPBS (1 short wash for 30 sec and 3 long washes for 10 min, on a shaker, at RT).

### 2.7.2.3 Staining of cells

- 1) The content of the 24 well plate was aspirated and the samples were washed with 1 ml of 0.1% Tween 20 in 1xPBS for 30 s.
- 2) 200 ul of 3% BSA in 1xPBS and 60 ul of Fc blocker was added to each sample and the samples were incubated for 1 hour.
- 3) After 1 hour the blocking solution was aspirated away and the samples were washed with 1 ml of 0.1% Tween 20 in 1xPBS for 30 s.
- 4) The primary antibody was prepared in advance by diluting it to the appropriate concentration (table 15) with 1% BSA in 1xPBS. 200  $\mu$ l of the primary antibody was added to each well followed by 1.5 hour incubation at RT.
- 5) The samples were washed 3 times with 1 ml of 1xPBS for 5 min at RT on a shaker followed by a single wash with 1 ml of 0.1% Tween 20 in 1xPBS for 30s.
- 6) The secondary antibody was prepared in advance by diluting it to the appropriate concentration (table 16) with 1% BSA in 1xPBS. 400 ul of the secondary antibody was added to each well followed by 45 min incubation at RT.
- 7) The samples were washed 4 times with 1 ml of 1xPBS for 5 min at RT on a shaker.
- 8) The slides were washed with 70% ethanol, air dried and labeled with a pencil.
- 9) 1 drop of DAKO aqueous fluorescent mounting media was pipetted onto the slides.
- 10) The cover slips were taken out of the well with a scalpel and small tweezers, flipped over (cells should be on bottom side of the cover slip) and mounted directly on the slide.
- 11) The slides were dried and stored in the dark at 4°C.

### 2.7.2.4 Confocal laser scanning microscopy (CLSM)

CLSM was performed using a Leica laser scanning spectral confocal microscope, model DM IRE2, equipped with an HCX PL Apo 63 ×/1.32 numeric aperture oil objective (Leica Microsystems, Wetzlar, Germany). Excitation was with an argon laser emitting at 488 nm, a krypton laser emitting at 568 nm, and a helium/neon laser emitting at 633 nm. Images were acquired using a TCS SP2 scanner and Leica Confocal software, version 2.5 (both from Leica Microsystems). All 2-color images were acquired using a sequential scan mode.

### 2.7.3 Flow cytometry

#### *Mitochondrial ROS detection by FACS*

Cells were cultured at concentration 1 million cells/ml for 6 days in ultra-low attachment 24 well plates.

- 1) The cells were kept on ice for 15 min and the supernatants were collected into FACS tube.
- 2) 200 ul of DPBS was added to the adherent cells, then the plate went back on ice for 15 more min (it was verified under microscope until the cells come off).
- 3) ROS staining solution was prepared in the dark (1ml –*enough for 10 measurements*) as instructed below:
  - a. 1 uL DCF working solution
  - b. 10 uL MitoTracker working solution
  - c. 100 uL MitoSOX working solution
  - d. 900 uL Culture medium
- 4) The wells with cells were washed with 500 ul of DPBS and transferred the DPBS into the same FACS tube.
- 5) Controls were prepared :
  - i. Negative control (stained cells)
  - ii. Negative control (unstained cells)
  - iii. Positive control with H<sub>2</sub>O<sub>2</sub>(stained cells)
- 6) The FACS tubes were spun at 420 g for 4 min. The supernatants were discarded.
- 7) 100 uL of ROS staining solution was added per FACS tube and vortexed briefly except negative unstained control. 100 uL DPBS was added to unstained control.
- 8) The cells were incubated in 37°C for 15 min in dark conditions.
- 9) Fluorescence was measured using FACS CANTO immediately. DCF staining was recorded using FITC channel to measure intracellular ROS; MitoTracker in APC channel for mitochondrial membrane potential; and MitoSOX in PE channel for mitochondrial ROS.

## 2.8 Protein-related techniques

### 2.8.1 Enzyme-linked Immunosorbent Assay (ELISA)

*Protocol for ELISA kits from R&D systems.*

All procedures were performed at RT unless stated otherwise. ELISA was performed according to the manufacturer's instructions.

- 1) The Capture Antibody was prepared without carrier protein at least 14 hours prior to beginning of the assay.
  - a. The dilution of the Capture Antibody was made in PBS to make a working concentration listed in the manufacturer instruction.
  - b. A micro plate for ELISA (a 96-well plate) was coated with 100 ul of the antibody solution above, sealed, and incubated until the beginning of the experiment in dark conditions protected away from the light.
- 2) After the incubation the micro-plate with capture antibody was washed 4 times in 350 ul wash buffer (for each well) with HydroFlex ELISA microplate washer.
- 3) 100 ul of fresh Reagent Diluent (1% BSA in PBS), which was prepared on the same day of the experiment or the day before was used to coat the plate in order to block unspecific binding sites, followed by 1 hour incubation period.
- 4) After 1 hour the Reagent Diluent in the wells was replaced with a fresh 100 ul reagent diluent for single washing. 100 ul of reagent diluent was pipetted into the first two rows of the plate later used for diluting the standards.
- 5) 100 µl of sample (supernatant) or 100 µl of standards diluted in Reagent Diluent was added per well. The plate was sealed and incubated for 2 hours in dark conditions protected away from the light.
- 6) The dilution of Detection Antibody was made in Reagent Diluent to attain the concentration listed in the manufacturer instruction (check the table below).
- 7) After 2 hours of incubation the plate was washed 4 times in 350 ul wash buffer with HydroFlex ELISA microplate washer.
- 8) 100 µl of Detection Antibodies was used to coat each well in the plate, sealed and incubated for 2 hours away from the light.
- 9) The dilution of Streptavidin-HRP was made in Reagent Diluent to attain the concentration listed in the manufacturer instruction (check the table below)
- 10) After the 2 hour incubation the plate containing detection antibody was washed 4 times in 350ul wash buffer with HydroFlex ELISA microplate washer.
- 11) 100 µl of Streptavidin-HRP was used to coat each well and incubated for 20 min in the dark.
- 12) After the 20 min the plate containing Streptavidin-HRP was washed 4 times in 350 ul wash buffer with HydroFlex ELISA microplate washer.
- 13) During the washing period a Substrate Solution was prepared. (Preparation of Substrate Solution was done by mixing 5 ml of Reagent A with 5 ml of Reagent B)
- 14) 100 µl of Substrate Solution was used to coat each well and incubated for 20 minutes in the dark.
- 15) After 20 minutes the reaction was terminated with 50 µl of Stop Solution (2N H<sub>2</sub>SO<sub>4</sub>), followed by detection of the absorbance at 450 nm on a Tecan Infinite 200 PRO reader.

In some cases of biomarkers tested the new dilution factors had to be established separately for M0, M1 and M2.



Required dilutions of ELISA reagents and supernatants:

**Table 13. YKL-40 (CHIT3L1) – dilutions of supernatants.**

Final Concentrations in the Wells	Dilutions
Supernatant of M0 1:50	980ul of 1%BSA in PBS with 20ul Supernatant
Supernatant of M1 1:1000	999ul of 1%BSA in PBS with 1ul Supernatant
Supernatant of M2 1:20	950ul of 1%BSA in PBS with 50ul Supernatant
Supernatant of M2/Ti 1:100	990ul of 1%BSA in PBS with 10ul Supernatant

**Table 14. YKL-40 (CHIT3L1) – reagent dilutions.**

Final Concentrations in the Wells	Dilutions
Capture Ab 1:180	10000ul PBS with 55.6ul Capture Ab
Standard 1:65	969ul 1%BSA in PBS with 30.8ul Standard
Detection 1:180	10000ul 1%BSA in PBS with 55.6ul Detection Ab
Streptavidin 1:200	10000ul 1%BSA in PBS with 50ul Streptavidin

**Table 15. CCL18 – reagent dilutions.**

Final Concentrations in the Wells	Dilutions
Capture Ab 1:180	10000ul of PBS with 55.6 ul Capture Ab
Standard 1:75	986ul 1%BSA in PBS with 13.3 ul Standard
Detection 1:180	10000ul 1%BSA in PBS with 55.6 ul Detection Ab
Streptavidin 1:200	10000ul 1%BSA in PBS with 50 ul Streptavidin

**Table 16. CCL18 – dilutions of supernatants.**

Final Concentrations in the Wells	Dilutions
Supernatant of M2 1:1000	999ul of 1%BSA in PBS with 1ul Supernatant

**Table 17. CCL18 – TNF- $\alpha$  – reagent dilutions.**

<i>Final Concentrations in the Wells</i>	Dilutions
<i>Capture Ab</i> 1:120	10000ul of PBS with 83.3 ul Capture Ab
<i>Standard</i> 1:135	927 ul 1%BSA in PBS with 7.4 ul Standard
<i>Detection</i> 1:60	10000ul 1%BSA in PBS with 167 ul Detection Ab
<i>Streptavidin</i> 1:200	10000ul 1%BSA in PBS with 50 ul Streptavidin

Estimating the concentration of the secretion protein of interest in a sample:

To determine precise concentration of the protein in a the sample, the system of numerical reference was attained by construction of a standard curve, for which the absorbance values of each standard detected by Tecan Infinite 200 PRO was plotted against the concentration.

### 2.8.2 Chitotriosidase activity assay

The Chit activity was detected in macrophage culture supernatants using Fluorimetric Chitinase Assay Kit from Sigma-Aldrich (St. Luis MO, USA). Chit activity was measured in black microplates from R&D systems by incubating 10ul of supernatents together with 90 ul of artificial substrate (4-Methylumbelliferyl N-acetyl- $\beta$ -D-glucosaminide) – a substrate suitable for exochitinase activity detection ( $\beta$ -N-acetylglucosaminidase activity or chitotriosidase activity). The reaction was stopped with a stop solution (Sodium Carbonate) provided by the kit and the fluorescence was measured at an excitation wavelength of 360 nm and an emission wavelength of 450 nm.

## 2.9 Statistical analysis

### 2.9.1 Statistical analysis of ELISA

- 1) The standard curve was fitted into a polynomial equation (describing the curve with  $R^2$  value not lower than 0.85), which was used in calculating the protein concentration in each sample of a well.
- 2) To estimate the original concentration of secreted protein found in each supernatant sample the values calculated using polynomial function of the standard curve were further multiplied by the corresponding dilution factor. The significance of difference between groups of experimental data in ELISA using Wilcoxon matched-pairs rank test or Student's paired t-test. A P-value less than 0.05 was considered statistically significant. The statistical analysis was performed in Excel and GraphPad.

### 2.9.2 Statistical analysis of RT-PCR

- 1) Preliminary statistical analysis to determine the error in the individual responses from target and reference measurements were performed by Lightcycler480 software.
- 2) The significance of difference between groups of experimental data RT-qPCR analysis was determined using Wilcoxon matched-pairs rank test or Student's paired t-test. A P-value less than 0.05 was considered statistically significant. The statistical analysis was performed in GraphPad Prism and Excel.

### 2.9.3 Statistics and bioinformatics for Affymetrix

- 1) A Custom CDF Version 21 with ENTREZ based gene definitions was used to annotate the arrays (Dai et. al, 2005). The raw fluorescence intensity values were normalized applying quantile normalization and RMA background correction. OneWay-ANOVA was performed to identify differential expressed genes using a commercial software package SAS JMP10 Genomics, version 15, from SAS (SAS Institute, Cary, NC, USA). A false positive rate of  $\alpha=0.05$  with FDR correction was taken as the level of significance.
- 2) Gene Set Enrichment Analysis (GSEA) was used to determine whether defined lists (or sets) of genes exhibit a statistically significant bias in their distribution within a ranked gene list using the fgsea package (Sergushichev, 2016), available and run with the R programming language running under the open-source computer software R v3.4.0 (R Core Team, 2017) and RStudio v1.1.456.

Pathways belonging to various cell functions such as cell cycle or apoptosis were obtained from public external databases (KEGG, <http://www.genome.jp/kegg>).

### 3 RESULTS

#### 3.1 Experimental design

CD14<sup>+</sup> primary human monocytes isolated from buffy coats were cultivated in serum-free medium (SFM). The SFM medium was produced on custom request as glucose free and supplemented with 5 mM or 25 mM glucose prior to use. SFM medium was supplemented with  $10^{-8}$  M dexamethasone and 5ng/ml M-CSF. Three prototypes of macrophage subpopulations were generated subsequently: M0 (no cytokine stimulation), M1 (stimulated with IFN $\gamma$ ) and M2 (stimulated with IL-4). Titanium disks were added to the cell culture prior to seeding the monocytes. The size of titanium discs was optimized (13.7 x 2 mm) to cover maximum surface in a well of a 24-well plate. Ti NPs were added to the cell culture media after seeding and stimulating the monocytes.  $3 \times 10^6$  cells per each well ( $2 \times 10^6$  cells/ml) were seeded in each well. The general design for the experiments with polished titanium disks and Ti NPs is illustrated by Figure 5.

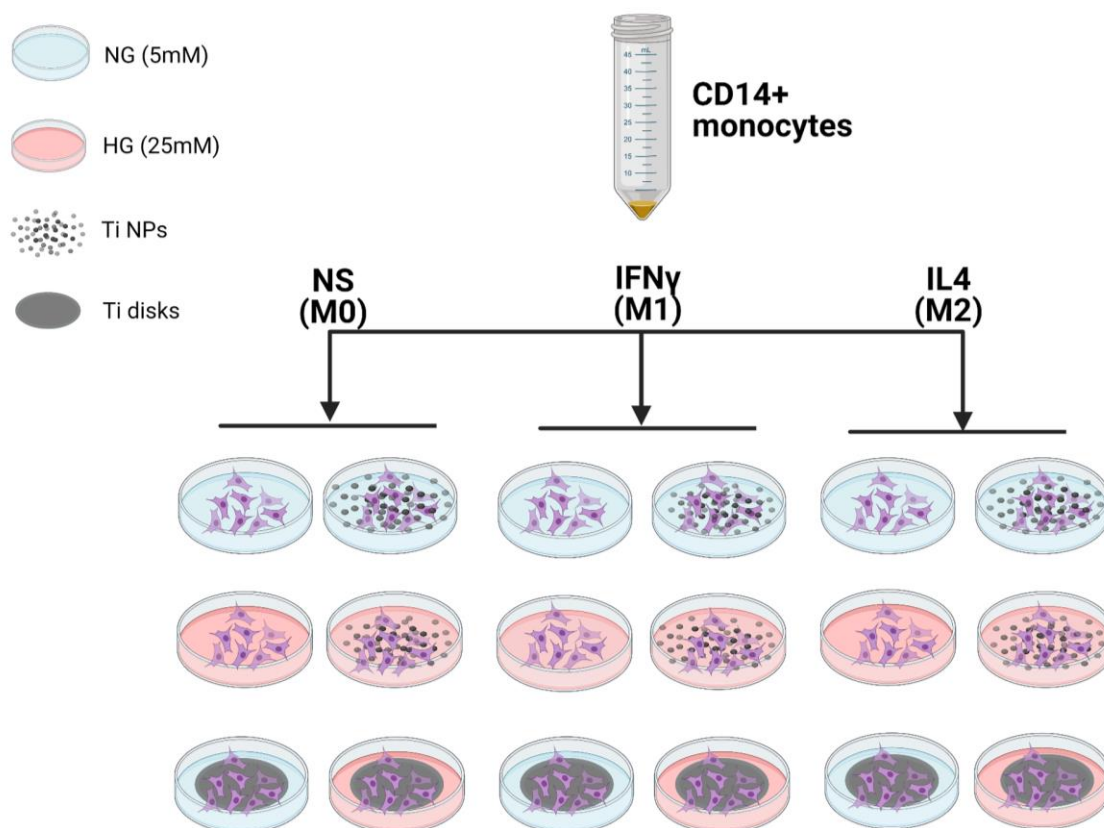
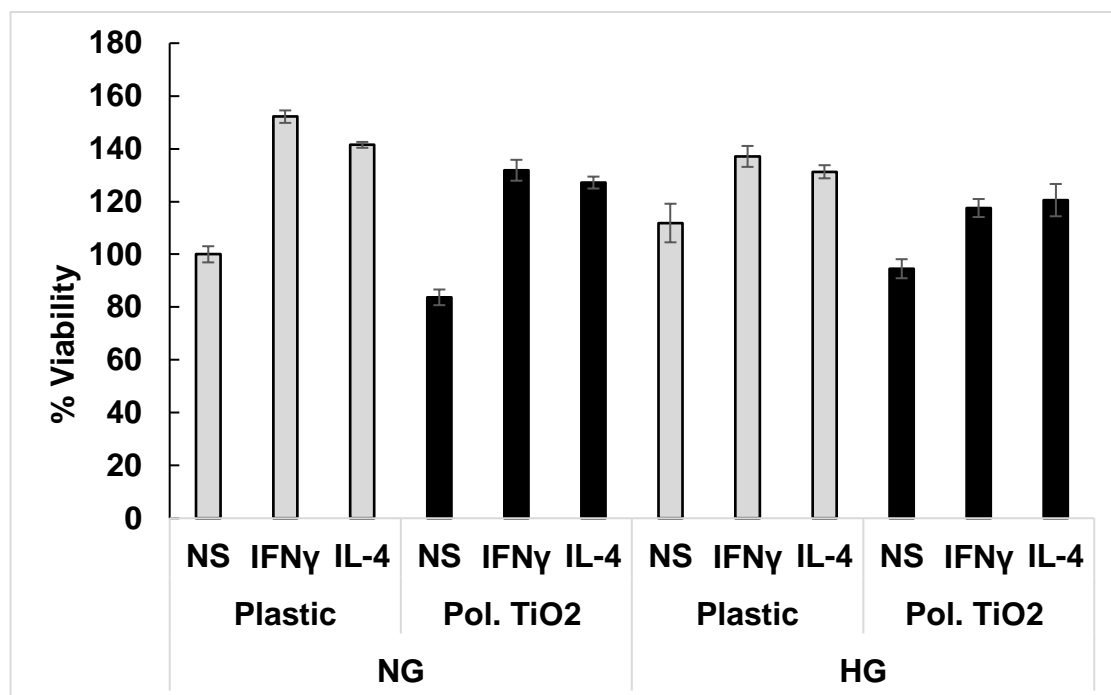


**Figure 5. Schematic representation of a model system for the experiment with polished titanium disks and titanium nanoparticles** (created with Biorender.com). Human peripheral blood monocytes were isolated from buffy coats by magnetic cell sorting using CD14 beads. M (IFN $\gamma$ ) and M (IL-4) macrophages have been generated by stimulating human monocytes with IFN $\gamma$  and IL-4, correspondingly, for 6 days in serum-free medium, supplemented with 5mM or 25mM glucose.

## 3.2 Analysis of titanium surfaces and nanoparticles on macrophage viability

### 3.2.1 Titanium disks do not affect macrophage viability

Metal implants often trigger adverse immune responses as a consequence of metal toxicity. Titanium materials are amongst most biocompatible materials since they are resistant to corrosion<sup>8,168</sup>. The effect of titanium surfaces on cell viability (measured by Alamar Blue test) was evaluated for M0, M1 and M2 cultured for 6 days in normal glucose (NG) and hyperglycemic conditions (HG); and in combination with or without Ti disks. Alamar Blue reagent was used for the viability assessment, which positively correlates with the level of fluorescent intensity (FI) measured at 590nm. The viability was normalized to unstimulated (M0) control as 100% (demonstrated by y-axis).



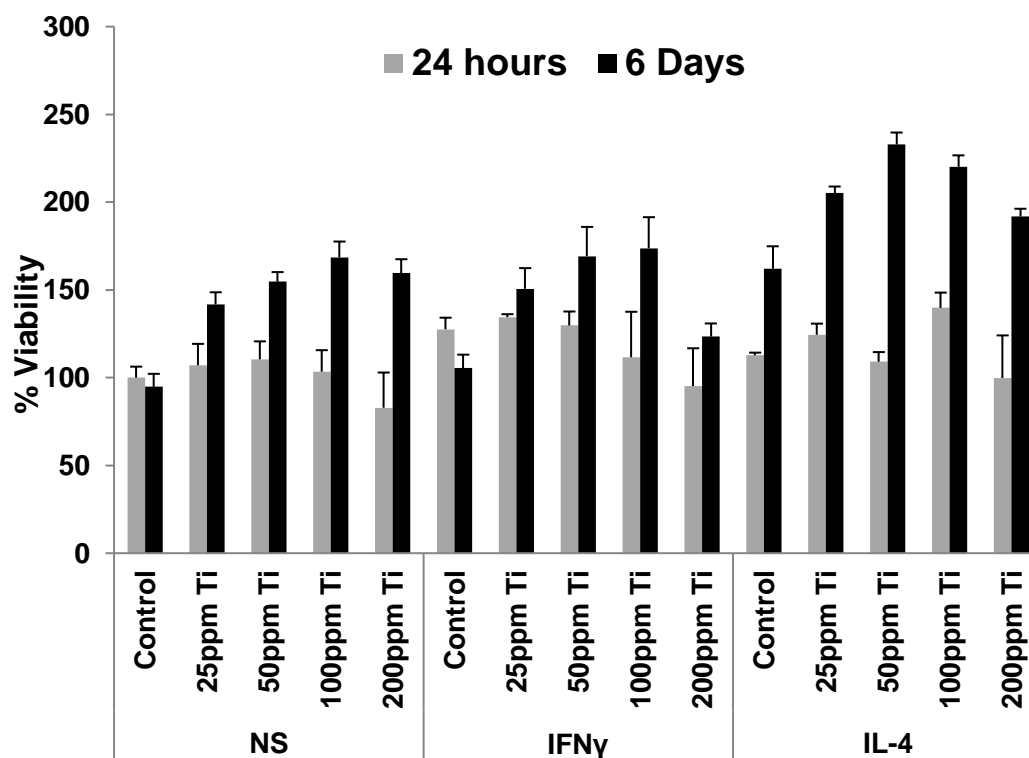
**Figure 6. Cell viability test performed with Alamar Blue for unstimulated (M0), IFN $\gamma$ -stimulated (M1) and IL-4-stimulated (M2) macrophages cultured on plastic or on the surface of polished titanium disks.** Each bar represents the mean value of % viability normalized to NS (control) on plastic as 100%, which was calculated from fluorescence intensity (FI) measured at 590nm. The mean value was obtained from 4 individual donors. The error bars are represented by SEM. Cell viability plotted for NS (M0), IFN $\gamma$  (M1) and IL-4 (M2) cultured on plastic or the surface of polished titanium disks, in normal glucose (NG) or high glucose (HG) conditions.

Figure 6 demonstrates that neither hyperglycemia nor titanium have any significant effect on viability of differentially activated macrophages. The viability signal of M0 macrophages in NG conditions cultured on plastic without titanium disks was taken as 100%. In NG the viability of M1 cultured on plastic was (152±2.37)% and M2 was (141±1.12)%. In presence of titanium disks, M0 in NG displayed the lowest viability signal, which was detected to be (85.7±2.97)%. M1 in NG cultured in presence of titanium disks was (132±3.96)% and M2 was (127±2.25)%. In HG, M0 on plastic displayed slightly higher viability, (111±7.31)%, than M0 in NG. In HG M1 on plastic was (137±3.97)% and M2 was (131±2.48)%. In presence of titanium disks and in HG

the viability for M0 was (94.5±3.61)%, for M1 was (117±3.41)% and for M2 was (120±6.11)%.

In total, there were no significant changes in cell viability of M0, M1 and M2 during the comparison of NG and HG environments. Also no significant changes were observed in macrophage responses comparing cells cultured on plastic with the cells cultured in presence of titanium disks. As expected, stimulation of macrophages with IFN $\gamma$  or IL-4 increased viability of macrophages in all the conditions tested.

### 3.2.2 Ti NPs at moderate concentrations do not affect macrophage viability



**Figure 7. Effect of increase in Ti NPs concentration on macrophage viability assessed with Alamar Blue test.** The test is performed for (M0) unstimulated (NS), (M1) IFN $\gamma$ -stimulated and (M2) IL-4-stimulated macrophages each cultured in absence of Ti NPs(control) and increasing concentration of Ti NPs (25, 50, 100 and 200) parts per million (ppm), which is represented by x-axis. The viability was measured after 24 hours and after 6 days the cells were in culture. Each bar represents the mean value of % viability normalized to M0 (24 hours) as 100% calculated from FI at 580nm. The mean values were obtained from 4 individual donors for 6 day experiment and 2 individual donors for 24 hours. The error bars are represented by SEM.

Macrophages have high tolerance for foreign materials and in comparison to other cells can handle higher concentrations of toxic substances<sup>169,170</sup>. It was essential to choose optimal concentration of the Ti NPs and determine its toxicity effects specifically in macrophages used in our model. To assess the effect of different nanoparticle concentrations on cell viability, Alamar Blue test was performed for M0, M1 and M2 macrophages cultured in absence of Ti NPs and with (0.0025, 0.0050, 0.0100 and 0.0200) wt% of Ti NP concentration, also represented by (25, 50, 100, 200)ppm (Figure 7). Alamar Blue test does not only represent cell viability, but also metabolic activity. The Alamar Blue signal was measured after 24 hours and after 6 days, to assess viabilities of, both, monocytes and differentially activated

macrophages. Ti NPs at all concentrations promoted increase in metabolic activity of M0, M1 and M2 macrophages, with one exception for M1 and 200 ppm Ti NPs. The highest viability signal amongst M0 macrophages was (168±9.00)%, which was detected after stimulation with 100 ppm Ti NPs; for M1 was (173±17.7)% also detected after stimulation with 100 ppm Ti NPs and for M2 was (232±6.80)% detected upon stimulation with 50 ppm Ti NPs.

In total, there was no difference in viability measured after 24 hours and 6 days in cells unexposed to Ti NPs and this viability was lower in comparison to cells stimulated with Ti NPs. In conclusion, Ti NPs induce higher metabolic activity in differentiated macrophages but not in monocytes. In all macrophage polarization states (M0, M1 and M2), 200 ppm of Ti NPs concentration showed decline in fluorescent intensity signal, however in comparison to M0 it was not significant. It was concluded that in fully mature macrophages, Ti NPs at 25, 50 and 100 ppm concentrations increase metabolic activity, however, at 200 ppm Ti NPs the metabolic activity start to decline in comparison to other concentrations. At concentration 100 ppm of Ti NPs, M0 and M1 macrophages were found to be most metabolically active and viable.

### **3.3 Effect of Ti NPs on gene expression of CHIT1, CHI3L1 and CCL18 in macrophages under normal glucose conditions**

#### **3.3.1 Ti NPs upregulate expression of CHIT1 and CHI3L1**

Chitotriosidase (CHIT1) and YKL-40(CHI3L1) are Glyco\_18 domain containing proteins are lectins, which are predominantly expressed and secreted by human monocyte-derived macrophages and are associated with macrophage activation<sup>171–173</sup>. CHI3L1 and CHIT1 are known pro-inflammatory factors and have been characterized as biomarkers of multiple chronic inflammatory conditions<sup>174–181</sup>. The mRNA expression levels of CHIT1 and CHI3L1 were measured by RT-PCR in monocytes after 6 days of monocyte differentiation to M0, M1 and M2. The effects were analyzed for 5 donors in M0 and M2 and 11 donors in M1. The expression of CHIT1 and CHI3L1 in monocytes (day 0) was not detected (Figure 8A, B). Figure 8A illustrates that there is a significant upregulation of YKL40 (CHI3L1) expression by Ti NPs in M0 and M2. In M1 macrophages Ti NPs slightly upregulate YKL40 (CHI3L1) expression, however, the differences do not reach the statistical significance.

In all macrophage subtypes (M0, M1 and M2) Ti NPs promoted upregulation in CHIT1 expression (Figure 8B). Stimulation of M0 macrophages with Ti NPs resulted in upregulation of CHIT1 expression by the average of 50 times. Stimulation of M1 macrophages with Ti NPs resulted in upregulation of CHIT1 expression by the average of 5.4 times. Stimulation of M2 macrophages with Ti NPs resulted in upregulation of CHIT1 expression by the average of 1.7 times. The effects were analyzed for 5 donors in M0, M1 and M2. In summary, Ti NPs promoted upregulation of CHIT1 expression in all macrophage subtypes and CHI3L1 in M0 and M2 macrophages.

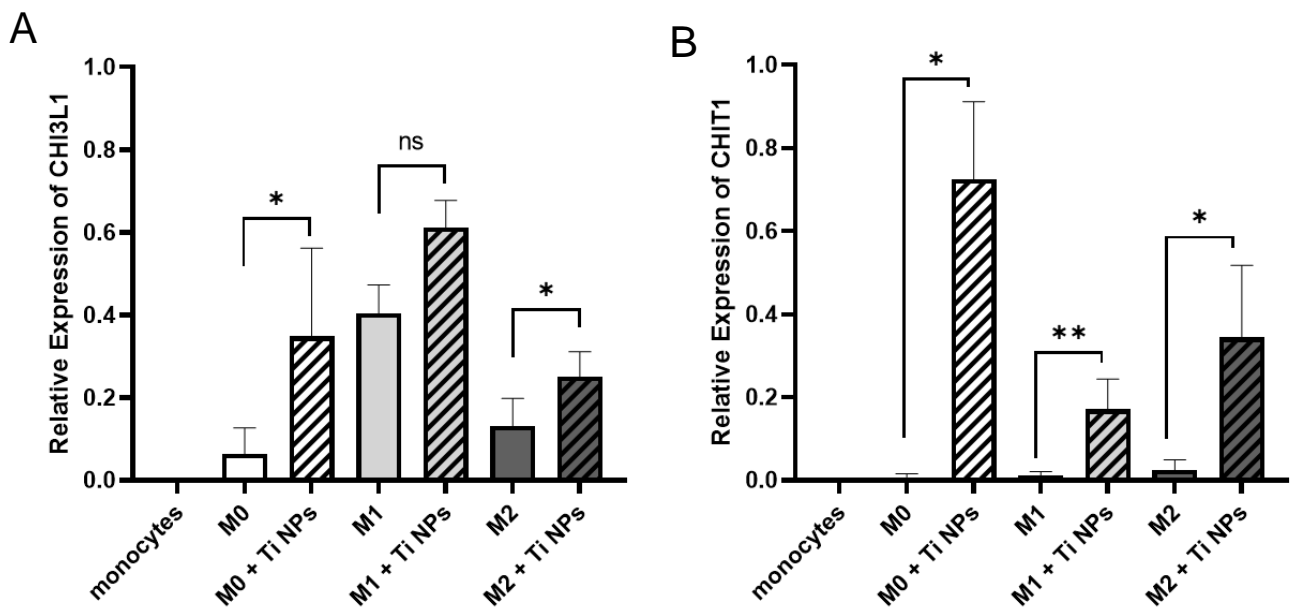


**Figure 8. Effect of titanium nanoparticles on CHIT1 and CHI3L1 expression in human macrophages.** Levels of gene expression were detected with RT-PCR for macrophages cultured for 6 days in presence or absence of 100ppm Ti NPs concentration. **A.** The expression of CHI3L1 in M0 (unstimulated), M1 (IFN $\gamma$ -stimulated) and M2 (IL4-stimulated) macrophages. **B.** The expression of CHIT1 in M0 (unstimulated), M1 (IFN $\gamma$ -stimulated) and for M2 (IL4-stimulated) macrophages. Each bar represents the mean value of expression from 5-10 individual donors, obtained after normalization of original expression to a maximum expression value as 1 in each donor. Statistical analysis was performed using paired two-tailed t test. \*\* $p < 0,01$  and \* $p < 0,05$ .

### 3.3.2 Ti NPs suppress CCL18 expression in dose-dependent manner

C-C motif chemokine 18 (CCL18) is strongly upregulated by IL-4 and is a key cytokine biomarker for M2<sup>93</sup>. Previously, in our laboratory it was found that all types of titanium material (polished Ti, porous Ti, micro Ti particles and Ti NPs) have an inhibitory effect on production of CCL18 in M2 macrophages in presence of dexamethasone; the strongest inhibitory effect was generated by Ti NPs (Gudima, 2017)<sup>182</sup>. In this study the effect of 25 ppm and 100 ppm Ti NPs on the mRNA expression levels of CCL18 were measured by RT-PCR in M2 macrophages cultured for 6 days in normal glucose conditions (Figure 9). Ti NPs at concentration 25 ppm suppressed CCL18 expression by the average of 10 times, with a maximum effect of 21 fold suppression. Ti NPs at concentration 100 ppm suppressed CCL18 expression by the average of 580 times, with a maximum suppression effect of 1297 fold change.



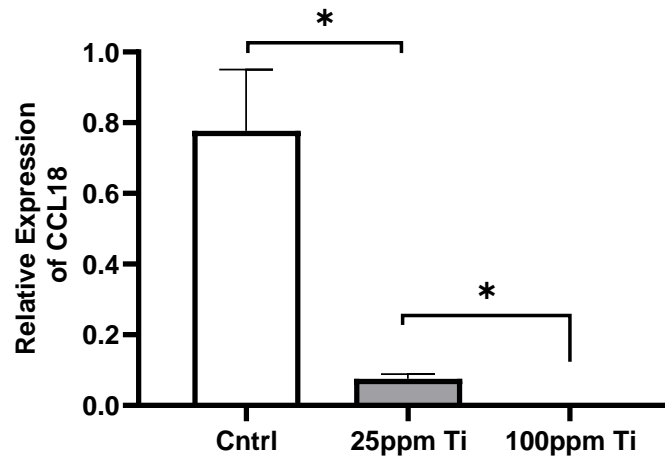


**Figure 9. Effect of titanium nanoparticles on CCL18 expression in human macrophages.** Levels of gene expression were detected with RT-PCR for M2 macrophages cultured for 6 days in absence or in presence of 25ppm and 100ppm Ti NPs concentration. Each bar represents the mean value of secretion from 6 individual donors. The error bars are represented by SEM. Statistical analysis was performed using paired two-tailed t test. \* $p < 0,05$

### 3.4 Effect of Ti NPs on macrophage secretion of TNF- $\alpha$ , CHI3L1, CCL18 and CHIT1 in normal glucose

#### 3.4.1 Ti NPs do not have an effect on TNF- $\alpha$ secretion

TNF- $\alpha$  is an inflammatory cytokine secreted by macrophages, and its production is stimulated by IFN $\gamma$ <sup>91</sup>. Elevated concentrations of TNF- $\alpha$  are detected upon exposure to Ti NPs<sup>183,184</sup>. Using ELISA, differences in the secretion levels of TNF- $\alpha$  in human macrophages exposed to Ti NPs were assessed. Figure 10 illustrates the effect of 25 ppm and 100 ppm Ti NPs concentration on TNF- $\alpha$  secretion measured in the supernatants obtained after 6 hours monocytes culturing. In M1 macrophages, the secretion levels of TNF- $\alpha$  were the highest (average 52 pg/ml), which was 1.77 times higher than the average secretion in M0 macrophages (29 pg/ml) and 1.83 times higher than in M2 (29 pg/ml). Both concentrations of Ti NPs (25 ppm and 100 ppm) did not generate any effect on TNF- $\alpha$  secretion in the cells cultured for 6 hours.

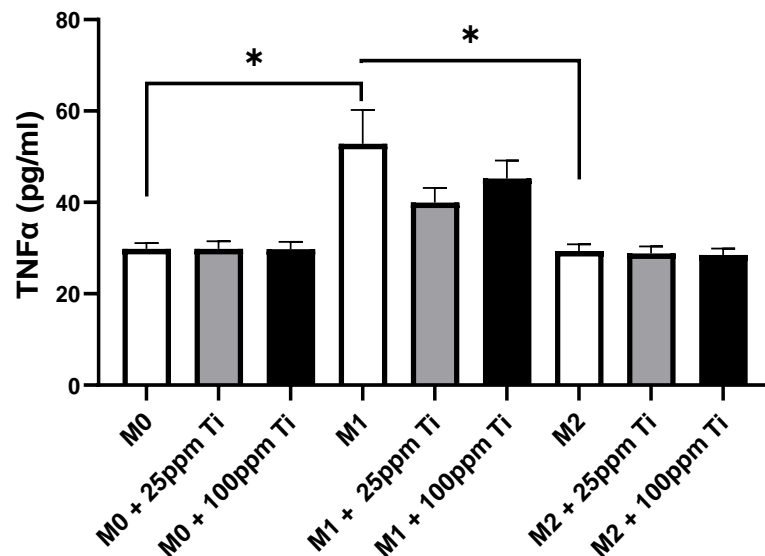


**Figure 10. Effect of titanium nanoparticles on TNF- $\alpha$  secretion in human macrophages.** Secretion levels were detected with ELISA in supernatants collected from M0, M1 and M2 macrophages cultured for 6 hours in presence or absence of 25ppm and 100ppm Ti NPs in NG. Each bar represents the mean value of secretion from 7 individual donors. The error bars are represented by SEM. Statistical analysis was performed using paired two-tailed t test. \* $p < 0.05$

#### 3.4.2 Ti NPs potentiate CHI3L1 secretion in dose-dependent manner

Next, the effect of Ti NPs on CHI3L1 secretion was examined. Figure 11 illustrates the effect of increasing concentration of Ti NPs on CHI3L1 secretion in M0, M1 and M2 macrophages cultured for 6 days.

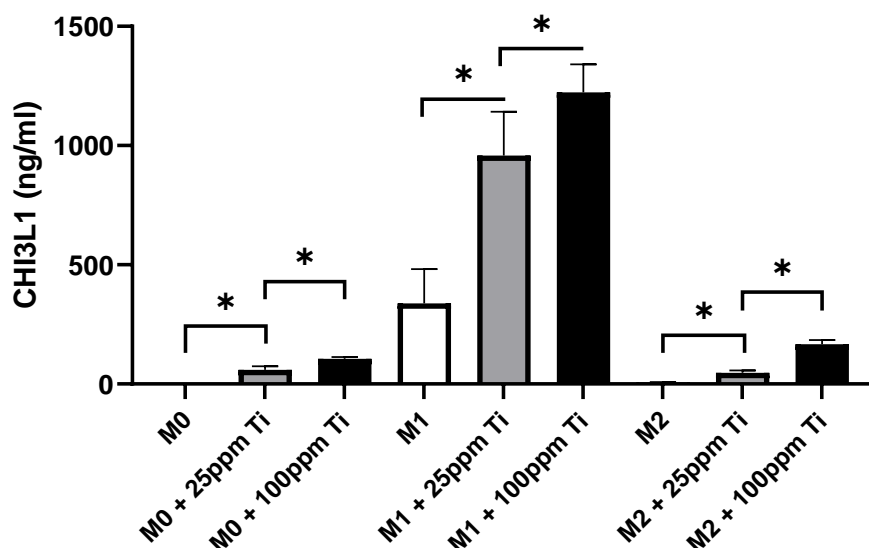


**Figure 11. Effect of titanium nanoparticles on CHI3L1 secretion by human macrophages.** Secretion levels were detected with ELISA in supernatants collected from M0, M1 and M2 macrophages cultured for 6 days in presence or absence of 25ppm and 100ppm Ti NPs in NG. Each bar represents the mean value of secretion from 6 individual donors. The error bars are represented by SEM. Statistical analysis was performed using paired two-tailed t test. \* $p < 0.05$ .

In M0 macrophages in absence of Ti NPs, the secretion levels of CHI3L1 were about 3.3 ng/ml. Stimulation of M0 with 25 ppm Ti NPs resulted in increased CHI3L1 secretion up to about 59 ng/ml, and 100 ppm Ti NPs resulted in increased CHI3L1 secretion to about 105 ng/ml. In M1 macrophages in absence of Ti NPs, the secretion levels of CHI3L1 were about 338 ng/ml, in presence of 25 ppm Ti NPs the levels increased up to 958 ng/ml and in presence of 100 ppm Ti NPs the levels were the highest (1222 ng/ml). In M2 macrophages in absence of Ti NPs, the secretion levels of CHI3L1 were about 7 ng/ml, in presence of 25 ppm Ti NPs the levels increased up to 46 ng/ml and in presence of 100 ppm Ti NPs the levels increased up to 167 ng/ml.

### 3.4.3 Ti NPs suppress CCL18 secretion in dose-dependent manner

The effect of Ti NPs on suppression of CCL18 secretion levels was assessed in supernatants collected from M2 macrophages cultured for 6 days (Figure 12). The average secretion of CCL18 from M2 cultured alone was 541 ng/ml. In presence of 25 ppm of Ti NPs, the average secretion of CCL18 was 317 ng/ml, which is by 1.71 times smaller than detected for M2 cultured in absence of Ti NPs. In presence of 100 ppm of Ti NPs, the secretion of CCL18 was significantly inhibited to the average of 20 ng/ml, which is by 15 times lower than in M2 cultured in presence of 25 ppm Ti NPs and by 26 times lower than in M2 cultured in absence of Ti NPs.

Similarly to the effect of Ti NPs on the expression of CCL18 gene (Figure 9), Ti NPs reduced secretion of CCL18. The reduction of secretion induced by 100 ppm Ti NPs was significantly greater than the reduction induced by 25 ppm Ti NPs. However, the magnitude of suppression in gene expression was significantly higher than the magnitude of reduction of CCL18 secretion. This can be explained by the fact that CCL18 can still be secreted while its gene expression is already switched off.

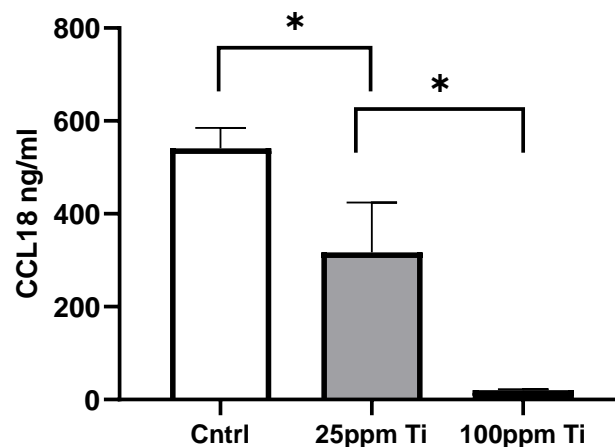


**Figure 12. Effect of titanium nanoparticles on CCL18 secretion in human macrophages.** Secretion levels were detected with ELISA in supernatants collected from M2 macrophages cultured for 6 days in presence or absence of 25ppm and 100ppm Ti NPs concentration in normoglycemic conditions. Each bar represents the mean value of secretion from 6 individual donors. The error bars are represented by SEM. Statistical analysis was performed using paired two-tailed t test. \* $p < 0,05$ .

### 3.4.4 Low concentrations of Ti NPs increase CHIT1 activity

CHIT1 possesses catalytic activity in contrast to CHI3L1. The mechanism of CHIT1 activity is a hydrolase function, which is responsible for digestion of chitin and defined by breakage of 1,4 beta glycosylic bonds, which connect all the monomers of sugar molecules into long chain heavy molecules<sup>171</sup>. Exochitinase activity was

assessed by using 4-Methylumbelliferyl N-acetyl- $\beta$ -D-glucosaminide as substrate of CHIT1 in M0, M1 and M2 macrophages in presence or in absence of Ti NPs at concentrations 25 ppm and 100 ppm (Figure 13). Interestingly, the lowest dose of Ti NPs (25 ppm) has shown a significant increase of CHIT1 activity by the average of 4.5 times in M0 macrophages, 1.5 times in M1 macrophages and 1.7 times in M2 macrophages. Surprisingly, the exochitinase activity measured from supernatants collected from macrophages cultured in presence of 100 ppm Ti NPs did not increase in all macrophage subtypes in comparison to controls. It may be that high concentration of Ti NPs blocked intracellular vesicular transport and commitment of CHIT1 for the secretory pathways.

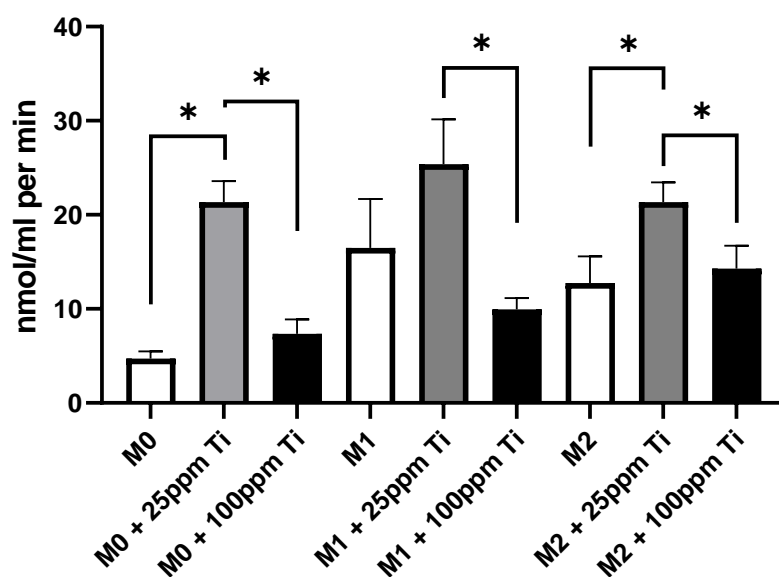


**Figure 13: Effect of titanium nanoparticles on CHIT1 exochitinase activity.** The enzymatic activity was measured in supernatants from M0, M1 and M2 macrophages collected from the cells cultured for 6 days in absence or presence of Ti NPs at concentrations 25ppm and 100ppm. Statistical analysis was performed using paired one-tailed and two-tailed t-test (\* $p < 0.05$ ).

### 3.5 Effect of hyperglycemia on Ti NPs-induced changes in TNF- $\alpha$ , CHI3L1, CHIT1 and CCL18 production

#### 3.5.1 Hyperglycemia and Ti NPs have no effect on TNF- $\alpha$ secretion

Increased production of TNF- $\alpha$  is found in diabetic patients<sup>185</sup>. Secretion levels of TNF- $\alpha$  are elevated in presence of high glucose in M0, M1 and M2 macrophages in the absence of dexamethasone<sup>49</sup>. Since glucocorticoids are always present in the tissues at low concentrations, 100 nM ( $10^{-8}$  M) dexamethasone was added in our model. The effect of hyperglycemic environment on the secretion of TNF- $\alpha$  in macrophages exposed to Ti NPs for 6 hours were assessed by ELISA. HG did not affect TNF- $\alpha$  secretion in all the conditions. HG did not affect TNF- $\alpha$  secretion in all the conditions. Ti NPs at both concentrations (25 ppm and 100 ppm), did not have stimulatory effect on secretion of TNF- $\alpha$  in the presence or absence of HG (Figure 14). This can potentially be explained by the fact that the experimental model used in this

study contained 100 nM dexamethasone, which contributed to the suppression of TNF- $\alpha$  production, because it is known that dexamethasone inhibits TNF- $\alpha$  secretion<sup>142</sup>.

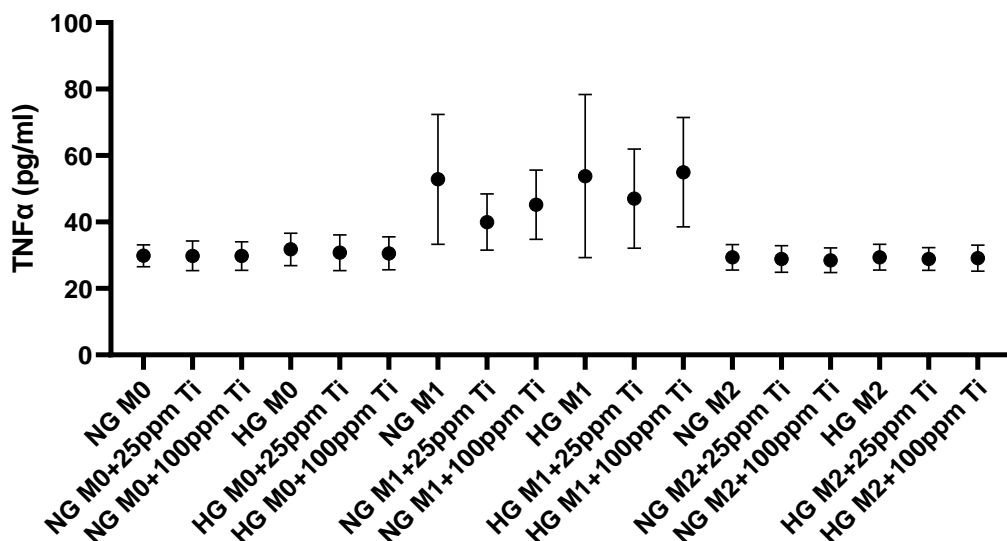


**Figure 14. Effect of hyperglycemia on TNF- $\alpha$  secretion in macrophages exposed to Ti NPs.** Secretion levels were detected with ELISA in supernatants collected from M0, M1 and M2 macrophages cultured for 6 hours in presence or absence of 25ppm and 100ppm Ti NPs in NG or HG. Each bar represents the mean value of secretion from 7 individual donors. The error bars are represented by SD.

### 3.5.2 Hyperglycemia cooperates with Ti NPs-induced expression of CHI3L1 in M1 and M2 macrophages

Increased serum levels of YKL40 (CHI3L1) are detected in patients with DM<sup>186</sup>. Elevated plasma levels of CHI3L1 can be used as marker of abnormal glucose tolerance in women with polycystic ovary syndrome<sup>187</sup>. However, in diabetic pregnant women there is no association between fetal exposure to maternal hyperglycemia and levels of CHI3L1 in their babies<sup>188</sup>. Production of CHI3L1 in presence of hyperglycemia in synergy with Ti NPs have not been studied before.

The expression of CHI3L1 in hyperglycemic macrophages exposed to Ti NPs was assessed via RT-PCR (Figure 15). Stimulation of M0 with 100 ppm Ti NPs in HG conditions resulted in upregulation of CHI3L1 expression by 25 times. 25 ppm Ti NPs in HG did not have any significant effect on upregulation of CHI3L1 expression, however, 25 ppm Ti NPs in NG promoted upregulation of CHI3L1 expression by the average of 5.5 times (Figure 15A). Stimulation of M1 macrophages with 100 ppm Ti NPs cultured in HG, resulted in upregulation of expression of CHI3L1 by the average of 2.8 times. The effects were similar in 6 donors analyzed and the strongest effect was 11 fold change. In M1 macrophages, there was no significant upregulation of CHI3L1 expression in presence of 25 ppm and 100 ppm Ti NPs in NG, however, stimulation with 100ppm Ti NPs in HG resulted in upregulation of CHI3L1 expression by 2.1 times (Figure 15B). In M2 macrophages cultured in HG, the effect was the strongest; 100 ppm Ti NPs promoted upregulation of CHI3L1 expression by the average of 35 times. Stimulation of M2 with 25 ppm Ti NPs in HG resulted in upregulation of CHI3L1 expression by the average of 22 times (Figure 15C). Hyperglycemia potentiated the effects of only 100 ppm Ti NPs-induced CHI3L1 expression in M1 and M2 macrophage subtypes and not of 25 ppm Ti NPs in any

macrophage subtypes. In total, HG significantly cooperated with 100 ppm Ti NPs in upregulation of CHI3L1 expression but not with 25 ppm Ti NPs.

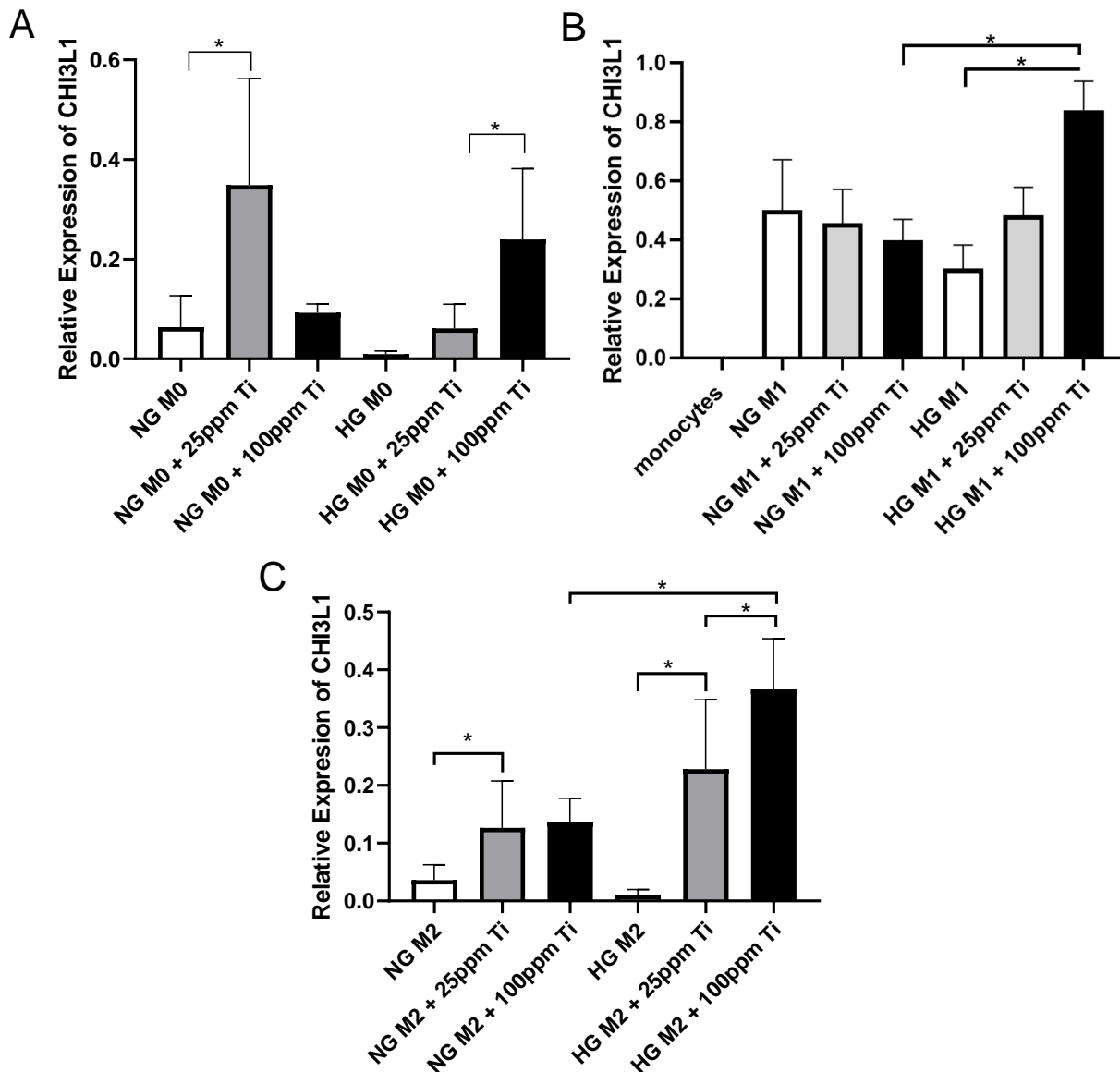


**Figure 15. Effect of hyperglycemia on CHI3L1 expression in primary human macrophages exposed to titanium nanoparticles.** Levels of gene expression were detected with RT-PCR for macrophages cultured in NG or HG for 6 days in presence or absence of 25ppm or 100ppm Ti NPs concentration. **A.** The expression of CHI3L1 from M0 (unstimulated), **B** from M1 (IFN $\gamma$ -stimulated) and **C** from M2 (IL4-stimulated) macrophages. Each bar represents the mean value of expression from 5 individual donors, obtained after normalization of original expression to a maximum expression value as 1 in each donor across all 18 conditions. Statistical analysis was performed using paired two-tailed t-test. \* $p < 0,05$ . The error bars are represented by SEM.

### 3.5.3 Hyperglycemia cooperates with Ti NPs-induced secretion of CHI3L1 in all macrophage subtypes

Next, the effect of hyperglycemia on Ti NPs-induced secretion of CHI3L1 in M0, M1 and M2 macrophages was evaluated (Figure 16 and 17). The ELISA was performed on supernatants collected from macrophages cultured for 6 days. The

secretion range was (3.0 – 134.1) ng/ml for M0 macrophages; (0.2 – 2.3) µg/ml for M1 macrophages and (5.8 – 272.3) ng/ml for M2 macrophages.

In M0 macrophages, the average CHI3L1 secretion levels were the lowest (3.3ng/ml). 100 ppm Ti NPs promoted CHI3L1 average secretion of 125 ng/ml and 25 ppm Ti NPs promoted CHI3L1 average secretion of 65 ng/ml. 100 ppm Ti NPs potentiated CHI3L1 secretion by the average of 32 times in NG and 38 times in HG. 25 ppm Ti NPs potentiated CHI3L1 secretion by the average of 18 times in NG and 32 times in HG (Figure 16A, 17). In M1 macrophages, Ti NPs at 100 ppm concentration promoted highest CHI3L1 secretion levels of about 2.1 µg/ml in HG. On average 100 ppm Ti NPs potentiated CHI3L1 secretion in M1 macrophages by the average of 3.6 times in NG and by 5.3 times in HG (Figure 16B, 17). In M2 macrophages, the levels of CHI3L1 secretion was less than in M1, and Ti NPs at 100 ppm concentration promoted CHI3L1 secretion up to 225 ng/ml. 100 ppm Ti NPs potentiated CHI3L1 secretion by the average of 24 times in NG and 31 times in HG, with a strongest effect of 39 fold change in one of the donors. 25 ppm Ti NPs potentiated secretion by the average of 8 times in NG and 12 times in HG (Figure 16C, 17).

Hyperglycemia potentiated the effects of 25 ppm Ti NPs-induced CHI3L1 secretion by the average of 1.4 times in M1 and 1.5 times in M2, and potentiated the effects of 100 ppm Ti NPs-induced CHI3L1 secretion by the average of 1.2 times in M0, 1.5 times in M1 and 1.3 times in M2. (Figure 17). In total, HG cooperates with Ti NPs in upregulation of CHI3L1 secretion in all macrophage subtypes. However, the effect of Ti NPs on CHI3L1 secretion was stronger than the effect of hyperglycemia on Ti NPs-induced CHI3L1 secretion in all macrophage subtypes.

In summary, CHI3L1 secretion data does not exactly correlate with the expression data, in particularly for M1 responses. In M1 macrophages, Ti NPs potentiate secretion of CHI3L1 in a dose-dependent manner, and HG cooperates with this effect working in synergy with both concentrations (25 ppm and 100 ppm) Ti NPs. However, Ti NPs have no effect on CHI3L1 expression in M1 macrophages in NG. In M1 macrophages, HG cooperates with 100 ppm but not with 25 ppm Ti NPs in upregulation of CHI3L1 gene expression. These findings imply that Ti NPs and HG cooperate on different levels resulting in the elevation of production of CHI3L1 by all types of macrophages.

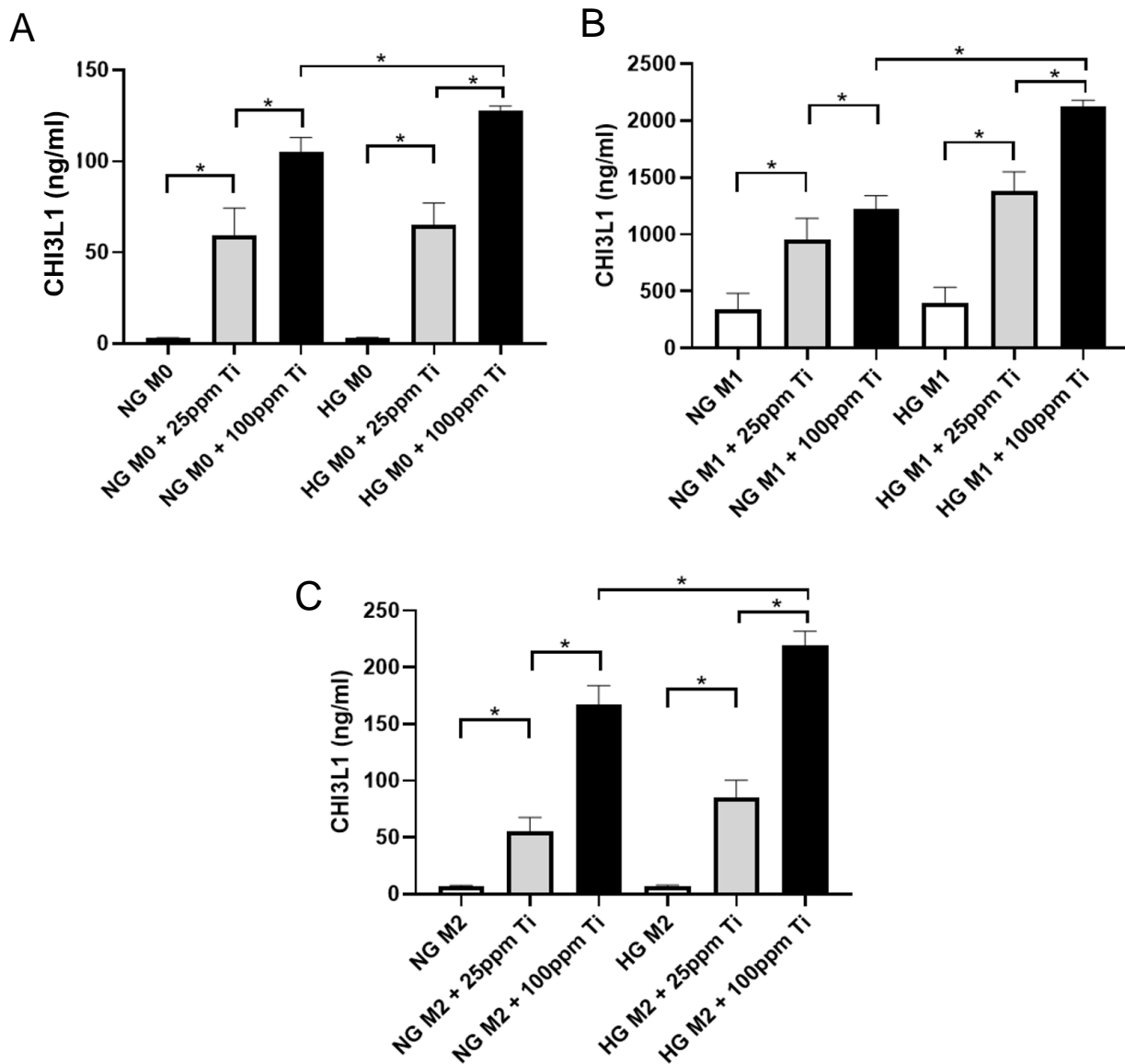


**Figure 16. Effect of hyperglycemia on CHI3L1 secretion in primary human macrophages exposed to titanium nanoparticles.** Supernatants were collected from monocytes-derived macrophages that were cultivated in NG and HG conditions for 6 days in absence or in presence of 25ppm and 100ppm concentrations of Ti NPs. The effects assessed, **A**, for M0 (NS), **B**, M1 (IFN $\gamma$ ) and **C**, M2 (IL4). All experiments were performed in duplicates. The results are presented separately from 6 individual donors (n=6). The error bars are represented by SEM. Statistical analysis was performed using paired two-tailed t-test. \*p<0.05.



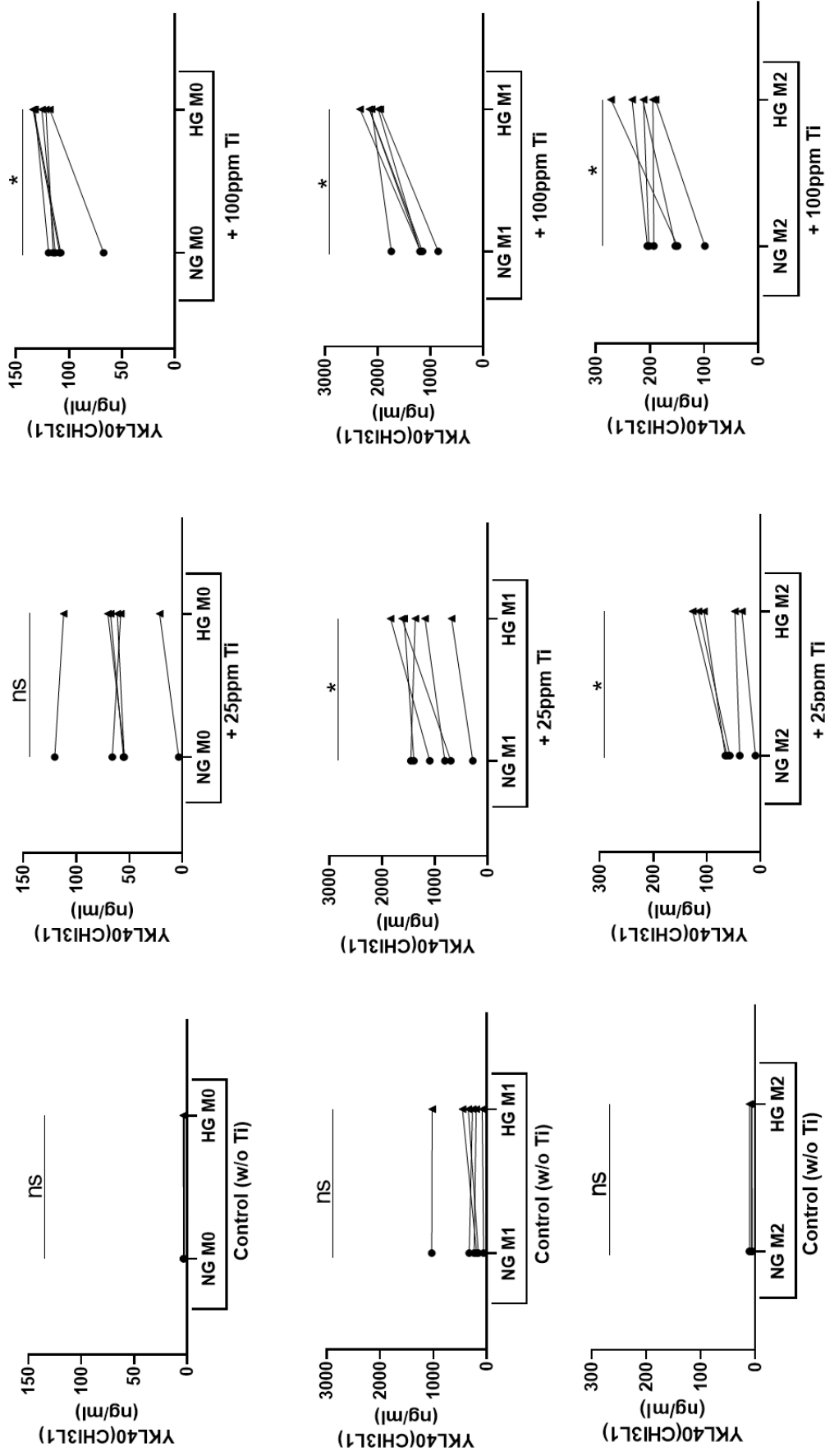


**Figure 17. Effect of hyperglycemia on CH13L1 secretion in primary human M0, M1 and M2 macrophages in absence or in presence of 25ppm and 100ppm concentration of titanium nanoparticles.** Supernatants were collected on day 6. Secretion levels were detected with ELISA. All experiments were performed in duplicates. The results are presented for individual donors (n=6) in normal and high glucose conditions. Statistical analysis was performed using paired two-tailed t-test. \*p<0.05.

### 3.5.4 Hyperglycemia cooperates with Ti NPs-induced expression of CHIT1 in M1 macrophages

Elevated levels of CHIT1 are observed in patients with type 2 diabetes (T2D) and associated with diabetic complications<sup>189</sup>. The aim of the study was to identify the effect of diabetic conditions on CHIT1 production in the context of Ti NPs. Analogously to CHI3L1, the expression of CHIT1 in hyperglycemic macrophages exposed to Ti NPs was analyzed (Figure 18).

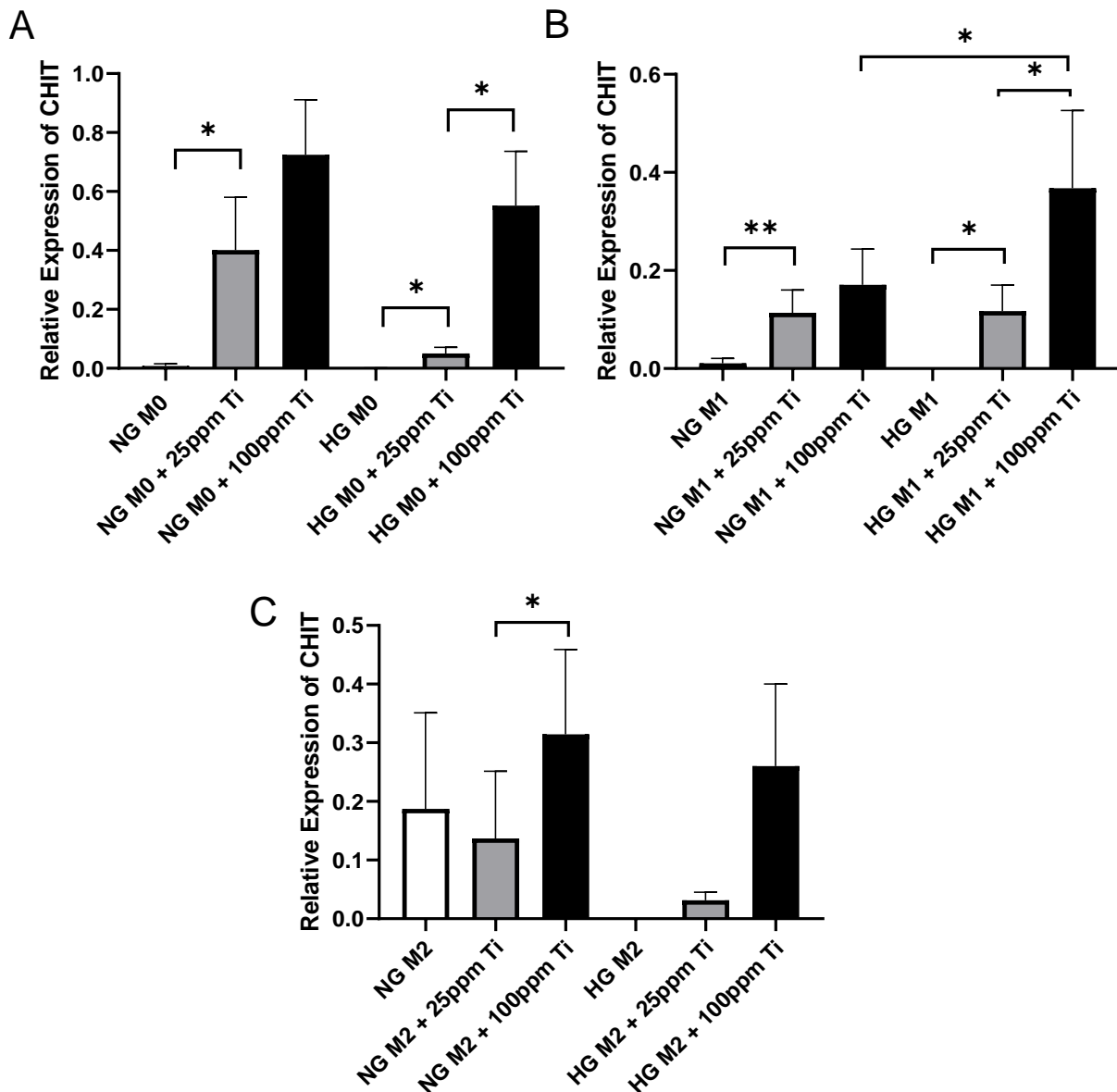


**Figure 18. Effect of hyperglycemia on CHIT1 expression in primary human macrophages exposed to titanium nanoparticles.** Levels of gene expression were detected with RT-PCR for macrophages cultured in NG or HG for 6 days in presence or absence of 25ppm or 100ppm Ti NPs concentration **A**. The expression of CHIT1 from M0 (unstimulated), **B** from M1 (IFN $\gamma$ -stimulated) and **C** from M2 (IL4-stimulated) macrophages. Each bar represents the mean value of expression from 5 individual donors, obtained after normalization of original expression to a maximum expression value as 1 in each donor across all 18 conditions. Statistical analysis was performed using paired two-tailed t-test (\* $p < 0,05$ ). The error bars are represented by SEM.

Stimulation of M0 macrophages with 25 ppm Ti NPs resulted in upregulation of CHIT1 expression by the average of 51 times in NG and 107 times in HG. Stimulation of M0 with 100 ppm Ti NPs resulted in upregulation of CHIT1 secretion by the average of 93 times in NG and 1167 times in HG. These upregulation effects occurred for all 6 donors analyzed (Figure 18A). Stimulation of M1 macrophages with 25 ppm Ti NPs resulted in upregulation of CHIT1 expression by the average of 11 times in NG and 1736 times in HG. Stimulation of M1 with 100 ppm Ti NPs resulted in upregulation of CHIT1 expression by the average of 16 times in NG and 5450 times in HG. These upregulation effects was detected in all 6 donors analyzed (Figure 18B). In M2 macrophages, 25 ppm and 100 ppm Ti NPs did not affect CHIT1 expression in NG. However, stimulation of M2 macrophages with Ti NPs resulted in upregulation of CHIT1 expression by the average of 181 times at 25 ppm concentration and 1501 times at 100 ppm concentration (Figure 18C). Hyperglycemia potentiated the effects of only 100 ppm Ti NPs-induced CHIT1 expression and only in M1 macrophages by the average of 5.8 times. In total, in all macrophage subtypes exposed to hyperglycemic environment, Ti NPs promoted upregulation of CHIT1 expression in a dose-dependent manner, which did not occur for NG conditions. However, hyperglycemia only cooperated with 100 ppm Ti NPs in M1 macrophages.

### **3.5.5 Hyperglycemia and Ti NPs cooperate in suppression of CCL18 production by M2**

Hyperglycemia suppresses production of CCL18 in primary human macrophages<sup>49</sup>. In the previous section, Figure 9 and 12 demonstrate that CCL18 is suppressed by Ti NPs. The effect of HG conditions on Ti NPs-induced suppression of CCL18 expression in M2 macrophages cultured for 6 days was examined by RT-PCR (Figure 19). 25 ppm Ti NPs suppressed CCL18 expression by the average of 10 times in NG and 22 times in HG. 100 ppm Ti NPs suppressed CCL18 by the average of 580 times in NG and 628 times in HG (Figure 19C). Hyperglycemia potentiated the effects of 25 ppm Ti NPs in suppression of CCL18 by the average of 2.4 times (Figure 19A). However, the suppressive effect of 100 ppm Ti NPs was very strong, and was not further affected by HG (Figure 19B).

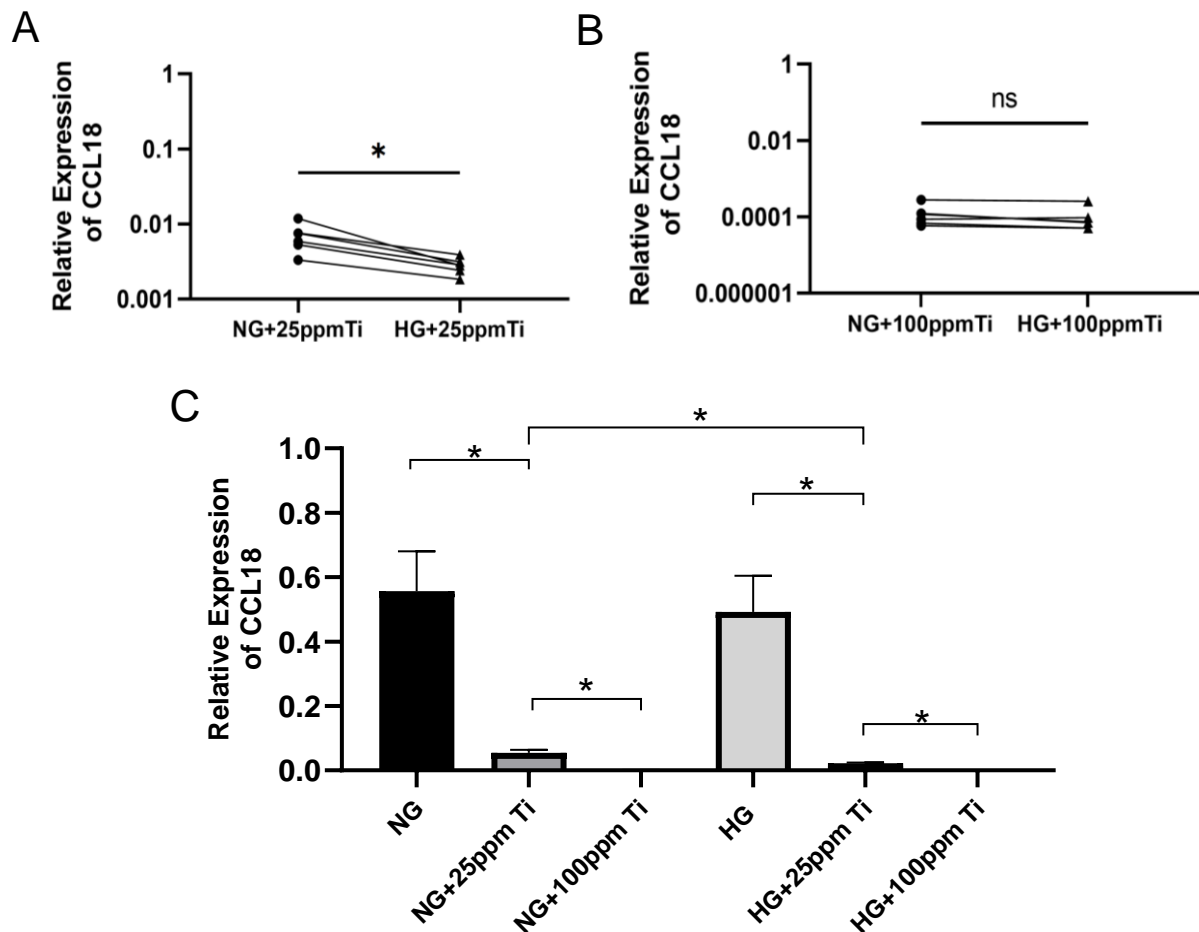


**Figure 19. Effect of hyperglycemia and titanium nanoparticles on CCL18 expression in human macrophages.** Expression levels were detected with RT-PCR from M2 macrophages cultured in NG or HG for 6 days in presence or absence of 25ppm and 100ppm Ti NPs concentration. **A.** Individual donor responses illustrating the NG and HG comparison with 25ppm Ti NPs. **B** 100ppm Ti NPs. **C.** Summary of 25ppm and 100ppm Ti NPs responses in NG and HG. Each bar represents the mean value of expression from 6 individual donors. The error bars are represented by SEM. Statistical analysis was performed using paired two-tailed t test. \* $p < 0,05$ .

Next, the effect of hyperglycemic environment on Ti NPs-induced suppression of CCL18 secretion was examined by ELISA (Figure 20). The protein secretion was detected from the supernatants collected from M2 macrophages cultured for 6 days in NG or HG conditions and in presence of 25 ppm or 100 ppm Ti NPs. Average secretion of CCL18 detected in macrophages was  $(541 \pm 39.8)$  ng/ml in NG conditions and  $(435 \pm 68.1)$  ng/ml in HG. In presence of 25 ppm Ti NPs, the secretion levels were reduced to the average of  $(316 \pm 98.0)$  ng/ml in NG and  $(237 \pm 88.5)$  ng/ml in HG. In presence of 100 ppm Ti NPs, the secretion levels were the lowest:  $(20.6 \pm 16.0)$  ng/ml in NG and  $(20.7 \pm 2.25)$  ng/ml in HG (Figure 20B). 25 ppm Ti NPs suppressed CCL18 secretion by the average of 1.7 fold in NG and by 1.8 fold in HG. 100 ppm Ti NPs suppressed CCL18 by the average of 26 times in NG and 21 times in HG (Figure 20C).

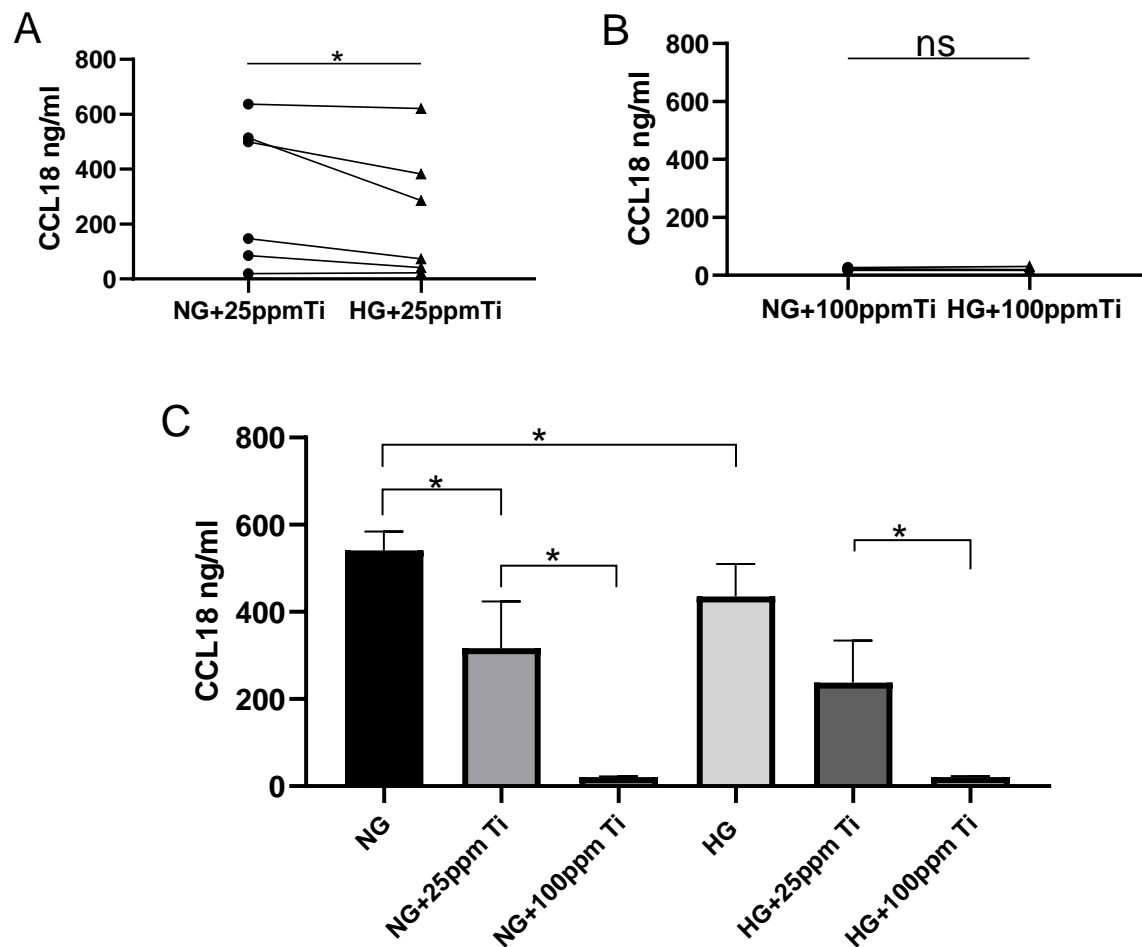


**Figure 20. Effect of hyperglycemia and titanium nanoparticles on CCL18 secretion in human macrophages.** Secretion levels were detected with ELISA in supernatants collected from M2 macrophages cultured in NG or HG for 6 days in presence or absence of 25ppm and 100ppm Ti NPs concentration. **A.** Individual donor responses illustrating the NG and HG comparison with 25ppm Ti NPs. **B** 100ppm Ti NPs. **C.** Summary of 25ppm and 100ppm Ti NPs responses in NG and HG. Each bar represents the mean value of secretion from 6 individual donors. The error bars are represented by SEM. Statistical analysis was performed using paired two-tailed t test. \* $p < 0,05$ .

Hyperglycemia potentiated the effects of 25 ppm Ti NPs in suppression of CCL18 secretion by the average of 1.3 fold (Figure 20A) and not in suppression of CCL18 induced by 100 ppm Ti NPs (Figure 20B). In conclusion, hyperglycemia cooperates with 25 ppm Ti NPs but not with 100 ppm Ti NPs in suppression of CCL18 secretion.

In total, the effect of suppression of CCL18 expression by Ti NPs was significantly larger than the effect of suppression of CCL18 secretion by Ti NPs. However, similarly to results of CCL18 secretion, hyperglycemia cooperates with 25 ppm Ti NPs but not with 100 ppm Ti NPs in suppression of CCL18 expression.

### 3.6 Effect of dexamethasone on CHI3L1 and CHIT1 expression in normal and hyperglycemic M1 exposed to Ti NPs

#### 3.6.1 Dexamethasone suppresses Ti NPs – induced CHI3L1 expression in HG and not in NG

Dexamethasone is a synthetic glucocorticoid, which is able to inhibit LPS-induced cytokine production of TNF- $\alpha$  and IL1- $\beta$ <sup>190,191</sup>. Dexamethasone reduces macrophage activation and used as a drug to treat implant-mediated inflammation<sup>192,193</sup>. The effect of 100 nM dexamethasone (Dex) on Ti NPs-induced expression changes of CHI3L1 in pro-inflammatory macrophages cultured for 6 days in NG or HG conditions was evaluated (Figure 21 and 22). Dex suppressed expression of CHI3L1 in M1 macrophages cultured in absence of Ti NPs by the average of 2.7 times in NG. These effects were similar in 5 individual donors (Figure 21A, Table 18). Dex had no effect on CHI3L1 expression in HG in absence of Ti NPs (Figure 21C). In presence of Ti NPs, Dex suppressed CHI3L1 expression in hyperglycemic M1 macrophages by the average of 2.0 times (Figure 21D, Table 18), however it had no effect on CHI3L1 expression in NG (Figure 21B).

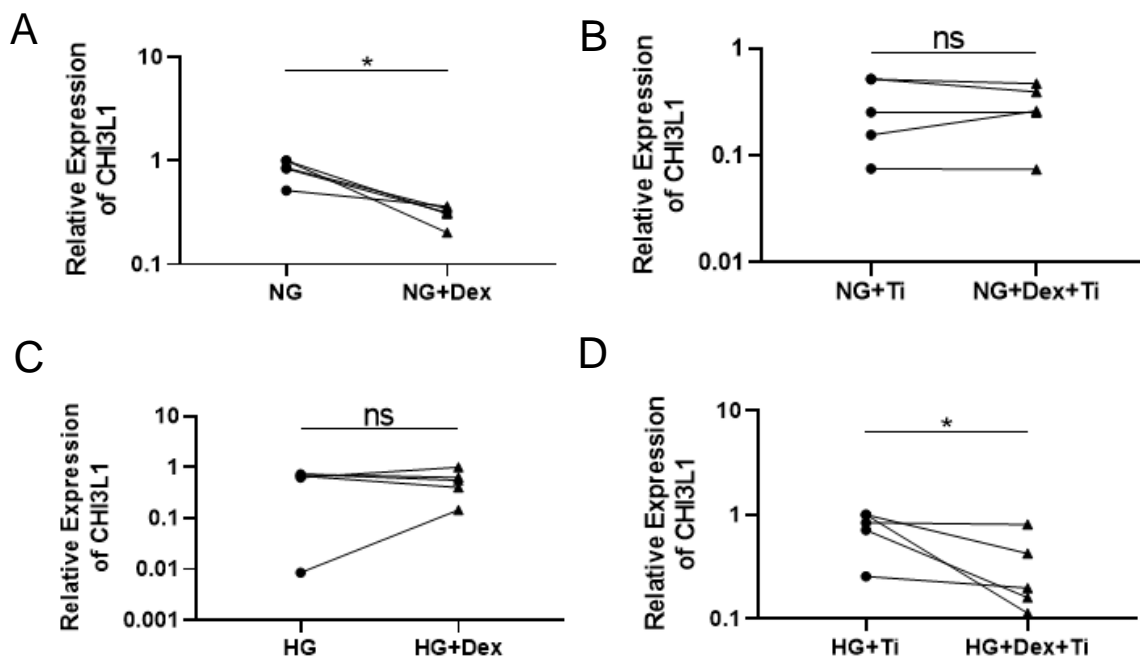


**Figure 21. Effect of dexamethasone on CHI3L1 expression in individual donors by M1 macrophages exposed to titanium nanoparticles in normal or high glucose conditions.** Expression levels were detected with RT-PCR from M1 macrophages cultured in NG or HG for 6 days in presence or absence of 100ppm Ti NPs. The results are presented for 5 individual donors. **A.** CHI3L1 expression in NG with or w/o Dex. **B.** CHI3L1 expression in NG with or w/o Dex exposed to Ti NPs. **C.** CHI3L1 expression in HG with or w/o Dex. **D.** CHI3L1 expression in HG with or w/o Dex exposed to Ti NPs.

**Table 18. Quantification of CHI3L1 suppression by dexamethasone in M1 macrophages for 5 individual donors.**

Donor number	Downregulation by Dex of CHI3L1 expression in M1 cultured in NG	Downregulation by Dex of CHI3L1 expression in M1 exposed to Ti NPs cultured in HG
1	2,65	8,83
2	3,26	1,04
3	2,48	2,36
4	1,41	4,45
5	4,95	1,30
<b>Average fold change</b>	<b>2,74</b>	<b>2,00</b>

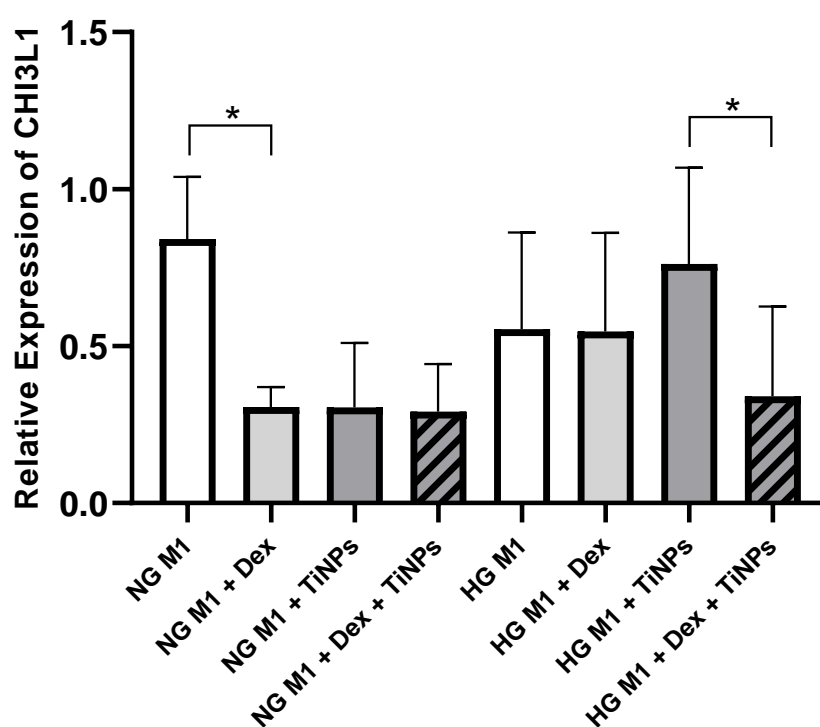


**Figure 22. Effect of dexamethasone on CHI3L1 expression by M1 macrophages exposed to titanium nanoparticles in normal or high glucose conditions.** Expression levels were detected with RT-PCR from M1 macrophages cultured in NG or HG for 6 days in presence or absence of Ti NPs at 100ppm concentration. Each bar represents the mean value of CHI3L1 expression from 5 individual donors, obtained after normalization of original expression to a maximum expression value as 1 in each donor across 8 conditions. Statistical analysis was performed using paired two-tailed t-test. \* $p < 0,05$ . The error bars are represented by SEM.

### 3.6.2 Dexamethasone upregulates Ti NPs – induced CHIT1 expression in NG and has no effect in HG

Next, the effect of Dex on Ti NPs-induced CHIT1 expression in M1 macrophages cultured for 6 days in NG or HG conditions was examined (Figure 23 and 24). Dex

downregulated CHIT1 expression in M1 macrophages by the average of 2.7 times, with a maximum suppression of 4.4 fold change (Figure 23A, Table 19). In absence of Dex, Ti NPs upregulated expression of CHIT1 by the average of 6.4 times with a maximum effect of 20 fold change (Figure 20). In presence of Dex, Ti NPs upregulated CHIT1 expression by the average of 36 times with a maximum upregulation effect of 56 fold change (Figure 20). In NG conditions, Dex enhanced Ti NPs-induced CHIT1 expression by the average of 2.9 times in all 5 individual donors (Figure 23B). In NG conditions, Dex suppressed CHIT1 expression by the average of 3.2 times without Ti NPs (Figure 23C). Dex had no effect on CHIT1 expression in hyperglycemic macrophages exposed to Ti NPs (Figure 23D). In hyperglycemic macrophages, in absence of Dex, Ti NPs upregulated CHIT1 expression by the average of 16 times; in presence of Dex, Ti NPs enhanced CHIT1 by the average of 46 times (Figure 24). In conclusion, dexamethasone cooperates with Ti NPs in upregulation of CHIT1 expression in NG but has no effect in HG. High glucose cooperates with Ti NPs-induced CHIT1 expression in absence of dexamethasone.

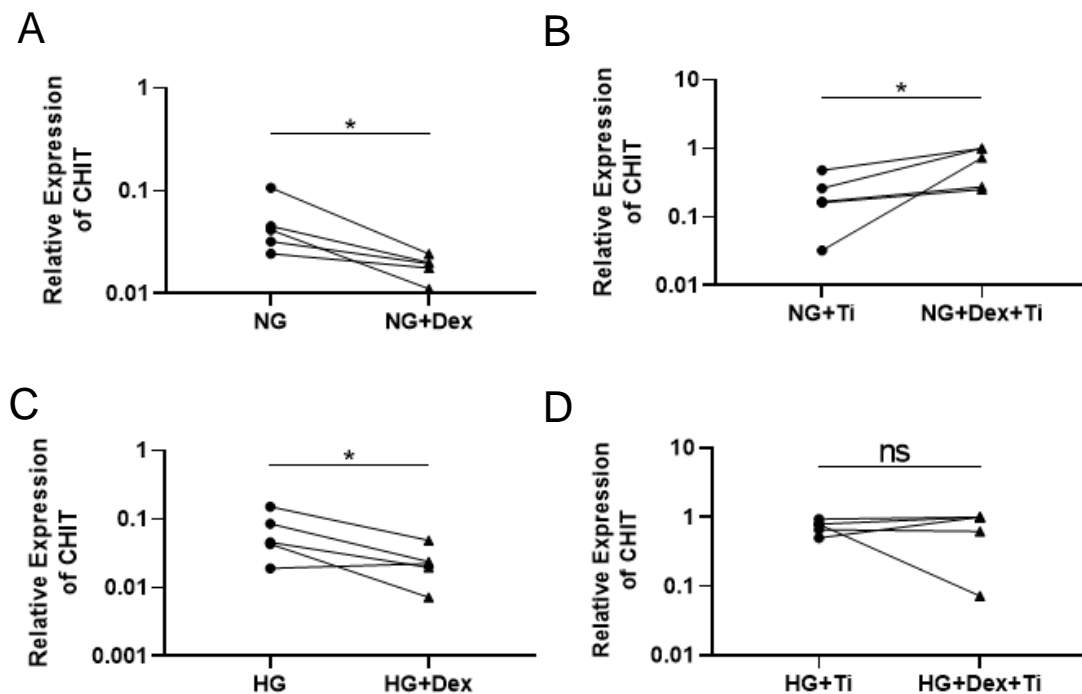


**Figure 23. Effect of dexamethasone on CHIT1 expression in individual donors by M1 macrophages exposed to titanium nanoparticles in normal or high glucose conditions.** Expression levels were detected with RT-PCR from M1 macrophages cultured in NG or HG for 6 days in presence or absence of 100ppm Ti NPs. The results are presented for 5 individual donors. **A.** CHIT1 expression in NG with or w/o Dex. **B.** CHIT1 expression in NG with or w/o Dex exposed to Ti NPs. **C.** CHIT1 expression in HG with or w/o Dex **D.** CHIT1 expression in HG with or w/o Dex exposed to Ti NPs.



**Table 19. Quantification of CHIT1 expression changes by dexamethasone in M1 macrophages for 5 individual donors.**

Donor Number	Downregulation by Dex of CHIT1 expression in M1 cultured in NG	Upregulation by Dex of CHI3L1 expression in M1 exposed to Ti NPs cultured in NG	Downregulation by Dex of CHIT1 expression in M1 cultured in HG
1	2,26	3,82	2,30
2	4,39	1,55	3,57
3	1,64	22,5	3,11
4	1,38	2,08	0,86
5	2,26	1,66	5,96
<b>Average fold change</b>	<b>2,70</b>	<b>2,95</b>	<b>3,16</b>

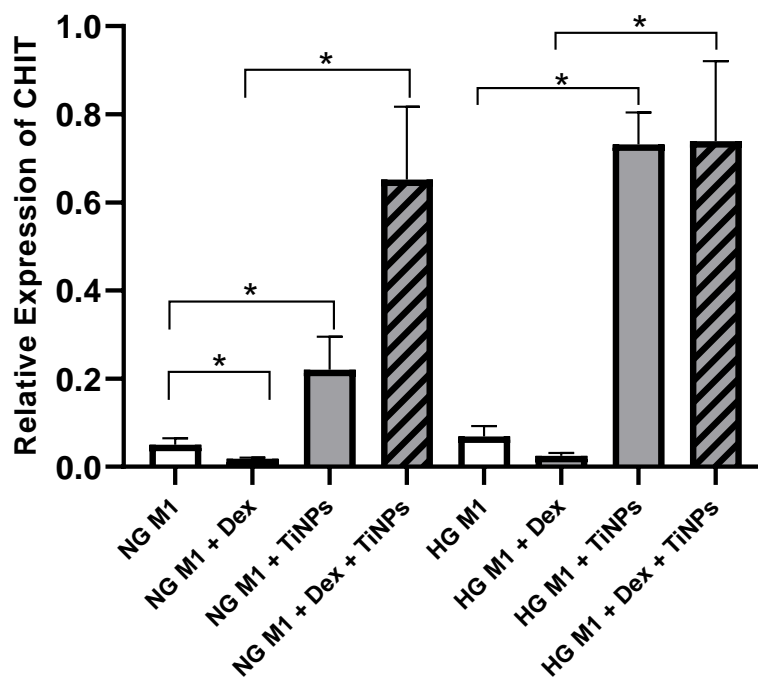


**Figure 24. Effect of dexamethasone on CHIT1 expression by M1 macrophages exposed to titanium nanoparticles in normal or high glucose conditions in summary.** Expression levels were detected with RT-PCR from M1 macrophages cultured in NG or HG for 6 days in presence or absence of Ti NPs at 100ppm concentration. Each bar represents the mean value of CHIT1 expression from 5 individual donors, obtained after normalization of original expression to a maximum expression value as 1 in each donor across 8 conditions. Statistical analysis was performed using paired two-tailed t-test. \* $p < 0,05$ . The error bars are represented by SEM.

### 3.7 Effect of Ti NPs on CHIT1 intracellular localization

Previous results of this study revealed that Ti NPs promote expression of CHIT1 in all macrophage subtypes. Using confocal microscopy and indirect immunofluorescence, intracellular localization of CHIT1 in M0, M1 and M2 macrophages cultured for 6 days in presence of 100 ppm Ti NPs was assessed. The cells were stained with antibody against CHIT1 and DRAQ5 and DAPI. CHIT1 was detected in cytoplasm and presumably on plasma membrane (PM) in M0 macrophages in control samples without Ti NPs (Figure 25A). Similarly to M0 macrophages without Ti NPs, presence of CHIT1 in M0 exposed to Ti NPs was also observed, however, it was more concentrated in some vesicular structures and slightly on PM (Figure 25B). Interestingly, most of the cells of M0 subtype exposed to Ti NPs were found to be heterogenous in size and shape in comparison to M0 without Ti NPs.

Using analogous staining and culture conditions the intracellular localization of CHIT1 in M1 macrophages was examined (Figure 26). Slight presence of CHIT1 has been observed in M1 macrophages without Ti NPs in cytoplasm and also in more diffused form (Figure 26A). Alternatively, in presence of Ti NPs significant overproduction of CHIT in up to 40% of M1 cells was observed. CHIT was mainly located on PM and in some large vesicular structures (Figure 26B).

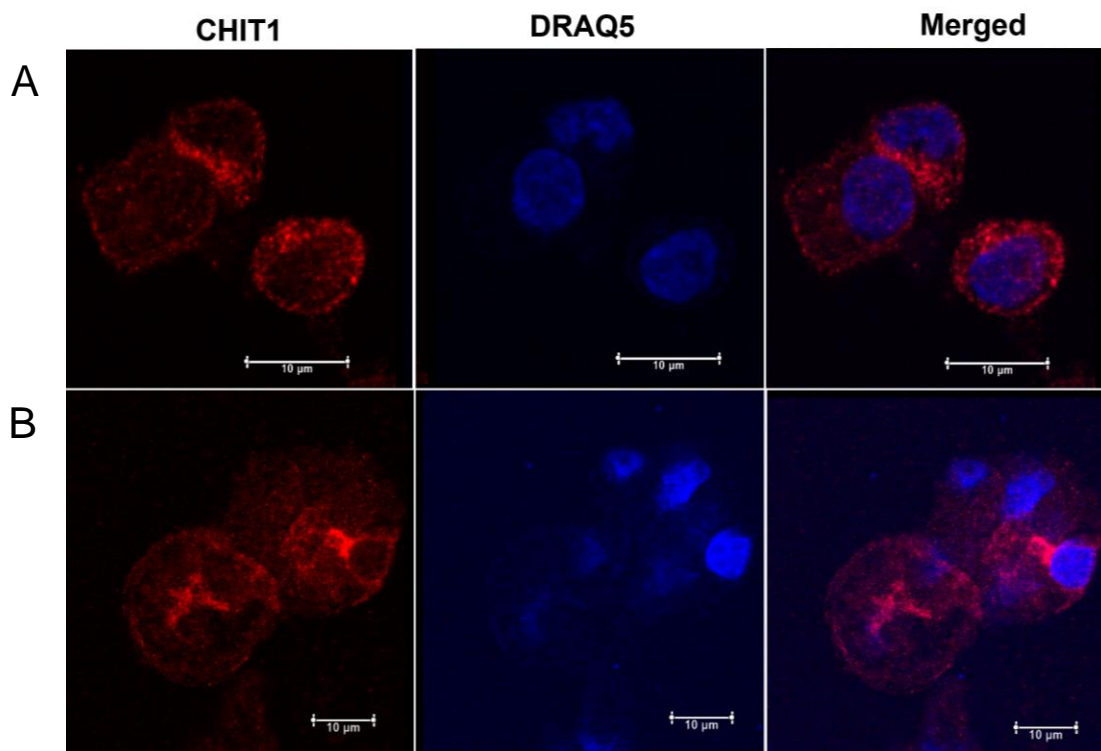


**Figure 25. Effect of titanium nanoparticles on the intracellular localization of CHIT1 in M0 macrophages.** PFA-fixed macrophages were stained with rabbit polyclonal anti-CHIT1 antibody and DRAQ5 nuclear stain. Secondary antibody was Cy3-conjugated goat anti-rabbit IgG. Red corresponds to CHIT1 staining. Scale bars are 10 µM. **A.** Representative M0 macrophage cultured for 6 days in absence of Ti NPs. **B.** Representative M0 macrophage cultured for 6 days in presence of 100ppm concentration of Ti NPs.

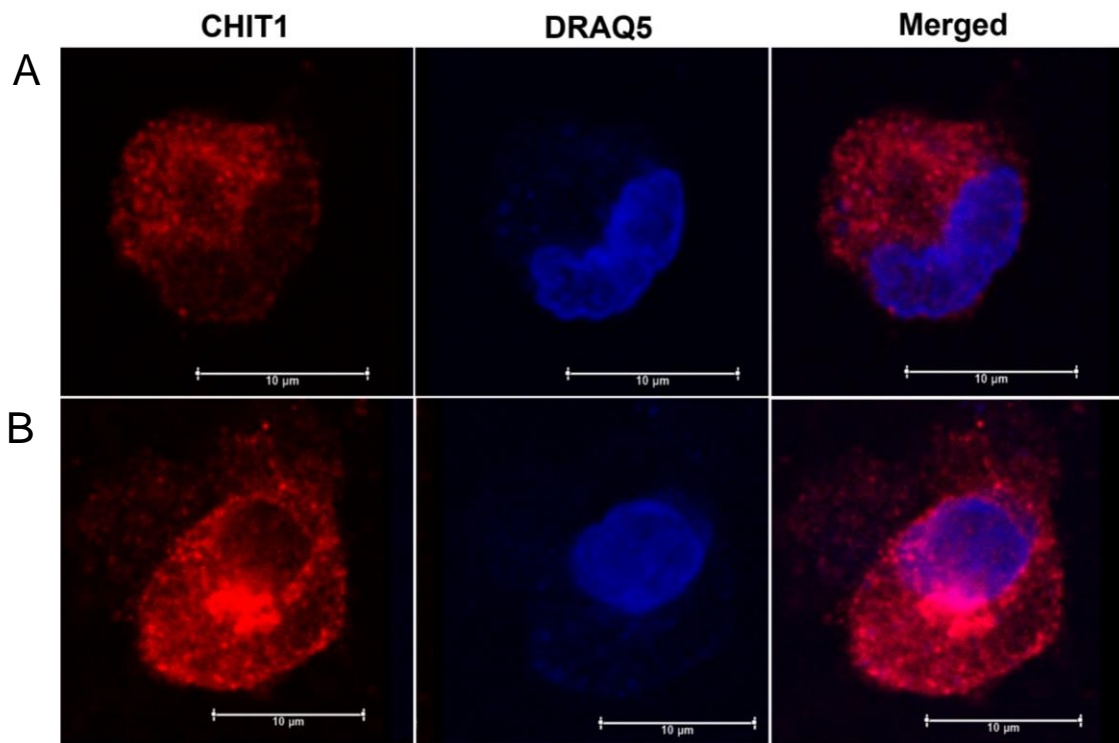


**Figure 26. Effect of titanium nanoparticles on intracellular localization of CHIT1 in M1 macrophages.** PFA-fixed macrophages were stained with rabbit polyclonal anti-CHIT1 antibody and DRAQ5 nuclear stain. Secondary antibody was Cy3-conjugated goat anti-rabbit IgG. Red corresponds to CHIT1 staining. Scale bars are 10 µm **A.** Representative M1 macrophage cultured for 6 days in absence of Ti NPs. **B.** Representative M1 macrophage cultured for 6 days in presence of 100ppm concentration of Ti NPs.

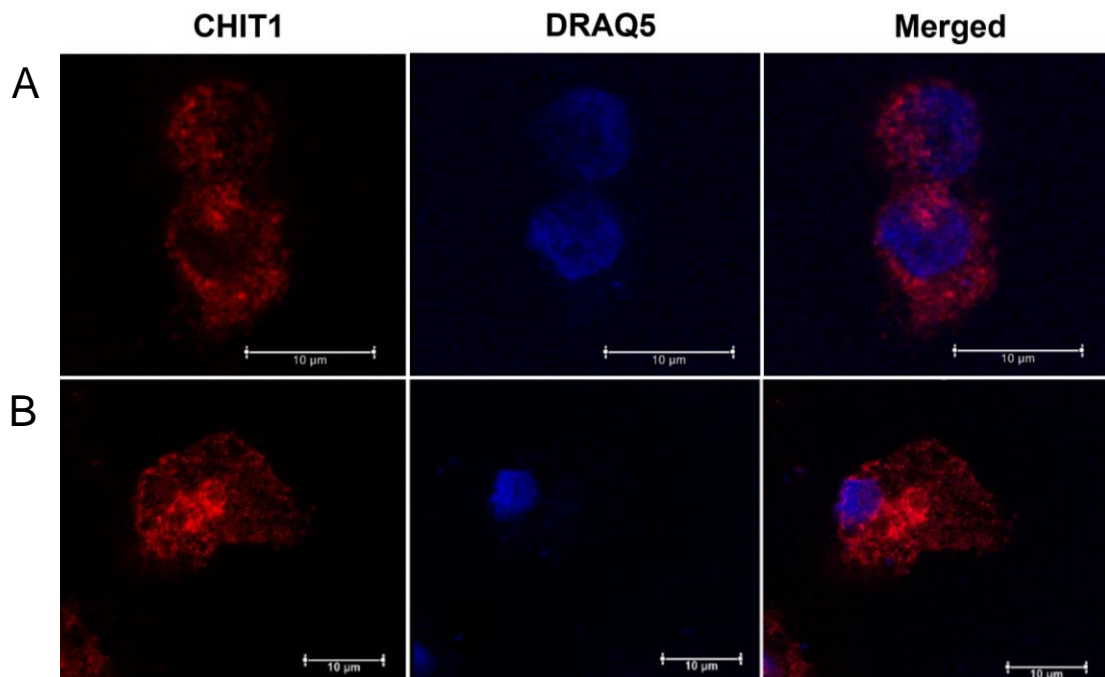


**Figure 27. Effect of titanium nanoparticles on intracellular localization of CHIT1 in M2 macrophages.** The cells were stained as indicated in the legends to Figure 25 and 26. **A.** Representative M2 macrophage cultured for 6 days in absence of Ti NPs. **B.** Representative M2 macrophage cultured for 6 days in presence of 100ppm concentration of Ti NPs.

The intracellular localization of CHIT1 in M2 was evaluated (Figure 27). Similar to M1 macrophages without Ti NPs, presence of CHIT1 was observed in cytoplasm also in a diffused form (Figure 27A). However, in presence of Ti NPs, we have observed significant amount of CHIT1 in some vesicular structures and not in the nuclei or on PM (Figure 27B). These vesicular structures did not resemble the ones visualized in M0 or M1 macrophages with Ti NPs.

Localization of CHIT1 within the trans-Golgi network (TGN) was investigated (Figure 28, 29). TGN corresponds to interconnected tubules and vesicles, at the trans face of the Golgi stack. TGN46 is a putative, cargo-binding protein that maintains a steady-state level in the dynamic TGN structure by active retention and recycling. Small level of colocalization between CHIT1 and TGN46 was observed only in M0 macrophages in control conditions w/o Ti NPs (Figure 28A), and no colocalization was detected in M1 and M2 for the same conditions (Figure 28B, C). Strong colocalization of CHIT1 and TGN46 was observed in M1 macrophages exposed to Ti NPs where it was apparent that CHIT1 accumulated in TGN vesicles and at PM (Figure 29B). The TGN signal was not detected in M0 and M2 macrophages exposed to Ti NPs (Figure 29A and C).

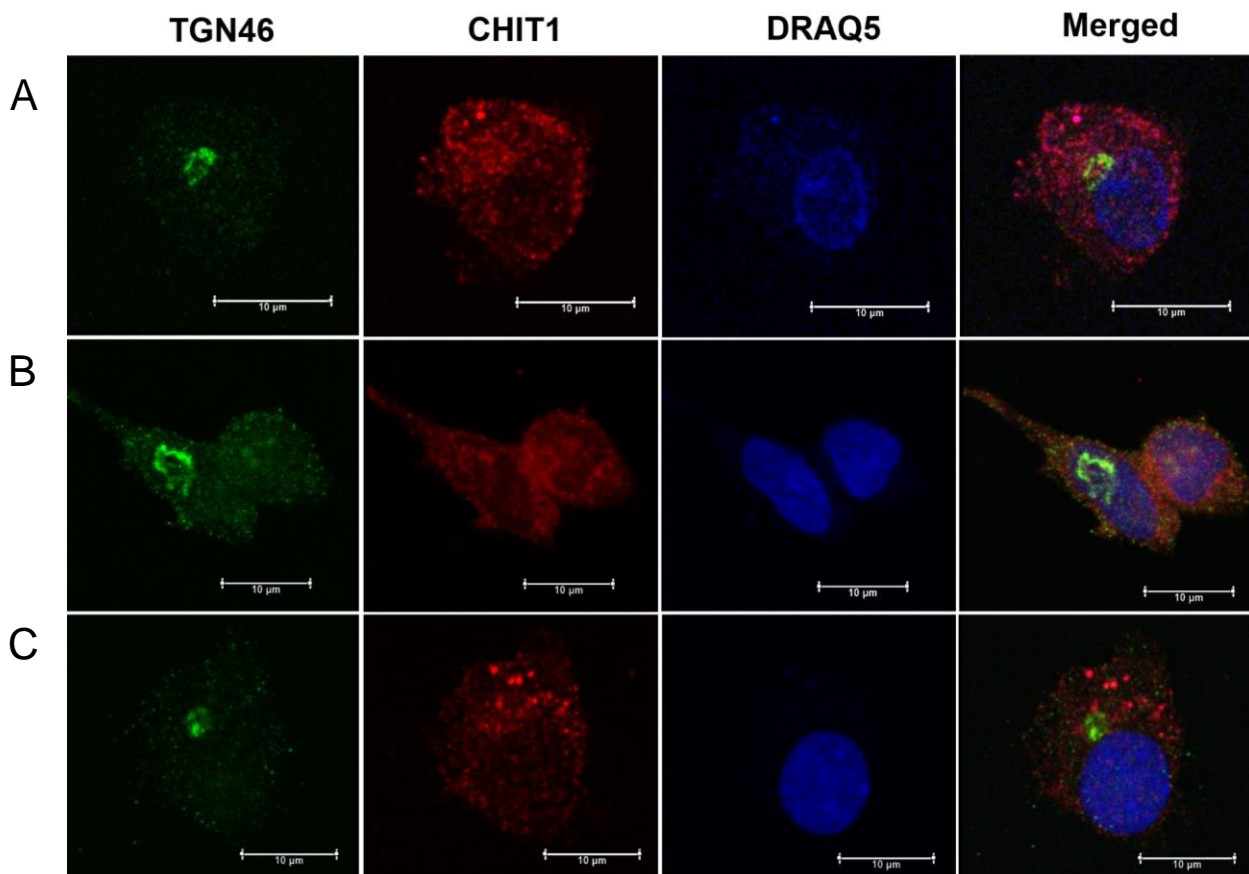


**Figure 28. Intracellular colocalization of CHIT1 and TGN46 in M0, M1 and M2 macrophages without Ti NPs (control conditions).** Macrophages were stained with rabbit polyclonal anti-CHIT1 antibody, mouse monoclonal anti-TGN46 antibody and nuclei dyes DRAQ5. Secondary antibody combination was Cy3-conjugated goat anti-rabbit IgG and Alexa488-conjugated goat anti-mouse IgG. Green corresponds to TGN46 staining, red corresponds to CHIT1 staining, and yellow corresponds to the area of colocalization (Merge). **A.** Representative M0 (unstimulated) macrophage. **B.** Representative M1 (IFN $\gamma$ -stimulated) macrophages and **C.** Representative M2 (IL4-stimulated) macrophage.



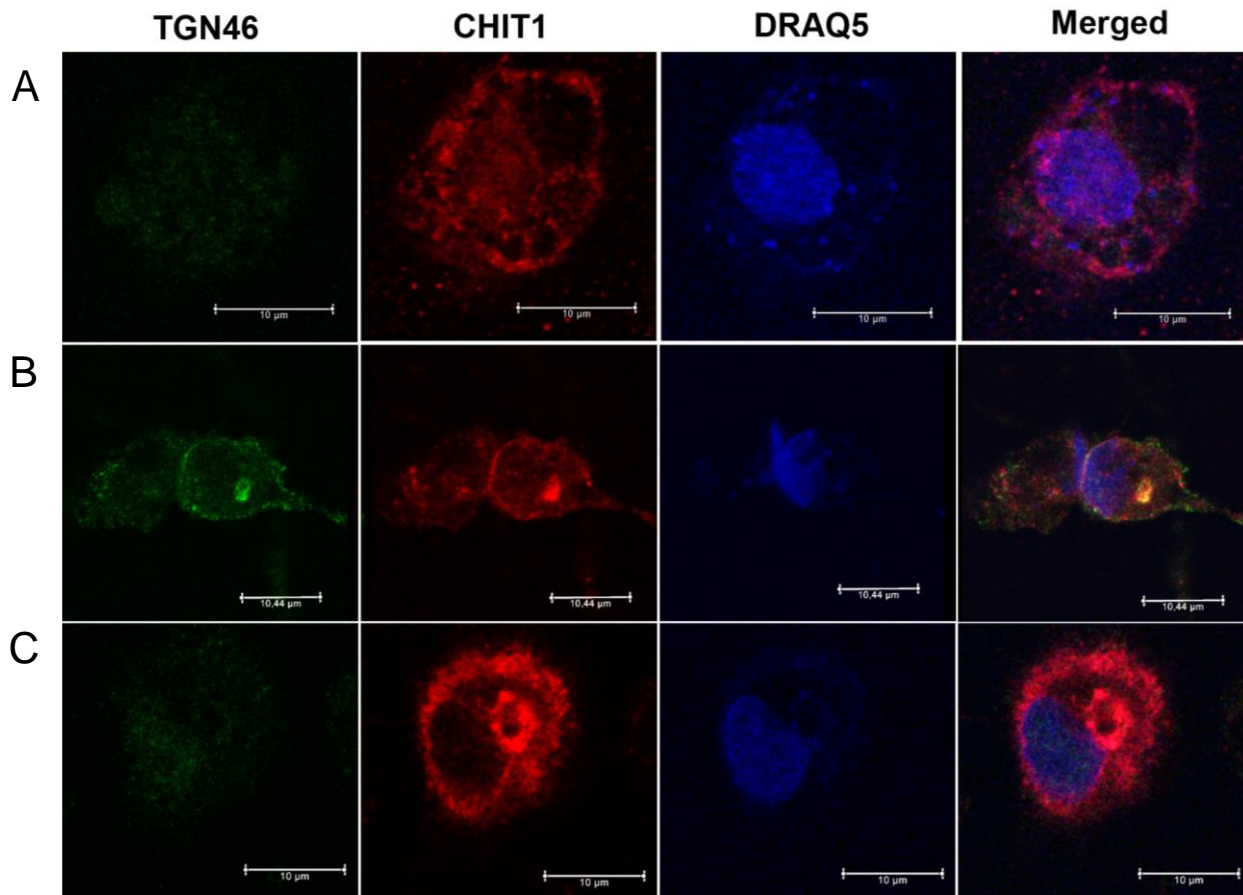


**Figure 29. Effect of Ti NPs on intracellular co-localization of CHIT1 and TGN46 in M0, M1 and M2 macrophages.** Macrophages were stained with rabbit polyclonal anti-CHIT1 antibody, mouse monoclonal anti-TGN46 antibody and nuclei dye DRAQ5. Secondary antibody combination was Cy3-conjugated goat anti-rabbit IgG and Alexa488-conjugated goat anti-mouse IgG. Green corresponds to TGN46 staining, red corresponds to CHIT1 staining, and yellow corresponds to the area of colocalization (Merge). The cells were exposed to 100ppm concentration of Ti NPs. **A.** Representative M0 (unstimulated) macrophage. **B.** Representative M1 (IFN $\gamma$ -stimulated) macrophages and **C.** Representative M2 (IL4-stimulated) macrophage..

TGN compartment of M0 and M2 macrophages was completely disrupted in most of the cells exposed to Ti NPs. In total, Ti NPs promoted CHIT1 trafficking to TGN compartment in M1 macrophages and blocked the normal sorting system by interrupting TGN for M0 and M2 macrophages sending CHIT1 to unusual locations.

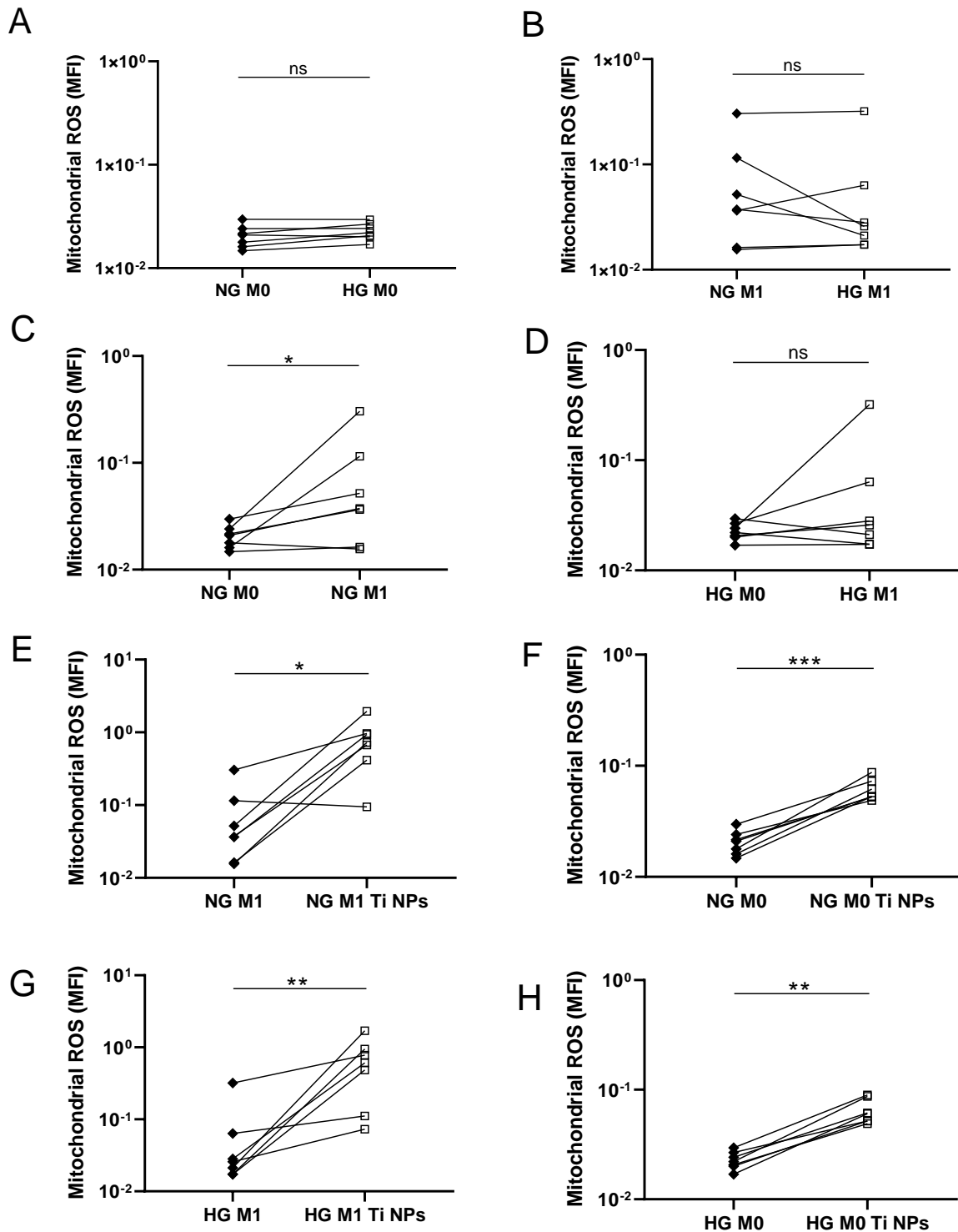
### 3.8 Effect of Ti NPs on mitochondrial ROS release

Ti NPs have been reported to exert toxicity by promoting the release of reactive oxygen species (ROS) and mitochondrial dysfunction<sup>188</sup>. It has been demonstrated that Ti NPs can induce endoplasmic reticulum (ER) stress in the cells by disrupting the mitochondrial-associated ER membranes and calcium ion balance via increasing the autophagy<sup>195</sup>. To determine the negative effects of Ti NPs through promoting toxicity by ROS activation, mitochondrial ROS release was measured by FACS in M0 and M1 macrophages cultured for 6 days. The cells were stimulated with 100 ppm of Ti NPs

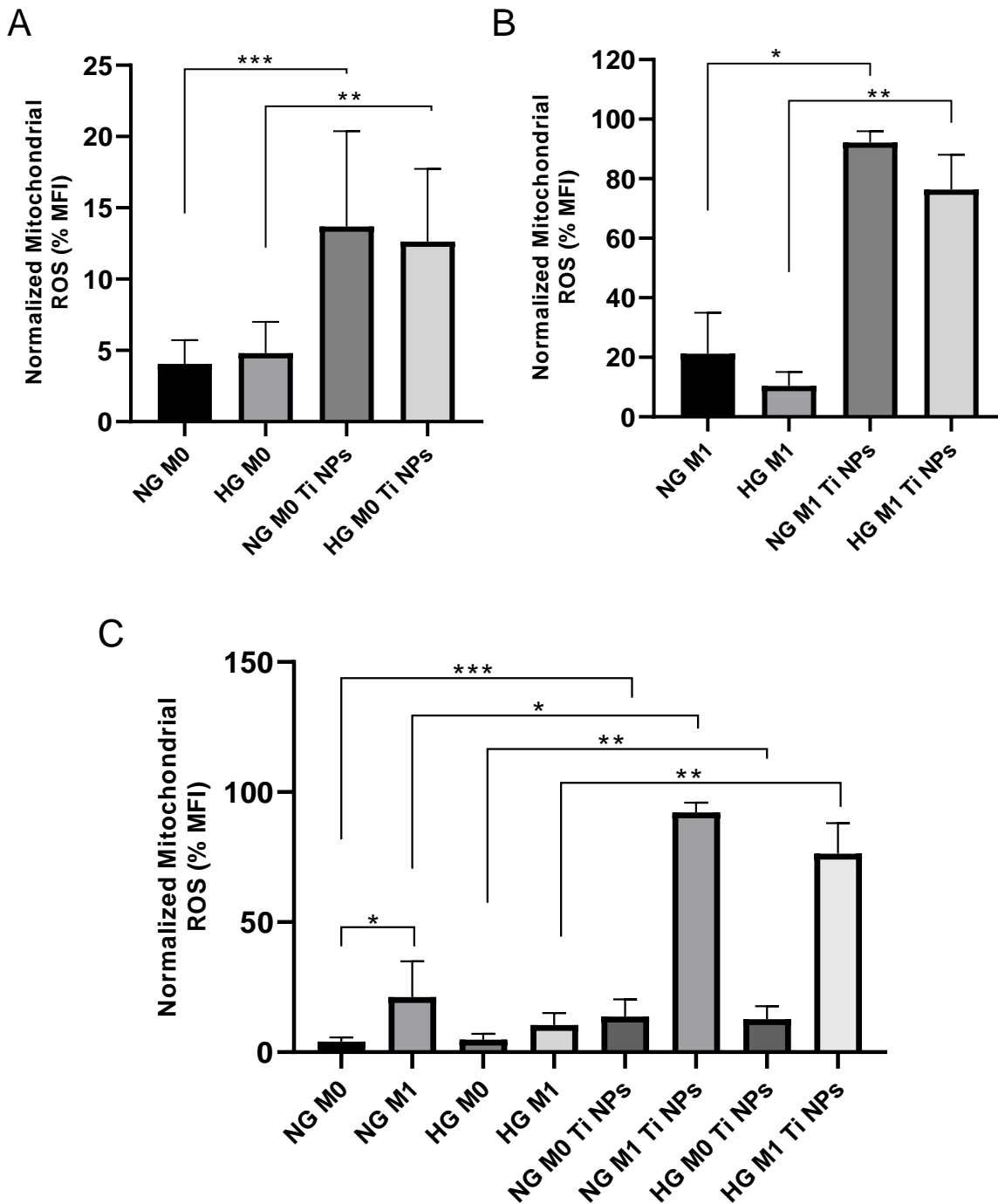
on day 5. High glucose was added 3 hours before the detection of ROS; dexamethasone was not included in the cell culture.

Figure 30 shows the differences in the mitochondrial ROS release for multiple pairs of macrophage conditions by comparing the medium fluorescence intensities (MFI), which represent a fraction of ROS per mitochondrion. In comparison to Ti NPs, high glucose had no effects on mitochondrial ROS release in both macrophage subtypes (Figure 30A, B). M1 macrophages produced significantly higher amount of ROS in comparison to M0 macrophages, which was by the average of 5.2 times higher for NG condition and 2.7 times higher for HG (Figure 30C, D). Ti NPs enhanced mitochondrial ROS release by the average of 3.4 times in M0 macrophages cultured in NG and 2.6 times in HG conditions (Figure 30F, H). In M1 macrophages, Ti NPs enhanced ROS release by the average of 4.3 times in NG and 7.3 times in HG conditions (Figure 30G, E).

The maximal ROS signal was detected in M1 macrophages exposed to Ti NPs, which is easier to see in the summary graph of all ROS normalized responses (Figure 31C). Although the effect in upregulation of ROS by Ti NPs was detected on average to be smaller in M0 macrophages, in comparison to M1 macrophages cultured in NG conditions, this effect was more significant (Figure 31A, B). To summarize, there was no potentiation of ROS release by hyperglycemia alone, however, hyperglycemia cooperated with Ti NPs in the enhancement of ROS release by M1 or M0 macrophages.



**Figure 30. Effect of titanium nanoparticles on mitochondrial ROS release in M0 and M1 macrophages cultured in normal and high glucose conditions.** Fluorescence was measured by FACS CANTO. DCF for measuring total intracellular ROS staining recorded in FITC channel; MitoTracker in APC channel for mitochondrial membrane potential; and MitoSOX in PE channel for mitochondrial ROS. MFI represent medium fluorescence intensity. The results are presented for 7 individual donors as a fraction of total ROS per mitochondrion. The cells were stimulated for 24 hours with 100ppm Ti NPs. Statistical analysis was performed using paired two-tailed t-test. \* $p < 0.05$ , \*\* $p < 0.01$ . **A.** ROS by M0 in NG versus HG **B.** ROS by M1 in NG versus HG. **C.** ROS by M0 versus M1 in NG. **D.** ROS by M0 versus M1 in HG. **E.** ROS by M1 versus M1 with Ti NPs in NG. **F.** ROS by M0 versus M0 with Ti NPs in NG. **G.** ROS by M1 versus M1 with Ti NPs in HG. **H.** ROS by M0 versus M0 with Ti NPs in HG.



**Figure 31. Effect of titanium nanoparticles on mitochondrial ROS release in summary.** Fluorescence was measured by FACS. Each bar represents the mean value from 7 individual donors calculated from the fraction of total ROS per mitochondrion. The values are normalized to maximum as 100%. The error bars are represented by SEM. Statistical analysis was performed using paired two-tailed t-test. \* $p < 0.05$ , \*\* $p < 0.01$ . **A.** Mitochondrial ROS released by M0 macrophages in NG or HG in presence or absence of 100ppm Ti NPs. **B.** Mitochondrial ROS released by M1 macrophages in NG or HG in presence or absence of 100ppm Ti NPs. **C.** Summary of A and B.



### 3.9 Affymetrix gene expression analysis of transcriptome in macrophages exposed to Ti NPs in normal and hyperglycemic conditions

To analyze the effect of Ti NPs on global transcriptional profiles of M1 and M2 polarized macrophages cultured in normal and high glucose conditions, Affymetrix GeneChips microarray assay was performed. According to the experimental model of this study, the monocytes were stimulated with pro(IFN $\gamma$ )/anti(IL4)-inflammatory factors and cultured in presence or absence of 100 ppm Ti NPs in NG or HG conditions. The macrophages cultured for 6 days were taken immediately for RNA isolation. The extracted samples with RNA yield at least 100 ng were used in microarray analysis. The samples were further tested for RNA integrity (RIN) by the services of the core Affymetrix facility. During the corresponding test, according to the recommendations by Affymetrix services, the RNA samples, which revealed RIN below 7 were taken for analysis. Microarray analysis of macrophage gene expression for the conditions listed above revealed only 4 different clusters of genes (Figure 32). A cluster represented by  $\alpha$ , corresponded to M1 macrophages cultured in presence of NG; cluster  $\beta$  to M2 macrophages cultured in NG; cluster  $\gamma$  to M1 macrophages exposed cultured in NG or HG in presence of Ti NPs and cluster  $\delta$  to M2 macrophages cultured in NG or HG in presence of Ti NPs.

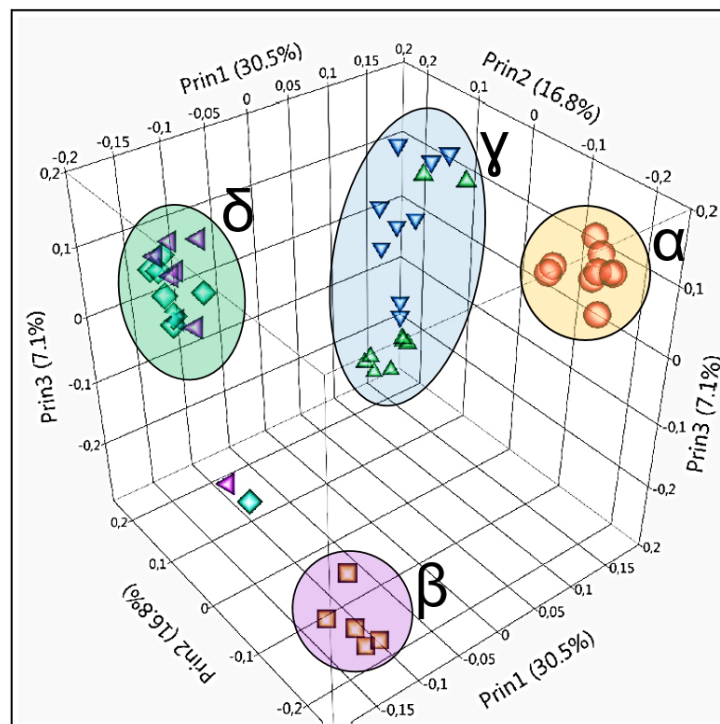


**Figure 32. Clustering of the microarray data in a 3D scatterplot.** Each sphere represents macrophages cultured for 6 days under different stimulations. Ti NPs of 100ppm concentration were used.  $\alpha$  (yellow) - stimulation with IFN $\gamma$ (M1) in normal glucose (NG= 5mM glucose) conditions;  $\beta$  (purple) - stimulation with IL4(M2) in NG;  $\gamma$  (blue) stimulation with IFN $\gamma$ (M1) and Ti NPs in NG (purple triangles) and HG (green squares) conditions;  $\delta$  (green) stimulation with IL4(M2) and Ti NPs in NG (blue triangles) and HG (green triangles) conditions.

A total of 6000 genes were differentially expressed after stimulation with Ti NPs for 6 days in M1 (IFN $\gamma$ ) macrophages and 5223 genes in M2 (IL4) macrophages (Figure

33A, B). In the comparison of M1 alone versus M1 with Ti NPs, 4950 genes were found statistically significant in NG and 3619 in HG; 2569 genes were in common with NG and HG (Figure 33A). In the comparison of M2 alone versus M2 with Ti NPs, 4269 genes were found in NG and 4091 in HG: 3137 genes were in common (Figure 33B). Figure 33C illustrates how the differences in gene expression used in characterization of M1 (IFN $\gamma$ ) and M2(IL-4) profiles change when the cells are stimulated with Ti NPs and HG. A total of 7915 genes were differentially expressed in comparison of M1 and M2 macrophages in all three conditions: control (w/o Ti NPs); exposed to Ti NPs alone and exposed to Ti NPs in synergy with HG (Figure 33C).

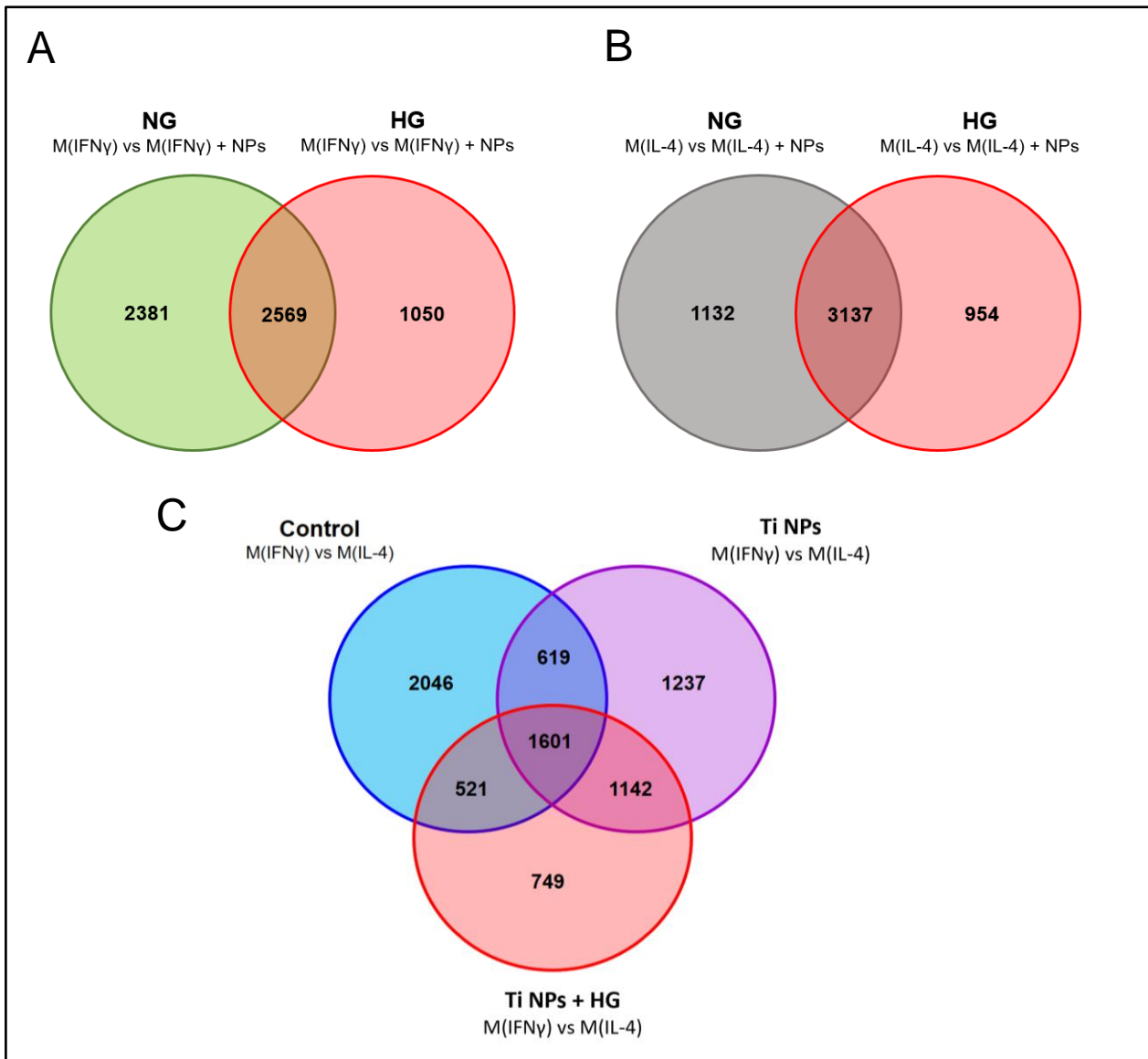


**Figure 33. Summary of Affymetrix microarray analysis of gene expression in macrophages exposed to Ti NPs in presence of NG and HG conditions. A.** Venn's diagram of differentially expressed genes by M1 versus M1 exposed to Ti NPs cultured in NG and HG. **B.** Venn's diagram of differentially expressed genes by M2 versus M2 exposed to Ti NPs cultured in NG (gray) and HG. **C.** Venn's diagram of differentially expressed genes in M1 (IFN $\gamma$ ) versus M2 (IL4) macrophages cultured in control (blue) - w/o Ti NPs and in presence of NG; Ti NPs (purple) - exposed to Ti NPs and in presence of NG and Ti NPs + HG – exposed to Ti NPs and in presence of HG.

4787 genes were differentially expressed between M1 and M2 in control. 4599 genes were found to be differentially expressed in presence of Ti NPs, in which 2220 (a half of those genes) remained the same between control and stimulation with Ti NPs, 4013 genes were found statistically significant in presence of Ti NPs in synergy with HG. Only 749 (less than a quarter) genes were differentially expressed in presence of HG with Ti NPs and not common with other genes.

For further analysis the focus was directed towards pro-inflammatory (M1) genes to narrow down the number of genes involved in regulation of macrophage responses by Ti NPs and hyperglycemia. A total of 10 genes that were differentially expressed in M1 versus M1 exposed to Ti NPs with maximal fold change were selected (Table 20). The threshold of P-value = 0.005 was chosen. In the comparison of M1 versus M1 exposed to Ti NPs in NG conditions, 4 genes were selected: MT1G, OLR1, MME, which were upregulated by the average of 3.4, 2.6 and 2.4 times and CXCL9 was downregulated by the average of 6.2 times. In the comparison of M1 versus M1 exposed to Ti NPs in HG conditions, 6 genes were selected: DCSTAMP, ORM1, CSF1, MT1X, CXCL8, which were upregulated by the average of 4.1, 3.9, 3.1, 3.1 and 2.6 times, and CXCL10 downregulated by the average of 6.2 times.

**Table 20: Differentially expressed genes in M1 macrophages exposed to Ti NPs in NG and HG.**

Gene name	Fold change	p-value	TPM* in inflammatory macrophages
<b>Comparison of M1 in NG with M1 in NG exposed to Ti NPs</b>			
<b>MT1G</b>	3,39	7,99E-09	165
<b>OLR1</b>	2,57	9,65E-06	27
<b>MME</b>	2,42	2,04E-11	15
<b>CXCL9</b>	-6,19	2,29E-23	3
<b>Comparison of M1 in HG with M1 in HG exposed to Ti NPs</b>			
<b>DCSTAMP</b>	4,12	5,93E-12	230
<b>ORM1</b>	3,87	9,97E-10	2
<b>CSF1</b>	3,13	4,85E-16	102
<b>MT1X</b>	3,06	1,03E-11	56
<b>CXCL8</b>	2,58	3,66E-03	395
<b>CXCL10</b>	-6,19	6,32E-24	5

\*Transcripts per million (TPM), is a normalized method for transcriptomic studies. TPM is a unit to estimate gene expression RNA-based and it is expressed as number/1X10<sup>6</sup> RNA counts<sup>196</sup>.

### 3.10 RT-PCR analysis and validation of selected Ti NPs-induced biomarkers

To confirm the results obtained by microarray analysis the following genes were validated via RT-PCR: DCSTAMP, OLR1, ORM1, MME and CSF1 (Figure 34); CXCL8, CXCL9, CXCL10, MT1X and MT1G (Figure 35). The expression of these genes was measured in M1 macrophages cultured for 6 days in presence or absence of 100 ppm Ti NPs in normal and high glucose conditions.

In macrophages cultured in NG, Ti NPs upregulated expression of DCSTAMP by the average of 10 times and in HG by the average of 20 times. These effects were similar in 5 individual donors and the strongest effect was 25 fold change in HG. Hyperglycemia enhanced Ti NPs-induced DCSTAMP expression by the average of 1.8 times (Figure 34A). Ti NPs upregulated expression of OLR1 by the average of 7.4 times in NG and by the average of 25 times in HG. These effects were similar in 5 individual donors and the strongest effect was 44 fold change in HG. Hyperglycemia enhanced Ti NPs-induced OLR1 expression by the average of 1.5 times (Figure 34B). Ti NPs upregulated expression of ORM1 by the average of 21 times in NG and by the average of 61 times in HG. The strongest effect was 3111 fold change in HG. Hyperglycemia enhanced Ti NPs-induced ORM1 expression by the average of 1.7 times (Figure 34C). Ti NPs upregulated MME expression by the average of 91 times in NG and by the average of 148 times in HG. The strongest effect was 266 fold change in NG. Hyperglycemia did not enhance Ti NPs-induced upregulation in expression of MME (Figure 34D). Ti NPs upregulated expression of CSF1 by the average of 4.5 times in NG and by the average of 8.5 times in HG. The strongest effect was 22 fold change in HG. Hyperglycemia enhanced Ti NPs-induced CSF1 expression by the average of 1.5 times (Figure 34E). Surprisingly, Ti NPs did not have an effect on expression of CXCL8 in presence of NG or HG; also, HG in absence of Ti NPs did not affect CXCL8 expression (Figure 35A). Ti NPs downregulated CXCL9 expression by the average of 88 times in NG and by the average of 122 times in HG. The strongest downregulation effect was 681 fold change in HG. Hyperglycemia did not potentiate Ti NPs-induced suppression CXCL9 expression (Figure 35B). Ti NPs downregulated CXCL10 expression by the average of 61 times in NG and by the average of 77 times in HG. The strongest downregulation effect was 302 fold change in HG. Hyperglycemia potentiated Ti NPs-induced suppression of CXCL10 expression by the average of 1.5 times (Figure 35C). Ti NPs upregulated MT1X expression by the average of 7 times in NG and by the average of 12 times in HG. The strongest effect was 54 fold change in HG. Hyperglycemia enhanced Ti NPs-induced upregulation in expression of MT1X by the average of 1.6 times (Figure 35D). Ti NPs upregulated MT1G expression by the average of 18 times in NG and by the average of 12 times in HG. The strongest effect was 177 fold change in NG. Hyperglycemia did not enhance Ti NPs-induced upregulation in expression of MT1G (Figure 35E).

In summary, hyperglycemia significantly cooperated with Ti NPs-induced expression of CSF1 and Ti NPs-induced suppression of CXCL10. It is still possible that hyperglycemia cooperates with other genes from the validation list, however, more sample size is required for statistical analysis. In total, the validation of genes was successful for all candidates except CXCL8, which did not match the calculation of fold change in gene expression. This could be explained by the highest P-value of CXCL8 listed in Table 20.

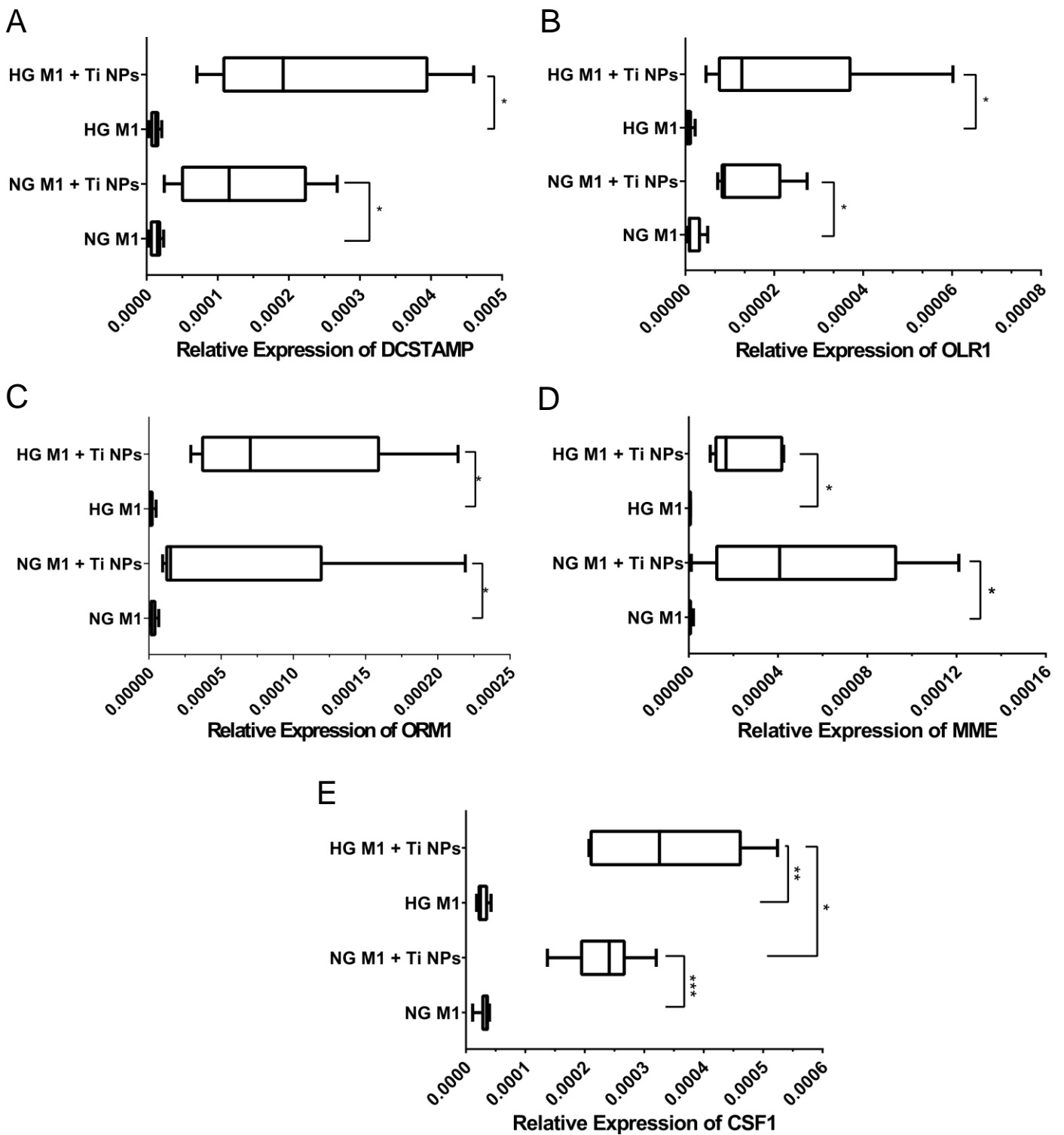


**Figure 34. Effect of Ti NPs and HG on expression of DCSTAMP, OLR1, ORM1, MME and CSF1 in M1 macrophages.** Levels of gene expression were detected with RT-PCR for macrophages cultured for 6 days in presence of absence of 100ppm Ti NPs. **A.** The expression of DCSTAMP, **B.** OLR1, **C.** ORM1, **D.** MME and **E.** CSF1. Each bar represents the mean value of expression from 5 individual donors. Statistical analysis was performed using paired two-tailed and one-tailed t-test. \*\* $p < 0,01$ , \* $p < 0,05$ . The error bars are represented by SEM.

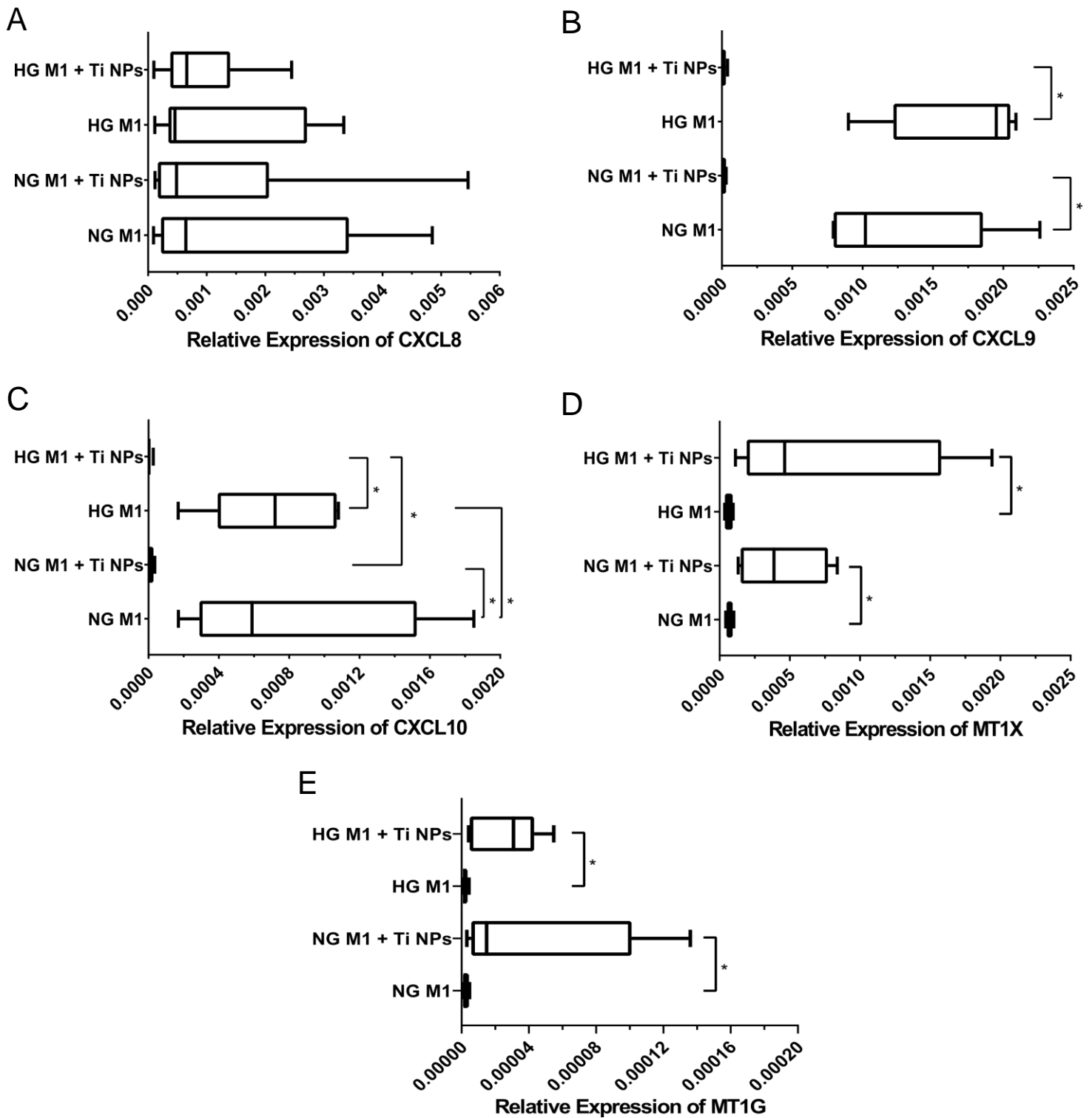


**Figure 35. Effect of Ti NPs and HG on expression of CXCL8, CXCL9, CXCL10, MT1X and MT1G in M1 macrophages.** Levels of gene expression were detected with RT-PCR for macrophages cultured for 6 days in presence of absence of 100ppm Ti NPs. **A.** The expression of CXCL8, **B.** CXCL9, **C.** CXCL10, **D.** MT1X and **E.** MT1G. Each bar represents the mean value of expression from 5 individual donors. Statistical analysis was performed using paired two-tailed and one-tailed t-test. \* $p < 0,05$ . The error bars are represented by SEM.

## 4 DISCUSSION

### 4.1 Interaction of Ti NPs with macrophages

It has been revealed by multiple studies that Ti NPs are toxic and promote sustained production of pro-inflammatory factors, which result in acute and chronic inflammation<sup>197–201</sup>. Titanium implants are a source of Ti NPs in human tissues. Despite good mechanical properties, corrosion resistance and low magnetic susceptibility of titanium, degradation of implants composed of titanium and titanium alloys is still a medical challenge<sup>202,203</sup>. The size of the particles released from implant surfaces range from the nanometer to micrometer scale, but the nanoparticles of smaller diameter size tend to generate the most biological toxicity<sup>12,38</sup>. In the present study, the rutile Ti NPs with a diameter of 15 nm were addressed as a major driving element of implant-related inflammation and were evaluated at different concentrations.

Periprosthetic osteolysis is a condition that originates from chronic inflammatory responses prompted by implant-derived particulate debris, which triggers recruitment of macrophages, fibroblasts, lymphocytes and osteoclasts<sup>133</sup>. The clearance of the foreign material, such as Ti NPs, is accomplished by phagocytosis, which is performed by pro-inflammatory macrophages<sup>38,204</sup>. However, the fibrotic tissues, which are primarily found in the peri-implant areas of patients with implants, are known to be rich in anti-inflammatory macrophages<sup>204,205</sup>. In this study, the effect of Ti NPs on macrophage responses was investigated in M0 (non-activated), M1 (pro-inflammatory) and M2 (anti-inflammatory macrophages).

In the first step of the study, the viability/metabolic activity of human M0, M1 and M2 macrophages was assessed in the presence of 25, 50, 100 and 200 ppm Ti NPs, which is equivalent to the concentrations of 25, 50, 100 and 200 µg/ml. After 24 h and 6 days of TI-NPs stimulation, macrophage viability was not reduced in the presence of Ti NPs in the entire range of concentrations. However, the viability in all macrophage subtypes cultured for 6 days was increased in the presence of all concentrations of Ti NPs tested in comparison to cells cultured only for 24 hours (section 3.2.2). In murine macrophages, pure rutile TiO<sub>2</sub> NPs of 30 and 100 nm diameter sizes at all concentrations (50, 100, 200, 300, and 400 mg/mL) decreased cell viability, phagocytic rate, and phagocytic index in a concentration-dependent manner, followed by autophagy<sup>206</sup>. In primary human osteoblasts, it was reported that anatase Ti NPs at concentrations 5, 10, 50 and 100 µg/ml do not affect cell viability<sup>207</sup>, which is in agreement with the results of this study. In contrast, silver nanoparticles (Ag NPs) induce significantly higher cell toxicity than Ti NPs. In murine macrophages, after 4 ppm Ag NPs, the cell viability started to decline, and 25 ppm Ag NPs is already considered very toxic<sup>208</sup>. However, zinc oxide nanoparticles (ZnO NPs) are considered to be less toxic than Ti NPs; in mouse alveolar macrophages, they didn't induce toxicity at concentrations of 3.5 mg/ml<sup>209</sup>. Therefore, the effects of Ti NPs are defined by affecting macrophages differentiation and polarization, but not their survival.

#### 4.1.1 Effect of Ti NPs on production of CHI3L1

A glycoprotein, CHI3L1, is expressed in humans and produced by macrophages, neutrophils, synoviocytes, chondrocytes, airway epithelial cells, vascular smooth muscle cells, and cancer cells<sup>210,211</sup>. In combination with other inflammatory molecules, CHI3L1 can be used as a biomarker in cancer, inflammation, tissue remodeling and fibrosis such as arthritis, asthma, multiple sclerosis, preclinical Alzheimer's disease,

heart failure and diabetic disorders<sup>176–179,212</sup>. Previously, the effect of Ti NPs, Ti microparticles and titanium surfaces on the expression and secretion of CHI3L1 was analyzed by Gudima, 2017, but Ti NPs-induced inflammation was not addressed in detail<sup>182</sup>. CHI3L1 is involved in inflammation and tissue remodeling and potentially can be associated with implant-related complications<sup>173</sup>. It is known that the fibrotic tissues often surround the titanium implant surfaces<sup>213</sup>. Using immunohistochemical analysis, positive staining for excessive production of CHI3L1 was detected in areas with fibrosis, concluding that excessive CHI3L1 production can cause extracellular matrix accumulation leading to tissue fibrosis<sup>214,215</sup>.

In this study, for the first time, the effect of two different concentrations of Ti NPs on the production of CHI3L1 was investigated. The data presented by Gudima, 2017 demonstrates that CHI3L1 production is primarily induced by M1 macrophages and the data of the current investigation is consistent with these findings<sup>182</sup>. In all macrophage subtypes, the secretion levels of CHI3L1 were increased in a concentration-dependent manner (section 3.4.2).

In the absence of Ti NPs, the secretion levels of CHI3L1 were about 3.3 ng/ml in M0 macrophages, 338 ng/ml in M1 macrophages and 7 ng/ml in M2 macrophages. In a study about osteoarthritis, it was demonstrated that the serum levels of CHI3L1 in healthy adults is 102 µg/l (ng/ml)<sup>216</sup>. In patients with severe trauma of the knee, the levels increase to 1277 ng/ml, and in patients with late-stage osteoarthritis the levels increase to 1928 ng/ml<sup>216</sup>. The present study reveals that in the presence of 100 ppm Ti NPs the secretion levels of CHI3L1 macrophages reach the average of 1222 ng/ml, which is very close to the pathological concentrations of CHI3L1 at the late stages of osteoarthritis and in severe trauma of the knee.

An increase in secretion of CHI3L1 induced by Ti NPs in M1 macrophages was found in all donors. However, the expression of CHI3L1 was not significantly upregulated in M1 macrophages by Ti NPs, because it was found only in about 50% of the donors; this data is also consistent with data presented by Gudima, 2017<sup>182</sup>. This suggests that there are differential mechanisms that control Ti NPs-induced CHI3L1 secretion and expression. Another possible explanation could be that the peak of CHI3L1 expression does not actually occur on day 6 (when the macrophages were harvested in the corresponding study) but sometime sooner, while the secreted levels of CHI3L1 accumulate over time and remain stable for protein detection. It has been shown that elevation of CHI3L1 levels in blood serum can be detected as soon as 3 hours after the stimulus<sup>214</sup>. Additional experiments need to be done to elaborate on the time peak of CHI3L1 expression induced by Ti NPs in human primary macrophages used as the experimental model of this study.

In contrast to the M1 results, in anti-inflammatory (M2) macrophages, the expression of CHI3L1 was upregulated by Ti NPs in a concentration-dependent manner similar to secretion (section 3.3.1 compared to 3.4.2). M2 macrophages can be present at the phase of resolution of inflammation, healing and in areas of fibrosis. It has been shown previously that increased production of CHI3L1 leads to tissue fibrosis<sup>173,215,217</sup>. Also it has been revealed that inhalation of Ti NPs induces renal fibrosis in mice via upregulation of the TGF-beta pathway<sup>218</sup>. It would be constructive to investigate the effect of Ti NPs on the production of TGF-beta in correlation with increased CHI3L1 production in M2 macrophages. Activation of CHI3L1 expression in M2 macrophages is probably physiologically important, because it could have a protective function against pathogenic invasion. It has been found that in CHI3L1-/- mice the protection against fungal-associated allergic airway inflammation is lost during M2 (IL-4)-type responses<sup>219</sup>.



#### 4.1.2 Effect of Ti NPs on production of CHIT1 and localization

Chitotriosidase (CHIT1) is a functional chitinase and contains a catalytically active Glyco\_18 domain, which is inactive in CHI3L1<sup>171,175</sup>. CHIT1 can also be secreted by human monocyte-derived macrophages and its pathological release makes it a key biomarker for the lysosomal storage Gaucher disease<sup>220</sup>. CHIT1 is associated with macrophage activation, it is expressed by macrophages and neutrophils and found in the lungs and circulation<sup>171,174</sup>. High levels of CHIT1 expression have been detected via RT-PCR analysis of periprosthetic soft tissue from osteolysis patients<sup>13</sup>. Gene expression profiling of peri-implant tissue around failing implants revealed upregulation of CHIT1 in synovial fluid from patients<sup>221</sup>. The effect of polished titanium disks (Ti disks) on CHIT1 expression in M0, M1 and M2 macrophages was evaluated for the first time by Gudima, 2017; the results did not reveal any significant effect of Ti disks on the upregulation of CHIT1 expression in all macrophage subtypes<sup>182</sup>. However, in the same study by Gudima, 2017, porous titanium and Ti NPs induced upregulation of CHIT1 expression in macrophages. These results are in agreement with the results of this study: Ti NPs promoted upregulation in CHIT1 expression in M0, M1 and M2 subtypes, with a maximum upregulation effect in M0.

Additionally, the effect of two concentrations of Ti NPs (25 and 100 ppm) on CHIT1 exochitinase activity, defined by the hydrolytic capacity of the enzyme was investigated in this study. Interestingly, the lowest dose (25 ppm) of Ti NPs induced a significant increase in CHIT1 activity in all macrophage subtypes, however, the higher dose (100 ppm) of Ti NPs did not influence any changes on the activity in comparison to the control conditions (section 3.4.4). It is possible that during the attempt to recycle Ti NPs, the higher dose clogged the vesicular trafficking machinery. Although CHIT1 was produced inside the cells, as the data with CHIT1 gene expression shows (section 3.3.1), it could not get secreted. The confocal analysis of CHIT1 localization in the presence of 100 ppm Ti NPs revealed a higher intensity of CHIT1 staining inside the cells in comparison to control conditions (section 3.7), which implies that there is a substantial amount of CHIT1 inside the cells in the presence of a higher dose of Ti NPs.

In M1 macrophages, Ti NPs promoted CHIT1 localization in the Trans-Golgi network (TGN) (section 3.7). However, in the presence of Ti NPs, the TGN signal was not detected at all in M0 and M2 macrophages in comparison to M0 and M2 unexposed to Ti NPs. The TGN compartment of M0 and M2 macrophages was completely disrupted in the cells that have been exposed to Ti NPs. In primary bone marrow-derived macrophages, it has been shown that the disruption of TGN can be caused by activators of the NLRP3 inflammasome, which leads to apoptosis through the activation of a caspase-1 and IL-1 $\beta$ -dependent mechanism<sup>222</sup>. *In vitro*, Ti NPs ingested by human macrophages and intestinal epithelial cells induce assembly of NLRP3-ASC-caspase-1 and NLRP3-dependent release of IL-1 $\beta$  and IL-8<sup>80</sup>. Studies in mice revealed that gold nanoparticles (Au NPs) trigger Golgi disruption, which can lead to a cell adhesion-related protein processing disorder<sup>223</sup>. It is possible that M1 macrophages could be more tolerant to apoptotic effects generated by Ti NPs in comparison to M0 and M2 macrophages. However, more studies need to be done to evaluate the effects of TGN disruption in M0 and M2 macrophages by Ti NPs.

One of the major evolutionary functions of CHIT1 is defense against pathogens through degradation of chitin. Chitin is a major component in a cell wall of fungi and exoskeleton of arthropods<sup>171</sup> and it is abundantly found in the environment and often inhaled by the lungs, damaging alveolar epithelial cells and phagocytosed by alveolar

macrophages<sup>224</sup>. CHIT1 has been implicated in pathogenesis and considered as a biomarker of pulmonary fibrosis, bronchial asthma, COPD and pulmonary infections<sup>224</sup>. Alternatively to implant materials, other routes of exposure to Ti NPs are through inhalation from industrial sources such as paints, plastic, rubber, papermaking and fiber. In this scenario, alveolar macrophages are interacting with Ti NPs. Since in mice inhalation of Ti NPs promotes upregulation of the TGF-beta pathway<sup>218</sup>, it is logical that CHIT1 enhances TGF- $\beta$ 1 receptor expression and signaling<sup>225</sup>. Several studies have shown that the uptake of the nanoparticles worsen respiratory disorders such as pulmonary fibrosis or LPS-induced lung inflammation<sup>74,76</sup>. It is feasible that Ti NPs start resembling nonspecific pathogenic invasion and as part of the defense mechanism the expression of CHIT1 in macrophages is significantly increased (section 3.3.1). For instance, toll-like receptors (TLRs) are responsible for recognizing specific pathogen-associated molecular patterns during activation of innate immunity; it has been revealed that gold nanoparticles immobilize with  $\alpha$ -mannose as carriers for a TLR7 ligand, which sequentially can act as a trigger to activation of a pathogenic response<sup>226</sup>. Ti NPs could also immobilize with several extracellular ligands, upstream components of the innate immune system, which promote activation of CHIT1 expression for the purposes of pathogen resolution. For instance, it has been found that upon entering the cell, Ti NPs interact with TLRs and promote the associated inflammatory responses<sup>227</sup>.

### 4.1.3 Effect of Ti NPs on CCL18 suppression

C-C motif chemokine 18 (CCL18) is secreted by anti-inflammatory macrophages and expressed in numerous organ tissues with the highest expression detected in the lungs and lymph nodes<sup>228–230</sup>. However, the presence of mRNA of CCL18 is only detected in monocytes/macrophages and dendritic cells<sup>231–233</sup>. In the literature, CCL18 can also be found by other names: macrophage inflammatory protein-4 (MIP-4), alternative macrophage activation associated CC chemokine-1 (AMAC-1) pulmonary and activation-regulated chemokine (PARC) and dendritic cell (DC)-chemokine 1 (DC-CK1)<sup>230,233–235</sup>. Elevated production of CCL18 has been detected in alternatively-activated macrophages<sup>233</sup> and represent pathological conditions connected to chronic inflammatory and fibrotic diseases, such as rheumatoid arthritis (RA) and Gaucher's disease<sup>231,236</sup>. In Gaucher disease and lung inflammation disorders, CCL18 is often investigated in association with CHIT1<sup>237</sup>. The effect of titanium surfaces, microparticles and nanoparticles on CCL18 production was investigated for the first time by Gudima, 2017, however, in this study different concentrations of Ti NPs were addressed<sup>182</sup>.

It was found that Ti NPs suppress CCL18 production in a dose-dependent manner (section 3.3.2 and section 3.4.3). The average secretion of CCL18 in M2 macrophages was suppressed by 25 ppm Ti NPs from 541 ng/ml to the average of 317 ng/ml, and by 100 ppm Ti NPs suppressed to the average of 20 ng/ml (section 3.4.3). Increased production of CCL18 in serum is predominantly a biomarker of numerous cancer types including leukemia, B lymphoma, and gastric, colorectal, ovarian and lung cancers<sup>238–240</sup>. In children with acute leukemia the levels of CCL18 in blood plasma were detected to be around 100 ng/ml<sup>239</sup>. In the lung cancer studies, it has been demonstrated that local concentration of CCL18 correlated with tumor size. Recently it has been revealed that TAMs and IL-4 activated macrophages promote the invasiveness of breast cancer cells via CCL18, which is achieved by binding to the PITPNM3 receptor and the interaction (CCL18-PITPNM3) is necessary to activate intracellular calcium response that plays critical roles in the invasiveness of breast cancer cells<sup>241</sup>. Since Ti NPs are so efficient at suppression of both secretion and

expression of CCL18, in combination with other drugs they can be potentially used in the treatment of cancer at concentrations such as 100 ppm.

## **4.2 Impact of hyperglycemia on Ti NPs-induced macrophage responses**

Hyperglycemia is a critical component in the diabetic pathology. DM patients have hyperglycemic blood and can suffer from consequences triggered by compromised immune responses. Amongst those consequences are the complications produced by metal implants<sup>32,46</sup>. Uncontrolled diabetes has been associated with a high risk of dental implant failures, but the mechanisms have not been clearly defined yet<sup>242</sup>. However, it is known that elevated concentrations of glucose stimulate implant corrosion<sup>31,53,54</sup>. It was found that the corrosion of titanium dental implants is caused by low pH values, which is related to biological inflammation and hyperglycaemic conditions and can be the potential explanation to the higher probability of implant failure in patients with diabetes<sup>54</sup>. Moreover, bone growth in a hyperglycemic environment is compromised<sup>243</sup>.

Monocytes and macrophages govern inflammatory reactions in diabetes and vascular complications<sup>58,130,131</sup>. In this study, the effect of a hyperglycemic environment on Ti NPs-induced reactions in human macrophages was assessed for the first time. It was previously found that increased levels of TNF- $\alpha$  are found in rats upon the exposure to Ti NPs<sup>183</sup>. Moreover, secretion levels of TNF- $\alpha$  are elevated in the presence of high glucose in M0 and M1 macrophages cultured for 6 days and in M0, M1 and M2 macrophages cultured for 6 hours<sup>49</sup>. The results of this study revealed no influence of high glucose on TNF- $\alpha$  production in M0, M1 and M2 macrophage in any combinations with or without Ti NPs (section 3.5.1). According to the data obtained in this study, the explanation could be that a low concentration of dexamethasone (100 nM), which was applied along with every stimulation condition, inhibited the potential enhancement of TNF- $\alpha$  responses by hyperglycemia or Ti NPs. In the study by Moganti et al 2016, dexamethasone was not applied to the cell cultures<sup>244</sup>. Dexamethasone is associated with an anti-inflammatory response and TNF- $\alpha$  with pro-inflammatory; in certain conditions they can counteract each other. For instance, dexamethasone inhibits LPS-induced secretion of TNF- $\alpha$  in RAW cells<sup>142</sup>.

Increased levels of CHI3L1 are detected in patients with both, T1D and T2D, and these patients are also known to be at high risk for the development of cardiovascular diseases in comparison to non-diabetic patients<sup>179</sup>. Amongst other markers, CHI3L1 is considered to be an inflammatory marker of diabetic complications<sup>245</sup>. In our study, it was found that hyperglycemia cooperates with 100 ppm Ti NPs inducing CHI3L1 secretion in all macrophage subtypes. However, hyperglycemia cooperates less with 25 ppm Ti NPs-induced CHI3L1 secretion and only in M1 and M2 macrophages (section 3.5.3). It is very likely that in the presence of high glucose and 100 ppm Ti NPs, macrophages are extremely active and secrete more CHI3L1 protein, which accumulates over the 6 days culturing of macrophages. An analogous assumption cannot be made for the gene expression of CHI3L1, which is measured only on day 6. Nevertheless, the results of this study show that hyperglycemia cooperates with 100 ppm Ti NPs-induced expression of CHI3L1 and not with 25 ppm Ti NPs, and only in M1 and M2 macrophages (section 3.5.2). Since in all macrophage subtypes the secretion levels of CHI3L1 are synergistically enhanced by Ti NPs and high glucose, excessive production of CHI3L1 in blood plasma of diabetic patients with existing

implants could be used in the prognosis of initiated chronic inflammation related to implant failure.

Chronic hyperglycemia is recognized as a major component in the pathogenesis of diabetes-induced atherosclerosis<sup>51</sup>. Elevated plasma levels of CHIT1 and CHI3L1, derived from macrophages, are associated with atherosclerotic plaque formation. It was found that increased plasma levels of CHIT1 and CHI3L1 are detected in patients with long-lasting T2D, however the major source of these proteins was neutrophils<sup>246</sup>. Similarly to CHI3L1, the effect of hyperglycemia on Ti NPs-induced CHIT1 production was investigated in human macrophages (section 3.5.4). CHIT1 is considered a biomarker of diabetic nephropathy pathogenesis and inflammation<sup>247</sup>. The results of this study revealed that in the presence of hyperglycemia, Ti NPs, in a dose-dependent manner, upregulate CHIT1 expression for all macrophage subtypes. However, Ti NPs-induced CHIT1 expression was only potentiated by hyperglycemia in M1 macrophages (section 3.5.4). In total, hyperglycemia cooperated in the enhancement of CHIT1 expression with only a higher concentration of Ti NPs (100 ppm) in pro-inflammatory macrophages and not in other macrophage subtypes. It is important to consider that CHIT1 is not only a biomarker of diabetes but also a biomarker for molecular pathogenesis of osteolysis, since osteolysis patients have increased expression of CHIT1 in periprosthetic soft tissue<sup>13</sup>. Considering that higher concentrations of Ti NPs and hyperglycemia work in synergy in the upregulation of CHIT1 expression in M1 macrophages, it is logical to conclude that pro-inflammatory macrophages are responsible for implant failure in diabetic patients through the potentiation of CHIT1 expression via chronic exposure to hyperglycemia and implant debris.

Hyperglycemia affects macrophage polarization in atherosclerotic plaques<sup>51,248</sup>. M1 and M2 produce distinct patterns of pro/anti-inflammatory factors; if CHI3L1 is produced in high concentrations by M1 macrophages, CCL18 is selectively produced by M2 macrophages<sup>93</sup>. The effect of hyperglycemia on the macrophage polarization profile through measuring CCL18 production was assessed for the first time by Moganti et al 2016; it was revealed that hyperglycemia suppresses the production of CCL18 in primary human macrophages. Suppression of CCL18 production by titanium materials in human macrophages was demonstrated by Gudima 2017<sup>182</sup>. The independent effects of hyperglycemia or titanium materials on the production of CCL18 by primary monocyte-derived macrophages have been studied separately, however, the effects from the cooperation of hyperglycemic stimulus simultaneously applied with titanium material have not been investigated until now. In this study, the effect of hyperglycemia on Ti NPs-induced suppression of CCL18 expression and secretion was addressed for the first time (section 3.5.5). In the negative control samples with normal glucose conditions, the secretion levels of CCL18 were the highest, however, in high glucose conditions, macrophages secreted less CCL18, which is consistent with previous findings<sup>49</sup>. However, the levels of CCL18 expression were not affected significantly by hyperglycemia, which is inconsistent with the findings of Moganti et al 2016. This inconsistency can be explained by the addition of dexamethasone to the macrophage cultures in the present study. In macrophages exposed to 25 ppm Ti NPs and cultured in normal glucose conditions, the levels of CCL18 were also reduced more significantly than in macrophages cultured with high glucose alone. However, high glucose potentiated the effect of 25 ppm Ti NPs in suppression of CCL18 secretion and expression, which was not the case for 100 ppm Ti NPs. In the presence of 100 ppm of TiO<sub>2</sub> NPs, the secretion of CCL18 was completely blocked in a normoglycemic or hyperglycemic environment, which implies that the inhibition of CCL18 is primarily driven by pro-inflammatory responses generated by Ti NPs and not by high glucose. However, it does not mean that there is no inhibition that comes from high glucose, but

the effect of Ti NPs has a much higher magnitude, and it hinders the effect of hyperglycemia. Nevertheless, Ti NPs shift the macrophage profile from the anti-inflammatory to pro-inflammatory subtype via suppression of CCL18 production and hyperglycemia can cooperate to some level with this effect, which explains why in diabetic patients the risk for implant-mediated inflammation is higher.

### 4.3 Role of dexamethasone in Ti NPs-induced CHIT and CHI3L1 responses

Glucocorticoids are often used as anti-inflammatory drugs to suppress inflammation in chronic inflammatory diseases<sup>249</sup>. Dexamethasone is a synthetic glucocorticoid with a higher potency than natural glucocorticoids, and is able to inhibit pro-inflammatory responses in macrophages and promote M2 polarization<sup>93,95</sup>. In this study, the effect of 100 nM dexamethasone on Ti NPs-induced expression of CHI3L1 and CHIT1 in pro-inflammatory macrophages was investigated (section 3.6). In normal glucose, dexamethasone decreased CHI3L1 expression in M1 macrophages by an average of 2.7 times, however it had no effect on Ti NPs-induced expression of CHIT1. This is consistent with the findings that CHI3L1 release from cultured human monocyte-derived macrophages is inhibited by dexamethasone especially in pro-inflammatory macrophages<sup>250</sup>. Dexamethasone is used in treatments with titanium implants to prevent metal wear debris-dependent aseptic loosening<sup>154</sup>. Dexamethasone-filled titanium nanotubes decrease pro-inflammatory responses (TNF- $\alpha$  and IL1 $\beta$ ) in macrophages and enhance osteoblast differentiation<sup>251</sup>. In the presence of 100 nM dexamethasone, the suppression of Ti NPs-induced CHI3L1 expression was not detected. It is possible that the concentration of dexamethasone used in this study was not high enough to have an effect; another explanation is that dexamethasone alleviates titanium implant-related inflammation through some independent mechanism to CHI3L1. In high glucose, dexamethasone had no effect on CHI3L1 expression in the absence of Ti NPs, however, in the presence of Ti NPs, dexamethasone downregulated CHI3L1 expression by an average of 2 times (section 3.6.1). It has been previously found that dexamethasone at 100nM inhibits glucose transport by causing translocation of glucose transporters from the plasma membrane to an internal location<sup>147,252</sup>. Since in high glucose the production of CHI3L1 is elevated in M1 macrophages exposed to Ti NPs (section 3.5.2 and 3.5.3), it is possible that dexamethasone inhibits the cooperation of Ti NPs and high glucose via inhibiting some intracellular transport component of glucose.

Previously, there have not been many direct studies conducted about the effects of dexamethasone on CHIT1 production. However, it has been revealed that treatment with corticosteroids causes a decrease in the CHIT1 activity in patients with active sarcoidosis<sup>232</sup>. Dexamethasone suppressed CHIT1 expression by an average of 3.2 times. In contrast to the CHI3L1 results, dexamethasone enhanced Ti NPs-induced CHIT1 expression by an average of 2.9 times in all 5 individual donors. In high glucose, dexamethasone downregulated the expression of CHIT1, however, it had no effect on Ti NPs-induced expression of CHIT1 (section 3.6.2). Dexamethasone is used in the prevention of osteolysis<sup>154</sup>, however, in the present study, it enhances CHIT1 expression in macrophages exposed to Ti NPs instead of inhibiting. These findings suggest that although dexamethasone is used in the treatment of acute inflammation, the anti-inflammatory function of it is not concrete and the mechanisms of its action are more complex than we think, since it may have pro-inflammatory characteristics on a

chronic level. Increased expression of CHIT1 is found in periprosthetic soft tissues and considered a biomarker of implant-mediated inflammation and osteolysis<sup>13</sup>. This topic needs to be further investigated and the positive effects of dexamethasone and the potential biomarker characteristics of CHIT1 in implant failure need to also be addressed.

### 4.4 Effect of Ti NPs on mitochondrial ROS release

ROS play an important role in many inflammatory disorders, skin aging, and cancer formation<sup>157,158,253</sup>. Production of ROS is induced by Ti NPs, which leads to activation of inflammatory responses in macrophages<sup>165,194</sup>. It has been revealed that Ti NPs trigger ROS release, induce inflammatory reactions in primary human macrophages and intestinal epithelial cells, and worsen acute colitis in mice after oral administration through accumulation in the spleen and inflammation<sup>80</sup>. Ti NPs can induce cell toxicity by disrupting the mitochondrial-associated ER membranes and calcium ion balance via increasing the autophagy<sup>195</sup>. In this study, the effect of Ti NPs on mitochondrial ROS release was investigated for M0 and M1 macrophages cultured in normal and high glucose conditions.

Initially, the experiment was performed in the presence of 100 nM dexamethasone, in which case, there was no total intracellular or mitochondrial ROS detected for any of the conditions (data not shown). These findings are consistent with published data. For instance, it has been previously found that 4 mg of dexamethasone injected intravenously into human subjects inhibited ROS generation by mononuclear cells and polymorphonuclear leukocytes<sup>254</sup>. Also it has been revealed that dexamethasone suppresses production of Nox-dependent ROS in activated microglial cells<sup>255</sup>. In contrast, dexamethasone promotes ROS generation and mitochondria-dependent apoptosis in RAW 264.7 cells<sup>256</sup>. However, in human macrophages, LPS-dependent ROS production is suspected to be inhibited by glucocorticoids<sup>140,141</sup>.

In the absence of dexamethasone, M1 macrophages generated a significant amount of ROS in comparison to M0 macrophages, which was by an average of 5.2 times higher in normal glucose and 2.7 times higher in high glucose conditions (section 3.8). Ti NPs enhanced ROS production in M1 macrophages by an average of 4.3 times in normal glucose and 7.3 times in high glucose. In M0 macrophages, Ti NPs induced ROS production to about the same level of M1 macrophages alone without Ti NPs, which was higher by an average of 3.4 times in normal glucose and 2.6 times in high glucose in comparison to M0 macrophages not exposed to Ti NPs.

It is known that chronic hyperglycemia induces oxidative stress and endothelial cell dysfunction via ROS-dependent mechanisms<sup>257</sup>. In this study, there was no potentiation of ROS release by hyperglycemia independently (section 3.8). This could be explained by the fact that the cells were stimulated with high glucose only for 3 hours, which rather represents an acute hyperglycemia. Both, acute and chronic high glucose in diabetes increases the production of ROS<sup>258</sup>. In the model of this study, monocytes were isolated from healthy individuals, but not from the diabetic patients, which can explain this inconsistency of the findings. Nevertheless, acute hyperglycemia cooperated with Ti NPs in the enhancement of ROS release by M1 or M0 macrophages.

In total, Ti NPs significantly enhance ROS production in pro-inflammatory macrophages and activate ROS release in the resting (M0) macrophages by, probably, promoting polarization of M0 towards the pro-inflammatory state. It is believed that in

macrophages the pro-inflammatory effects of NPs in the induction of ROS are dependent on size and duration of exposure, and are comparable to LPS-induced production of ROS<sup>259</sup>. Based on the results of this study, it is reasonable to conclude that the ROS-dependent toxicity of metal NPs is not only related to the physicochemical properties of the NPs, such as size and composition, but also is related to their interaction with distinct biological systems and their biochemical microenvironment.

#### **4.5 Affymetrix gene expression analysis and validation of Ti NPs-induced biomarkers**

The effect of polished and porous titanium surfaces on gene expression (whole transcriptome) in macrophages was first analyzed by Gudima, 2017<sup>182</sup>. However, the effect of Ti NPs in combination with high glucose has been first addressed in this study (section 3.9). In the analysis by Gudima, 2017, it was revealed that, both polished and porous titanium display similar trends with the highest number of differences between titanium and control settings (w/o titanium) found in M2 macrophages<sup>182</sup>. However, in the present study, the number of differences between Ti NPs and control settings was found to be higher for M1 macrophage genes in comparison to M2 genes. Due to the small size, metal nanoparticles can penetrate inside the cells and be poorly eliminated in comparison to metal surfaces<sup>260</sup>. Hence it is not surprising to see large differences in regulation of the genes by metal surfaces and nanoparticles.

In addition to the differences between Ti NPs versus control (w/o Ti NPs), the differences in gene expression of M1 (IFN $\gamma$ ) versus M2 (IL-4) were evaluated in the presence of Ti NPs alone and in the presence of Ti NPs in synergy high glucose. A total of 7915 genes were differentially expressed in the comparison of M1 and M2 macrophages in all three conditions. 60% of these genes were differentially expressed between M1 and M2 alone (control). A total of 4599 genes were found to be differentially expressed in the presence of Ti NPs, in which 52% of these genes were differentially expressed by Ti NPs alone and not common with the control. 4013 genes were found statistically significant in the presence of Ti NPs in synergy with HG. Only 17% of these genes were differentially expressed in the presence of HG with Ti NPs and not common with other genes. In summary, high glucose did not have as large of an effect on the change in gene expression in comparison to the effect of Ti NPs.

Since the results of microarray analysis have shown that Ti NPs have a greater effect on the regulation of pro-inflammatory (M1) genes, the focus was directed towards the M1 profile. A total of 10 genes that were differentially expressed and displayed maximal fold change in the comparison of M1 versus M1 exposed to Ti NPs were selected for further evaluation. These 10 genes were validated by RT-PCR. (Table 21). 9 genes (DCSTAMP, OLR1, ORM1, MME and CSF1, CXCL9, CXCL10, MT1X and MT1G) passed the validation analysis. One gene (CXCL8) did not pass, which could be explained by the highest P-value indicated in the Affymetrix analysis.

**Table 21: Validation via RT-PCR of Ti NPs-induced biomarkers in pro-inflammatory macrophages cultured in normal and high glucose conditions.**

Gene symbol	Regulation $\Delta$	Fold change in NG (M1 vs M1 + Ti NPs)	Fold change in HG (M1 vs M1 + Ti NPs)
CSF1	↑	4.5	8.5
CXCL8	N/A	N/A	N/A
CXCL9	↓	88	122
CXCL10	↓	61	77
DCSTAMP	↑	10	20
MME	↑	91	148
MT1G	↑	18	12
MT1X	↑	7.0	12
OLR1	↑	7.4	25
ORM1	↑	21	61

Colony stimulating factor-1 (CSF1), also known as macrophage stimulating factor or M-CSF1, regulates survival, proliferation, and differentiation of macrophages<sup>261</sup>. It has been demonstrated by Gudima, 2017 that CSF1 is upregulated in response to polished and porous titanium<sup>182</sup>. In the present study, it was revealed that CSF1 is also upregulated by Ti NPs in both normal or high glucose conditions. All the data together suggests that all titanium material despite its form and morphology universally promote CSF1 expression in human macrophages.

C-X-C motif chemokine ligand 9 and 10 (CXCL9 and CXCL10) are inflammatory chemokines and are predominantly induced by IFN $\gamma$  and share a chemokine receptor known as chemokine receptor 3 (CXCR3)<sup>262</sup>. Macrophage-derived CXCL9 and CXCL10 are considered to be important for antitumor immune responses; their expression is significantly upregulated in the tumor microenvironment in response to cancer therapy<sup>263</sup>. The findings by Gudima, 2017, revealed that CXCL9 and CXCL10 were significantly downregulated on porous titanium, while there were no effects on polished titanium<sup>182</sup>. In the present study with Ti NPs, the results were similar to the effects of porous titanium: the expression of CXCL9 and CXCL10 was greatly suppressed by Ti NPs in normal or high glucose environments. Since both CXCL9 and CXCL10 are associated with adverse local tissue reactions, their downregulation by porous titanium and Ti NPs is indicative for the suppression of specific inflammatory reactions. However, the suppression of CXCL9 and CXCL10 by titanium materials would not be beneficial to cancer patients. Therefore, cancer patients should pay attention to the materials that they use in implants and the overall stability of the implants in a context of potential osteolysis and the corresponding metal corrosion, which is responsible for the release of Ti NPs.

Dendritic cell-specific transmembrane protein (DCSTAMP) is involved in modulating cell–cell fusion in both osteoclasts and macrophages that form foreign body giant cells (FBGCs), and also interacts with TNF Superfamily Member 11<sup>264</sup>. DCSTAMP plays a role in the regulation of dendritic cell (DC) antigen presentation activity by controlling phagocytic activity and is involved in the maintenance of immune self-tolerance and avoidance of autoimmune reactions<sup>265,266</sup>. DCSTAMP is a potential biomarker for molecular pathogenesis of osteolysis<sup>13</sup>. Ti NPs induce inflammation and osteolysis<sup>267</sup>. The results of this study have shown that expression of DCSTAMP is upregulated by Ti NPs. In hyperglycemic conditions, Ti NPs upregulate DCSTAMP expression twice as much as in normoglycemic conditions, which implies that in patients with poorly controlled diabetes, the osteolysis via the DCSTAMP-dependent mechanism should be more prevailed.



The membrane metalloendopeptidase (MME) gene encodes neprilysin (NEP), a zinc-dependent metalloprotease expressed in most tissues, which includes the central and peripheral nervous systems<sup>268</sup>. MME is expressed in macrophages and is known to modulate inflammation responses by degrading neuropeptides<sup>269,270</sup>. Overexpression of MME is a gene therapy approach to prevent amyloid beta aggregation in the treatment of Alzheimer's disease<sup>270</sup>. The validation analysis of the microarray results revealed that Ti NPs exceedingly upregulate expression of MME, which can be potentially applied in a combination treatment of Alzheimer's disease.

Metallothioneins (MTs) are cysteine-rich proteins with a molecular weight of approximately 6000 Da, and have a specific binding capacity to group II metal ions<sup>271,272</sup>. During oxidative stress, biosynthesis of MTs is increased by several times, which protects the cells from cytotoxicity and DNA damage<sup>273</sup>. The results of this study have shown that MTs are upregulated in response to Ti NPs exposure. Since MTs are known to serve a protective function against heavy metal ion toxicity, this probably implies that titanium ions are recognized as a toxic substance, which activates intracellular defense mechanisms against metal toxicity via the upregulation of MTs expression. More specifically, the validation analysis of microarray results revealed that Ti NPs significantly upregulate the expression of only two MTs isoforms, which are MT1G and MT1X. MT1G acts as a tumor suppressor gene in hepatocellular carcinoma (HCC)<sup>274</sup>. Induction of the hMT1G promoter by VEGF and heavy metals occurs through the utilization of different transcription factors, however, the mechanisms of MT1G silencing are related to promoter hypermethylation<sup>275</sup>. Analogously to MT1G, MT1X is known to inhibit progression of HCC. MT1X promotes cell cycle arrest and apoptosis by inactivating NF- $\kappa$ B signaling<sup>273</sup>. Both, MT1X and MT1G serve as candidates for a prognostic indicator of HCC<sup>273,274</sup>. In combination with other reagents, Ti NPs can be potentially employed in the treatment of HCC. Ti NPs are commonly used in photodynamic therapy, sonodynamic therapy and drug delivery systems for potential treatments of cancers<sup>276</sup>.

Oxidized low density lipoprotein receptor 1 (OLR1), also known as lectin-like oxidized low-density lipoprotein receptor-1 (LOX-1), is the main OxLDL receptor of endothelial cells, and is also expressed in macrophages and smooth muscle cells<sup>277,278</sup>. OLR1 is a marker for atherosclerosis, and once activated by ox-LDL or other ligands in macrophages and vascular endothelial cells, it stimulates the expression of adhesion molecules, pro-inflammatory signaling pathways and proangiogenic proteins, including NF- $\kappa$ B and VEGF<sup>279</sup>. In the present study, the results of the Affymetrix analysis confirmed by validation via RT-PCR, have shown that Ti NPs significantly upregulate expression of OLR1 in pro-inflammatory macrophages. Overexpression of OLR1 in mice results in an accelerated atherosclerotic lesion formation which is associated with increased inflammation. In humans, OLR1 gene polymorphisms were associated with increased susceptibility to myocardial infarction<sup>280</sup>. It has been known that electronegative low-density lipoprotein LDL(-) promotes differentiation of human monocytes to M1 macrophages through a OLR1-dependent pathway<sup>281</sup>. In the present study, high glucose enhanced the Ti NPs-induced expression of OLR1. OLR1 expression was upregulated about 3 times higher in a diabetic environment in comparison of OLR1 induced by Ti NPs alone. It has been previously revealed that activation of OLR1 contributes to pervasive inflammation in early diabetic nephropathy<sup>282</sup>. It is possible that these effects are attributed to hyperglycemic blood.

Orosomucoid 1 (ORM1) is a human alpha-1 acid glycoprotein (AGP, a 44 kD immunosuppressive glycoprotein), which is detected in plasma of healthy individuals<sup>283,284</sup>. However, the levels of ORM1 are significantly elevated in patients

with metastatic tumors and in severely burned patients<sup>285–288</sup>. Also, ORM1 is known to promote M2 macrophage polarization<sup>284</sup>. Ti NPs induced expression of ORM1 in normal and high glucose. Hyperglycemia enhanced Ti NPs-induced ORM1 expression by an average of 1.7 times. Considering the fact that ORM1 promotes M2 polarization and Ti NPs upregulate expression of ORM1 by a significant amount, it is not unreasonable to conclude Ti NPs can also promote M2 polarization via an ORM1-dependent mechanism and high glucose plays an assisting role in this process. It has been previously found that in mouse BMDMs, gold NPs (size 13nm diameter) are capable of promoting polarization of M1 macrophages to M2<sup>289</sup>. In the human THP-1 cell line, Ti NPs (nanotubes, sizes: 92 and 142 nm), promote polarization of M0 macrophages to M2 macrophages<sup>290</sup>. Ti NPs used in the present study are 15nm in diameter and previously there were no studies conducted with this particular size of Ti NPs together with a corresponding macrophage model.

In summary, Ti NPs in synergy with hyperglycemia had the strongest upregulation effect on MME expression and the strongest suppression effect on CXCL9 expression. Overall, it is very challenging to detect degradation of implant materials once they are already inserted inside the body<sup>291</sup>. However, in patients with titanium implants, increased levels of CHIT1, DCSTAMP, MME, CHI3L1, OLR1, CSF1, ORM1 and MT1X and suppressed levels of CXCL9 and CXCL10 can be detected in blood and potentially used in combination as biomarkers of implant wear-off particle release and upcoming implant failure. Especially in diabetic patients with titanium implants, these biomarkers should be highly monitored.

## 5 SUMMARY

Titanium biomaterials are widely used for implantation. Titanium implants release titanium nanoparticles (Ti NPs), known as implant debris. Ti NPs induce inflammation and are amongst the driving forces that contribute to the disruption of the mechanical stability of implant devices causing aseptic loosening and triggering adverse immune reactions that lead to chronic health complications. Macrophages are innate immune cells present in virtually all tissues. Macrophages are responsible for the recognition of foreign material and foreign body response. Pathological activation of macrophages can result in the failure of implants. Patients with Diabetes Mellitus (DM) have elevated blood sugar levels and can suffer from consequences triggered by compromised immune responses. Amongst those consequences are the complications produced by metal implants. Hyperglycemia is a major factor of diabetic pathology, which also promotes implant corrosion contributing to the release of metal wear-off particles. Macrophages are essential regulators of inflammation and play a critical role in DM and diabetic complications.

The aim of the study was to investigate the interacting effect of Ti NPs and hyperglycemia on innate immune responses, which can be responsible for the implant failure in diabetic patients. In the current study, the effects of titanium debris on primary human macrophages in hyperglycemic conditions were explored. Monocytes were isolated out of buffy coats by CD14+ positive selection and differentiated into the following subtypes: M0 (control or unstimulated), M1 (stimulated with IFN $\gamma$ ) and M2 (stimulated with IL-4). Macrophages were exposed to high concentrations of glucose (25mM) to mimic a diabetic environment. For the assessment of the effects of titanium debris, the cells were stimulated with 25 ppm and 100 ppm of Ti NPs. The results of the Alamar Blue assay revealed that Ti NPs at moderate concentrations do not affect macrophage viability. Using RT-PCR and ELISA, the expression and secretion of CHI3L1, CHIT1, CCL18 and TNF- $\alpha$  were quantified.

Ti NPs stimulated gene expression of CHI3L1 in M0 and M2 macrophages, however, the secretion of CHI3L1 was potentiated in all macrophage subtypes. Ti NPs stimulated gene expression of CHIT1 in all macrophage subtypes. Gene expression and secretion of CCL18 was suppressed by Ti NPs. In the presence of Ti NPs, the secretion of TNF- $\alpha$  was not changed. Hyperglycemia cooperated with Ti NPs-induced gene expression of CHI3L1 in M1 and M2 and Ti NPs-induced secretion of CHI3L1 in all macrophage subtypes. Hyperglycemia cooperated with Ti NPs-induced CHIT1 expression in all macrophage subtypes. Suppressed production of CCL18 by Ti NPs was enhanced by hyperglycemia. In the presence of a hyperglycemic environment, secretion of TNF- $\alpha$  was not changed. Dexamethasone suppressed Ti NPs-induced CHI3L1 expression in a high glucose environment but not in normal glucose. However, dexamethasone upregulated Ti NPs-induced CHIT1 expression in normal glucose and had no effect in high glucose.

Confocal microscopy demonstrated that Ti NPs promote intracellular accumulation of CHIT1 in the trans-Golgi network (TGN) in M1 macrophages, however, in M2 macrophages, Ti NPs trigger degradation of TGN. Flow cytometry demonstrated that Ti NPs induce ROS release in M0 macrophages and enhance ROS production in M1 macrophages. The results of Affymetrix gene expression analysis identified a group of differentially expressed genes induced by Ti NPs: DCSTAMP, OLR1, ORM1, MME, CSF1, CXCL8, CXCL9, CXCL10, MT1X and MT1G. RT-qPCR validation analysis of the differentially expressed genes revealed that hyperglycemia enhances Ti NPs-

induced expression of CSF1, DCSTAMP, CSF1, MT1X, OLR1 and ORM1; and favors Ti NPs-induced suppression of CXCL9 and CXCL10.

In total, Ti NPs induced increased production of ROS, CHIT1, CHI3L1, DCSTAMP, OLR1, ORM1, MME, CSF1, MT1X and MT1G, and suppressed production of CCL18, CXCL9 and CXCL10 in primary human monocyte-derived macrophages. Hyperglycemia cooperated with the effects of Ti NPs in the production of CHIT1, CHI3L1, CSF1, DCSTAMP, MT1X, OLR1, ORM1, CXCL9 and CXCL10. In summary, the results of the study clearly demonstrated that Ti NPs and hyperglycemia have synergistic effects, while the dominant effects are induced by the Ti NPs. The synergistic effect of Ti NPs and hyperglycemia are characterized by the system of biomarkers including CHIT1, DCSTAMP, CHI3L1, OLR1, CSF1, ORM1 and MT1X that can potentially be used to predict the detrimental effect of Ti implants in diabetic patients.

## 6 REFERENCES

1. Schindhelm, K. & Milthorpe, B. K. An overview of biomaterials. *Australasian physical & engineering sciences in medicine / supported by the Australasian College of Physical Scientists in Medicine and the Australasian Association of Physical Sciences in Medicine* vol. 9 29–32 (2003).
2. Tsukimura, I. *et al.* Assessment of magnetic field interactions and radiofrequency-radiation-induced heating of metallic spinal implants in 7 T field. *J. Orthop. Res.* **35**, 1831–1837 (2017).
3. Zou, Y. F., Chu, B., Wang, C. B. & Hu, Z. Y. Evaluation of MR issues for the latest standard brands of orthopedic metal implants: Plates and screws. *Eur. J. Radiol.* **84**, 450–457 (2015).
4. Griggs, J. A. Dental Implants. *Dent. Clin. North Am.* **61**, 857–871 (2017).
5. Miller, R. J. H., Teuteberg, J. J. & Hunt, S. A. Innovations in ventricular assist devices for end-stage heart failure. *Annu. Rev. Med.* **70**, 33–44 (2019).
6. Zhang, L. C. & Chen, L. Y. A Review on Biomedical Titanium Alloys: Recent Progress and Prospect. *Adv. Eng. Mater.* **21**, 1–29 (2019).
7. Li, Y. *et al.* New developments of ti-based alloys for biomedical applications. *Materials (Basel)*. **7**, 1709–1800 (2014).
8. Kzhyshkowska, J. *et al.* Macrophage responses to implants: prospects for personalized medicine. *J. Leukoc. Biol.* **98**, 953–962 (2015).
9. Lausmaa, J., Kasemo, B. & Mattsson, H. Surface spectroscopic characterization of titanium implant materials. *Appl. Surf. Sci.* **44**, 133–146 (1990).
10. Stuart Goodman<sup>1</sup>, Y. T. K. and M. T. Joint Replacement Surgery and the Innate Immune System. 253–257 (2014).
11. Wang, K. The use of titanium for medical applications in the USA. *Mater. Sci. Eng. A* **213**, 134–137 (1996).
12. Matusiewicz, H. Potential release of in vivo trace metals from metallic medical implants in the human body: From ions to nanoparticles - A systematic analytical review. *Acta Biomater.* **10**, 2379–2403 (2014).
13. Koulouvaris P, Ly K, Ivashkiv LB, Bostrom MP, Nestor BJ, Sculco TP, P. P. Expression Profiling Reveals Alternative Macrophage Activation and Impaired Osteogenesis in Periprosthetic Osteolysis. *J. Orthop. Res.* **26**, 106–116 (2007).
14. Levi, M., Keller, T. T., Van Gorp, E. & Ten Cate, H. Infection and inflammation and the coagulation system. *Cardiovasc. Res.* **60**, 26–39 (2003).
15. Stavropoulos, A., Bertl, K., Eren, S. & Gotfredsen, K. Mechanical and biological complications after implantoplasty—A systematic review. *Clin. Oral Implants Res.* **30**, 833–848 (2019).
16. Moore, L. B. & Kyriakides, T. R. Molecular characterization of macrophage-biomaterial interactions. *Advances in Experimental Medicine and Biology* vol. 865 109–122 (2015).
17. Hannahan, J. P. & Eleazer, P. D. Comparison of Success of Implants versus Endodontically Treated Teeth. *J. Endod.* **34**, 1302–1305 (2008).
18. Sharkey, P. F., Lichstein, P. M., Shen, C., Tokarski, A. T. & Parvizi, J. Why are total knee arthroplasties failing today-has anything changed after 10 years? *J. Arthroplasty* **29**, 1774–1778 (2013).
19. Ulrich, S. D. *et al.* Total hip arthroplasties: What are the reasons for revision? *Int. Orthop.* **32**, 597–604 (2008).
20. Mok, J. M. *et al.* Reoperation after primary fusion for adult spinal deformity: Rate, reason, and timing. *Spine (Phila. Pa. 1976)*. **34**, 832–839 (2009).

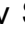
21. Revell, P. A. The combined role of wear particles, macrophages and lymphocytes in the loosening of total joint prostheses. *J. R. Soc. Interface* **5**, 1263–1278 (2008).
22. Klinge, U., Dievernich, A., Tolba, R., Klosterhalfen, B. & Davies, L. CD68+ macrophages as crucial components of the foreign body reaction demonstrate an unconventional pattern of functional markers quantified by analysis with double fluorescence staining. *J. Biomed. Mater. Res. - Part B Appl. Biomater.* **108**, 3134–3146 (2020).
23. Mariani, E., Lisignoli, G., Borzi, R. M. & Pulsatelli, L. Biomaterials: Foreign bodies or tuners for the immune response? *Int. J. Mol. Sci.* **20**, (2019).
24. Purdue, P. E., Koulouvaris, P., Potter, H. G., Nestor, B. J. & Sculco, T. P. The cellular and molecular biology of periprosthetic osteolysis. *Clin. Orthop. Relat. Res.* 251–261 (2007) doi:10.1097/01.blo.0000238813.95035.1b.
25. Eastgate, J. A., Symonns, J. A., Wood, N. C., Capper, S. J. & Duff, G. W. Plasma levels of interleukin-1-alpha in rheumatoid arthritis. *Rheumatology* **30**, 295–297 (1991).
26. Rabolli, V. *et al.* The alarmin IL-1 $\alpha$  is a master cytokine in acute lung inflammation induced by silica micro- and nanoparticles. *Part. Fibre Toxicol.* **11**, 1–15 (2014).
27. Wynn, T. A. & Barron, L. Macrophages: Master regulators of inflammation and fibrosis. *Semin. Liver Dis.* **30**, 245–257 (2010).
28. Gittens, R. A., Olivares-Navarrete, R., Tannenbaum, R., Boyan, B. D. & Schwartz, Z. Electrical implications of corrosion for osseointegration of titanium implants. *J. Dent. Res.* **90**, 1389–1397 (2011).
29. Evrard, L. Titanium: A New Allergen. *Implant Dent. - A Rapidly Evol. Pract.* (2011) doi:10.5772/19931.
30. Lechner, J., Noubissi, S. & von Baehr, V. Titanium implants and silent inflammation in jawbone—a critical interplay of dissolved titanium particles and cytokines TNF- $\alpha$  and RANTES/CCL5 on overall health? *EPMA J.* **9**, 331–343 (2018).
31. Messer, R. L. W. *et al.* Corrosion of machined titanium dental implants under inflammatory conditions. *Journal of Biomedical Materials Research - Part B Applied Biomaterials* vol. 88 474–481 (2009).
32. Kotsovilis, S., Karoussis, I. K. & Fourmouis, I. A comprehensive and critical review of dental implant placement in diabetic animals and patients. *Clin. Oral Implants Res.* **17**, 587–599 (2006).
33. Tengvall, P., Lundström, I., Sjöqvist, L., Elwing, H. & Bjursten, L. M. Titanium-hydrogen peroxide interaction: model studies of the influence of the inflammatory response on titanium implants. *Biomaterials* **10**, 166–175 (1989).
34. Cheng, X. & Roscoe, S. G. Corrosion behavior of titanium in the presence of calcium phosphate and serum proteins. *Biomaterials* **26**, 7350–7356 (2005).
35. Khan, M. A., Williams, R. L. & Williams, D. F. The corrosion behaviour of Ti-6Al-4V, Ti-6Al-7Nb and Ti-13Nb-13Zr in protein solutions. *Biomaterials* **20**, 631–637 (1999).
36. Kaesche, H. *Galvanic Corrosion Cells.* (2003). doi:10.1007/978-3-642-96038-3\_11.
37. Eliaz, N. Corrosion of metallic biomaterials: A review. *Materials (Basel).* **12**, (2019).
38. Buzea, C., Pacheco, I. I. & Robbie, K. Nanomaterials and nanoparticles: Sources and toxicity. *Biointerphases* **2**, MR17–MR71 (2007).
39. Hanaor, D. A. H. & Sorrell, C. C. Review of the anatase to rutile phase

- transformation. *J. Mater. Sci.* **46**, 855–874 (2011).
40. Bourikas, K., Kordulis, C. & Lycourghiotis, A. Titanium dioxide (Anatase and Rutile): Surface chemistry, liquid-solid interface chemistry, and scientific synthesis of supported catalysts. *Chem. Rev.* **114**, 9754–9823 (2014).
  41. Tsou, H. & Hsieh, P. Anticorrosive, Antimicrobial, and Bioactive Titanium Dioxide Coating for Surface-modified Purpose on Biomedical Material. *Appl. Titan. Dioxide* (2017) doi:10.5772/intechopen.68854.
  42. Mark J. Jackson, W. A. Titanium Dioxide Coatings in Medical Device Applications. *Surf. Eng. Surg. Tools Med. Devices* 49–63 (2007) doi:10.1007/978-0-387-27028-9\_3.
  43. Jiao, H., Xiao, E. & Graves, D. T. Diabetes and Its Effect on Bone and Fracture Healing. *Curr. Osteoporos. Rep.* **13**, 327–335 (2015).
  44. Khader, Y. S., Dauod, A. S., El-Qaderi, S. S., Alkafajei, A. & Batayha, W. Q. Periodontal status of diabetics compared with nondiabetics: A meta-analysis. *J. Diabetes Complications* **20**, 59–68 (2006).
  45. Hwang, D. & Wang, H. L. Medical contraindications to implant therapy: Part II: relative contraindications. *Implant Dent.* **16**, 13–23 (2007).
  46. De Moraes, J. A. N. D. *et al.* Effect of diabetes mellitus and insulin therapy on bone density around osseointegrated dental implants: A digital subtraction radiography study in rats. *Clin. Oral Implants Res.* **20**, 796–801 (2009).
  47. Promsudthi, A., Poomsawat, S. & Limsricharoen, W. The role of Toll-like receptor 2 and 4 in gingival tissues of chronic periodontitis subjects with type 2 diabetes. *J. Periodontal Res.* **49**, 346–354 (2014).
  48. Verhaeghe, J. *et al.* Bone and mineral metabolism in BB rats with long-term diabetes: Decreased bone turnover and osteoporosis. *Diabetes* **39**, 477–482 (1990).
  49. Moganti, K. *et al.* Hyperglycemia induces mixed M1/M2 cytokine profile in primary human monocyte-derived macrophages. *Immunobiology* **222**, 952–959 (2017).
  50. Gardner, A. B., Lee, S. K. C., Woods, E. C. & Acharya, A. P. Biomaterials-based modulation of the immune system. *Biomed Res. Int.* **2013**, (2013).
  51. Aronson, D. & Rayfield, E. J. How hyperglycemia promotes atherosclerosis: Molecular mechanisms. *Cardiovasc. Diabetol.* **1**, 1–10 (2002).
  52. Ariganello, M. B. *et al.* Surface nanocavitation of titanium modulates macrophage activity. *Int. J. Nanomedicine* **13**, 8297–8308 (2018).
  53. Faverani, L. P. *et al.* Effects of dextrose and lipopolysaccharide on the corrosion behavior of a Ti-6Al-4V alloy with a smooth surface or treated with double-acid-etching. *PLoS One* **9**, (2014).
  54. Tamam, E. & Turkyilmaz, I. Effects of pH and elevated glucose levels on the electrochemical behavior of dental implants. *J. Oral Implantol.* **40**, 153–159 (2014).
  55. Abduljabbar, T., Al-sahaly, F., Al-kathami, M., Afzal, S. & Vohra, F. Comparison of periodontal and peri-implant inflammatory parameters among patients with prediabetes, type 2 diabetes mellitus and non-diabetic controls. *Acta Odontol. Scand.* **75**, 319–324 (2017).
  56. Farnsworth, C. W. *et al.* Obesity/type 2 diabetes increases inflammation, periosteal reactive bone formation, and osteolysis during *Staphylococcus aureus* implant-associated bone infection. *Journal of Orthopaedic Research* vol. 36 (2018).
  57. Al-Sowygh, Z. H., Ghani, S. M. A., Sergis, K., Vohra, F. & Akram, Z. Peri-implant conditions and levels of advanced glycation end products among patients with

- different glycemic control. *Clinical Implant Dentistry and Related Research* vol. 20 345–351 (2018).
58. Dasu, M. R., Devaraj, S. & Jialal, I. High glucose induces IL-1 $\beta$  expression in human monocytes: Mechanistic insights. *Am. J. Physiol. - Endocrinol. Metab.* **293**, 337–346 (2007).
59. Devaraj, S. *et al.* Knockout of toll-like receptor-2 attenuates both the proinflammatory state of diabetes and incipient diabetic nephropathy. *Arterioscler. Thromb. Vasc. Biol.* **31**, 1796–1804 (2011).
60. Devaraj, S., Tobias, P. & Jialal, I. Knockout of toll-like receptor-4 attenuates the pro-inflammatory state of diabetes. *Cytokine* **55**, 441–445 (2011).
61. Lalla, E., Lamster, I. B., Drury, S., Fu, C. & Schmidt, A. M. Hyperglycemia, glycooxidation and receptor for advanced glycation endproducts: Potential mechanisms underlying diabetic complications, including diabetes-associated periodontitis. *Periodontol. 2000* **23**, 50–62 (2000).
62. Ghiraldini, B. *et al.* Influence of Glycemic Control on Peri-Implant Bone Healing: 12-Month Outcomes of Local Release of Bone-Related Factors and Implant Stabilization in Type 2 Diabetics. *Clin. Implant Dent. Relat. Res.* **18**, 801–809 (2016).
63. Shi, H., Magaye, R., Castranova, V. & Zhao, J. Titanium dioxide nanoparticles: A review of current toxicological data. *Part. Fibre Toxicol.* **10**, (2013).
64. Kuku, G. & Culha, M. Investigating the origins of toxic response in TiO<sub>2</sub> nanoparticle-treated cells. *Nanomaterials* **7**, (2017).
65. Weir, A., Westerhoff, P., Fabricius, L., Hristovski, K. & Von Goetz, N. Titanium dioxide nanoparticles in food and personal care products. *Environ. Sci. Technol.* **46**, 2242–2250 (2012).
66. Bettini, S. *et al.* Food-grade TiO<sub>2</sub> impairs intestinal and systemic immune homeostasis, initiates preneoplastic lesions and promotes aberrant crypt development in the rat colon. *Sci. Rep.* **7**, 1–13 (2017).
67. Kiser, M. A. *et al.* Titanium nanomaterial removal and release from wastewater treatment plants. *Environ. Sci. Technol.* **43**, 6757–6763 (2009).
68. Westerhoff, P., Song, G., Hristovski, K. & Kiser, M. A. Occurrence and removal of titanium at full scale wastewater treatment plants: Implications for TiO<sub>2</sub> nanomaterials. *J. Environ. Monit.* **13**, 1195–1203 (2011).
69. Stark, W. J., Stoessel, P. R., Wohlleben, W. & Hafner, A. Industrial applications of nanoparticles. *Chem. Soc. Rev.* **44**, 5793–5805 (2015).
70. Skocaj, M., Filipic, M., Petkovic, J. & Novak, S. Titanium dioxide in our everyday life; Is it safe? *Radiol. Oncol.* **45**, 227–247 (2011).
71. Shandilya, N., Le Bihan, O., Bressot, C. & Morgeneyer, M. Emission of titanium dioxide nanoparticles from building materials to the environment by wear and weather. *Environ. Sci. Technol.* **49**, 2163–2170 (2015).
72. Oberdorster, G., Ferin, J. & Lehnert, B. E. Correlation between particle size, in vivo particle persistence, and lung injury. *Environ. Health Perspect.* **102**, 173–179 (1994).
73. Rossi, E. M. *et al.* Airway exposure to silica-coated TiO<sub>2</sub> nanoparticles induces pulmonary neutrophilia in mice. *Toxicol. Sci.* **113**, 422–433 (2009).
74. Inoue, K. ichiro *et al.* Effects of inhaled nanoparticles on acute lung injury induced by lipopolysaccharide in mice. *Toxicology* **238**, 99–110 (2007).
75. Li, B. *et al.* Molecular Mechanisms of Nanosized Titanium Dioxide-Induced Pulmonary Injury in Mice. *PLoS One* **8**, (2013).
76. A. Jasim, F., K.Suker, D. & I .AL- Badran, A. TiO<sub>2</sub> Nanoparticles Induce Lung Fibrosis and Proteinosis through Influence on Matrix Metalloproteinase



- Expression. *Int. J. Sci.* **3**, 1–13 (2017).
77. Messer, R. L. W. *et al.* Interactions between stainless steel, shear stress, and monocytes. *J. Biomed. Mater. Res. - Part A* **87**, 229–235 (2008).
  78. Hong, F., Yu, X., Wu, N. & Zhang, Y. Q. Progress of: In vivo studies on the systemic toxicities induced by titanium dioxide nanoparticles. *Toxicology Research* vol. 6 115–133 (2017).
  79. Hewitt, R. E., Vis, B., Pele, L. C., Faria, N. & Powell, J. J. Imaging flow cytometry assays for quantifying pigment grade titanium dioxide particle internalization and interactions with immune cells in whole blood. *Cytom. Part A* **91**, 1009–1020 (2017).
  80. Ruiz, P. A. *et al.* Titanium dioxide nanoparticles exacerbate DSS-induced colitis: Role of the NLRP3 inflammasome. *Gut* **66**, 1216–1224 (2017).
  81. Dréno, B., Alexis, A., Chuberre, B. & Marinovich, M. Safety of titanium dioxide nanoparticles in cosmetics. *J. Eur. Acad. Dermatology Venereol.* **33**, 34–46 (2019).
  82. Rouse, J. G., Yang, J., Ryman-Rasmussen, J. P., Barron, A. R. & Monteiro-Riviere, N. A. Effects of mechanical flexion on the penetration of fullerene amino acid-derivatized peptide nanoparticles through skin. *Nano Lett.* **7**, 155–160 (2007).
  83. Pflücker, F. *et al.* The human stratum corneum layer: An effective barrier against dermal uptake of different forms of topically applied micronised titanium dioxide. *Skin Pharmacol. Appl. Skin Physiol.* **14**, 92–97 (2001).
  84. Sadrieh, N. *et al.* Lack of significant dermal penetration of titanium dioxide from sunscreen formulations containing nano- and submicron-size TiO<sub>2</sub> particles. *Toxicol. Sci.* **115**, 156–166 (2010).
  85. Bennat, C. & Müller-Goymann, C. C. Skin penetration and stabilization of formulations containing microfine titanium dioxide as physical UV filter. *Int. J. Cosmet. Sci.* **22**, 271–283 (2000).
  86. Commission, S. C. on C. S. (ScCs) of the E. Report for clarification of the meaning of the term " sprayable applications / products " for the nano forms of Carbon Black CI 77266 , Titanium Oxide and Zinc Oxide. 13 (2014) doi:10.2772/49208.
  87. Mantovani, A. *et al.* The chemokine system in diverse forms of macrophage activation and polarization. *Trends Immunol.* **25**, 677–686 (2004).
  88. Murray, P. J. *et al.* Macrophage Activation and Polarization: Nomenclature and Experimental Guidelines. *Immunity* **41**, 14–20 (2014).
  89. Mantovani, A., Biswas, S. K., Galdiero, M. R., Sica, A. & Locati, M. Macrophage plasticity and polarization in tissue repair and remodelling. *J. Pathol.* **229**, 176–185 (2013).
  90. Gratchev, A. *et al.* M $\phi$ 1 and M $\phi$ 2 can be re-polarized by Th2 or Th1 cytokines, respectively, and respond to exogenous danger signals. *Immunobiology* **211**, 473–486 (2006).
  91. Martinez, F. O. & Gordon, S. The M1 and M2 paradigm of macrophage activation: Time for reassessment. *F1000Prime Rep.* **6**, 1–13 (2014).
  92. Stein, M., Keshav, S., Harris, N. & Gordon, S. Interleukin 4 potently enhances murine macrophage mannose receptor activity: A marker of alternative immunologic macrophage activation. *J. Exp. Med.* **176**, 287–292 (1992).
  93. Kzhyshkowska, J., Gudima, A., Moganti, K., Gratchev, A. & Orekhov, A. Perspectives for Monocyte/Macrophage-Based Diagnostics of Chronic Inflammation. *Transfus. Med. Hemotherapy* **43**, 66–77 (2016).
  94. Torres, M. A., Jones, J. D. G. & Dangl, J. L. Reactive oxygen species signaling

- in response to pathogens. *Plant Physiol.* **141**, 373–378 (2006).
95. Gratchev, A., Kzhyshkowska, J., Utikal, J. & Goerdts, S. Interleukin-4 and dexamethasone counterregulate extracellular matrix remodelling and phagocytosis in type-2 macrophages. *Scandinavian Journal of Immunology* vol. 61 10–17 (2005).
  96. Gratchev, A. *et al.* Activation of a TGF- $\beta$ -Specific Multistep Gene Expression Program in Mature Macrophages Requires Glucocorticoid-Mediated Surface Expression of TGF- $\beta$  Receptor II. *J. Immunol.* **180**, 6553–6565 (2008).
  97. Nurgazieva, D. *et al.* TGF- $\beta$ 1, but Not Bone Morphogenetic Proteins, Activates Smad1/5 Pathway in Primary Human Macrophages and Induces Expression of Proatherogenic Genes. *J. Immunol.* **194**, 709–718 (2015).
  98. Kzhyshkowska, J. *et al.* Novel stabilin-1 interacting chitinase-like protein (SI-CLP) is up-regulated in alternatively activated macrophages and secreted via lysosomal pathway. *Blood* **107**, 3221–3228 (2006).
  99. Gratchev, A. *et al.* Expression of osteoarthritis marker YKL-39 is stimulated by transforming growth factor beta (TGF-beta) and IL-4 in differentiating macrophages. *Biomark. Insights* **2008**, 39–44 (2008).
  100. Gratchev, A. Antigen-Presenting Cells: Molecular Repertoire, Immune Regulation, and Healing. 272–279 (2001).
  101. Klopffleisch, R. & Jung, F. The pathology of the foreign body reaction against biomaterials. *J. Biomed. Mater. Res. - Part A* **105**, 927–940 (2017).
  102. Anderson, J. M., Rodriguez, A. & Chang, D. T. Foreign body reaction to biomaterials. *Semin. Immunol.* **20**, 86–100 (2008).
  103. Zaveri TD, Lewis JS, Dolgova NV, Clare-Salzler MJ, K. B. Integrin-Directed Modulation of Macrophage Responses to Biomaterials. *Biomaterials* **35**, 3504–3515 (2014).
  104. Nakashima, Y. *et al.* Signaling pathways for tumor necrosis factor- $\alpha$  and interleukin-6 expression in human macrophages exposed to titanium-alloy particulate debris in vitro. *J. Bone Jt. Surg. - Ser. A* **81**, 603–615 (1999).
  105. Love, R. J. & Jones, K. S. The recognition of biomaterials: Pattern recognition of medical polymers and their adsorbed biomolecules. *J. Biomed. Mater. Res. - Part A* **101 A**, 2740–2752 (2013).
  106. Dhupal, M. *et al.* Immunotoxicity of titanium dioxide nanoparticles via simultaneous induction of apoptosis and multiple toll-like receptors signaling through ROS-dependent SAPK/JNK and p38 MAPK activation. *Int. J. Nanomedicine* **13**, 6735–6750 (2018).
  107. Arredouani, M. S. *et al.* The macrophage scavenger receptor SR-AI/II and lung defense against pneumococci and particles. *Am. J. Respir. Cell Mol. Biol.* **35**, 474–478 (2006).
  108. Zlotnik, A. & Yoshie, O. Chemokines: A new classification system and their role in immunity. *J. Cult. Herit.* **1**, 121–127 (2000).
  109. Özçelik, H. *et al.* Harnessing the Multifunctionality in Nature: A Bioactive Agent Release System with Self-Antimicrobial and Immunomodulatory Properties. *Adv. Healthc. Mater.* **4**, 2026–2036 (2015).
  110. Stankevich KS, Gudima A, Filimonov VD, Klüter H, Mamontova EM, Tverdokhlebov SI, K. J.  Surface modification of biomaterials based on high-molecular polylactic acid and their effect on inflammatory.pdf.
  111. Stankevich, K. S. *et al.* Modification of PCL Scaffolds by Reactive Magnetron Sputtering: A Possibility for Modulating Macrophage Responses. *ACS Biomater. Sci. Eng.* **6**, 3967–3974 (2020).
  112. Nurulain T. Zaveri. A Foreign Body Response-on-a-Chip Platform Fatemeh.

- Physiol. Behav.* **176**, 139–148 (2016).
113. Mesure, L., de Visscher, G., Vranken, I., Lebacqz, A. & Flameng, W. Gene expression study of monocytes/macrophages during early foreign body reaction and identification of potential precursors of myofibroblasts. *PLoS One* **5**, (2010).
  114. Lackey, D. E. & Olefsky, J. M. Regulation of metabolism by the innate immune system. *Nat. Rev. Endocrinol.* **12**, 15–20 (2016).
  115. Sataloff, R. T., Johns, M. M. & Kost, K. M. *Biomaterials in regenerative medicine and immune system*. (Springer, 1995).
  116. Germolec, D. R., Shipkowski, K. A., Frawley, R. P. & Evans, E. Markers of inflammation. *Methods Mol. Biol.* **1803**, 57–79 (2018).
  117. Abdulkhaleq, L. A. *et al.* The crucial roles of inflammatory mediators in inflammation: A review. *Vet. World* **11**, 627–635 (2018).
  118. Krzyszczyk, P., Schloss, R., Palmer, A. & Berthiaume, F. The role of macrophages in acute and chronic wound healing and interventions to promote pro-wound healing phenotypes. *Front. Physiol.* **9**, 1–22 (2018).
  119. Akdis, M. *et al.* Interleukins, from 1 to 37, and interferon- $\gamma$ : Receptors, functions, and roles in diseases. *J. Allergy Clin. Immunol.* **127**, 701-721.e70 (2011).
  120. Kajal Hamidzadeh, Stephen M. Christensen, Elizabeth Dalby, Prabha Chandrasekaran, and D. M. M. Macrophages and the Recovery from Acute and Chronic Inflammation. *Annu Rev Physiol.* **79**, 567–592 (2017).
  121. Yao, C. & Narumiya, S. Prostaglandin-cytokine crosstalk in chronic inflammation. *Br. J. Pharmacol.* **176**, 337–354 (2019).
  122. Gautier, E. L., Ivanov, S., Lesnik, P. & Randolph, G. J. Local apoptosis mediates clearance of macrophages from resolving inflammation in mice. *Blood* **122**, 2714–2722 (2013).
  123. Grabiec, A. M. & Hussell, T. The role of airway macrophages in apoptotic cell clearance following acute and chronic lung inflammation. *Semin. Immunopathol.* **38**, 409–423 (2016).
  124. Chiurchiù, V. & MacCarrone, M. Chronic inflammatory disorders and their redox control: From molecular mechanisms to therapeutic opportunities. *Antioxidants Redox Signal.* **15**, 2605–2641 (2011).
  125. Cochain, C. & Zerneck, A. Macrophages in vascular inflammation and atherosclerosis. *Pflugers Arch. Eur. J. Physiol.* **469**, 485–499 (2017).
  126. Saltiel, A. R. & Olefsky, J. M. Inflammatory linking obesity and metabolic disease and metabolic disease. *J. Clin. Invest.* **127**, 1–4 (2017).
  127. Torres-Castro, I. *et al.* Human monocytes and macrophages undergo M1-type inflammatory polarization in response to high levels of glucose. *Immunol. Lett.* **176**, 81–89 (2016).
  128. Fadini, G. P. *et al.* Monocyte-macrophage polarization balance in pre-diabetic individuals. *Acta Diabetol.* **50**, 977–982 (2013).
  129. Nagareddy, P. R. *et al.* Hyperglycemia promotes myelopoiesis and impairs the resolution of atherosclerosis. *Cell Metab.* **17**, 695–708 (2013).
  130. You, H., Gao, T., Cooper, T. K., Reeves, W. B. & Awad, A. S. Macrophages directly mediate diabetic renal injury. *Am. J. Physiol. - Ren. Physiol.* **305**, (2013).
  131. Tesch, G. H. Macrophages and diabetic nephropathy. *Semin. Nephrol.* **30**, 290–301 (2010).
  132. Kimball, A. S. *et al.* Notch regulates macrophage-mediated inflammation in diabetic wound healing. *Front. Immunol.* **8**, (2017).
  133. Noordin, S. & Masri, B. Periprosthetic osteolysis: Genetics, mechanisms and potential therapeutic interventions. *Can. J. Surg.* **55**, 408–417 (2012).
  134. Desgeorges, T., Caratti, G., Mounier, R., Tuckermann, J. & Chazaud, B.

- Glucocorticoids shape macrophage phenotype for tissue repair. *Front. Immunol.* **10**, 1–12 (2019).
135. Lee, S. W. *et al.* Glucocorticoids selectively inhibit the transcription of the interleukin 1 $\beta$  gene and decrease the stability of interleukin 1 $\beta$  mRNA. *Proc. Natl. Acad. Sci. U. S. A.* **85**, 1204–1208 (1988).
  136. Kern, J. A., Lamb, R. J., Reed, J. C., Daniele, R. P. & Nowell, P. C. Dexamethasone inhibition of interleukin 1 beta production by human monocytes. Posttranscriptional mechanisms. *J. Clin. Invest.* **81**, 237–244 (1988).
  137. Burnstein, K. L. & Cidlowski, J. A. Multiple mechanisms for regulation of steroid hormone action. *J. Cell. Biochem.* **51**, 130–134 (1993).
  138. Bridgham, J. T. *et al.* Protein Evolution by Molecular Tinkering : Diversification of the Nuclear Receptor Superfamily from a Ligand- Dependent Ancestor. **8**, (2010).
  139. Weikum, E. R., Knuesel, M. T., Ortlund, E. A. & Yamamoto, K. R. Glucocorticoid receptor control of transcription : precision and plasticity via allostery. *Nat. Publ. Gr.* doi:10.1038/nrm.2016.152.
  140. Ehrchen, J. M., Roth, J. & Barczyk-Kahlert, K. More than suppression: Glucocorticoid action on monocytes and macrophages. *Front. Immunol.* **10**, (2019).
  141. Meßmer, U. K., Winkel, G., Briner, V. A. & Pfeilschifter, J. Glucocorticoids potently block tumour necrosis factor- $\alpha$ - and lipopolysaccharide-induced apoptotic cell death in bovine glomerular endothelial cells upstream of caspase 3 activation. *Br. J. Pharmacol.* **127**, 1633–1640 (1999).
  142. Chuang, T. Y. *et al.* Suppression of LPS-induced inflammatory responses by the hydroxyl groups of dexamethasone. *Oncotarget* **8**, 49735–49748 (2017).
  143. Luedke, C. E. & Cerami, A. Interferon- $\gamma$  overcomes glucocorticoid suppression of cachectin/tumor necrosis factor biosynthesis by murine macrophages. *J. Clin. Invest.* **86**, 1234–1240 (1990).
  144. Ehrchen, J. *et al.* Glucocorticoids induce differentiation of a specifically activated, anti-inflammatory subtype of human monocytes. *Blood* **109**, 1265–1274 (2007).
  145. Barczyk, K. *et al.* Glucocorticoids promote survival of anti-inflammatory macrophages via stimulation of adenosine receptor A3. *Blood* **116**, 446–455 (2010).
  146. James, B. Y., Ann, E. B. & Rosenthal, A. S. GLUCOCORTICOID SUPPRESSION OF MACROPHAGE MIGRATION INHIBITORY FACTOR. **137**, 1031–1041 (1973).
  147. Norton, J. M. & Munck, A. In vitro actions of glucocorticoids on murine macrophages: Effects on glucose transport and metabolism, growth in culture, and protein synthesis. *J. Immunol.* **125**, 259–266 (1980).
  148. Khalil, N., Whitman, C., Zuo, L., Danielpour, D. & Greenberg, A. Regulation of alveolar macrophage transforming growth factor- $\beta$  secretion by corticosteroids in bleomycin-induced pulmonary inflammation in the rat. *J. Clin. Invest.* **92**, 1812–1818 (1993).
  149. Heasman, S. J. *et al.* Interferon  $\gamma$  suppresses glucocorticoid augmentation of macrophage clearance of apoptotic cells. *Eur. J. Immunol.* **34**, 1752–1761 (2004).
  150. Franchimont, D. *et al.* Tumor Necrosis Factor alpha Decreases, and Interleukin-10 Increases, the Sensitivity of Human Monocytes to Dexamethasone: Potential Regulation of the Glucocorticoid Receptor. *J. Clin. Endocrinol. Metab.* **84**, 2834–2839 (1999).
  151. Song, E. *et al.* Influence of alternatively and classically activated macrophages

- on fibrogenic activities of human fibroblasts. *Cell. Immunol.* **204**, 19–28 (2000).
152. Giles, K. M. *et al.* Glucocorticoid Augmentation of Macrophage Capacity for Phagocytosis of Apoptotic Cells Is Associated with Reduced p130Cas Expression, Loss of Paxillin/pyk2 Phosphorylation, and High Levels of Active Rac. *J. Immunol.* **167**, 976–986 (2001).
  153. Heideveld, E. *et al.* Glucocorticoids induce differentiation of monocytes towards macrophages that share functional and phenotypical aspects with erythroblastic Island macrophages. *Haematologica* **103**, 395–405 (2018).
  154. Rivera, M. C., Perni, S., Sloan, A. & Prokopovich, P. Anti-inflammatory drug-eluting implant model system to prevent wear particle-induced periprosthetic osteolysis. *Int. J. Nanomedicine* **14**, 1069–1084 (2019).
  155. Isaguliants, M. G., Bartosch, B. & Ivanov, A. V. Redox Biology of Infection and Consequent Disease. *Oxid. Med. Cell. Longev.* **2020**, (2020).
  156. Reczek, C. R. & Chandel, N. S. ROS-dependent signal transduction. *Curr. Opin. Cell Biol.* **33**, 8–13 (2015).
  157. Rendra, E. *et al.* Reactive oxygen species (ROS) in macrophage activation and function in diabetes. *Immunobiology* **224**, (2019).
  158. Kohchi, C., Inagawa, H., Nishizawa, T. & Soma, G. I. ROS and innate immunity. *Anticancer Res.* **29**, 817–822 (2009).
  159. Pawate, S., Shen, Q., Fan, F. & Bhat, N. R. Redox regulation of glial inflammatory response to lipopolysaccharide and interferony. *J. Neurosci. Res.* **77**, 540–551 (2004).
  160. Liu, F. T., Newland, A. C. & Jia, L. Bax conformational change is a crucial step for PUMA-mediated apoptosis in human leukemia. *Biochem. Biophys. Res. Commun.* **310**, 956–962 (2003).
  161. Rani, V., Deep, G., Singh, R. K., Palle, K. & Yadav, U. C. S. Oxidative stress and metabolic disorders: Pathogenesis and therapeutic strategies. *Life Sci.* **148**, 183–193 (2016).
  162. Li, J., Wuliji, O., Li, W., Jiang, Z. G. & Ghanbari, H. A. Oxidative stress and neurodegenerative disorders. *Int. J. Mol. Sci.* **14**, 24438–24475 (2013).
  163. Andersson-Sjöland, A., Karlsson, J. C. & Rydell-Törmänen, K. ROS-induced endothelial stress contributes to pulmonary fibrosis through pericytes and Wnt signaling. *Lab. Investig.* **96**, 206–217 (2016).
  164. Pitocco, D., Tesauro, M., Alessandro, R., Ghirlanda, G. & Cardillo, C. Oxidative stress in diabetes: Implications for vascular and other complications. *Int. J. Mol. Sci.* **14**, 21525–21550 (2013).
  165. Tsugita, M., Morimoto, N. & Nakayama, M. SiO<sub>2</sub> and TiO<sub>2</sub> nanoparticles synergistically trigger macrophage inflammatory responses. *Part. Fibre Toxicol.* **14**, 1–9 (2017).
  166. Feng, Y. *et al.* Effect of reactive oxygen species overproduction on osteogenesis of porous titanium implant in the present of diabetes mellitus. *Biomaterials* **34**, 2234–2243 (2013).
  167. Suzuki, R., Muyco, J., Mckittrick, J. & Frangos, J. A. Reactive oxygen species inhibited by titanium oxide. (2002).
  168. Yoshinori Onuki, Ph.D., 1, Upkar Bhardwaj, M.Pharm., 1, Fotios Papadimitrakopoulos, Ph.D., 2 & Diane J. Burgess, P. D. . A Review of the Biocompatibility of Implantable Devices: Current Challenges to Overcome Foreign Body Response. *J. Diabetes Sci. Technol.* **2**, 1003–1015 (2008).
  169. Al-Maawi, S., Orłowska, A., Sader, R., James Kirkpatrick, C. & Ghanaati, S. In vivo cellular reactions to different biomaterials—Physiological and pathological aspects and their consequences. *Semin. Immunol.* **29**, 49–61 (2017).

170. Lanone, S. *et al.* Comparative toxicity of 24 manufactured nanoparticles in human alveolar epithelial and macrophage cell lines. *Part. Fibre Toxicol.* **6**, 1–12 (2009).
171. Di Rosa, M., Distefano, G., Zorena, K. & Malaguarnera, L. Chitinases and immunity: Ancestral molecules with new functions. *Immunobiology* **221**, 399–411 (2015).
172. Recklies, A. D., White, C. & Ling, H. The chitinase 3-like protein human cartilage glycoprotein 39 (HC-gp39) stimulates proliferation of human connective-tissue cells and activates both extracellular signal-regulated kinase- and protein kinase B-mediated signalling pathways. *Biochem. J.* **365**, 119–126 (2002).
173. Lee, C. G. *et al.* Role of chitin and chitinase/chitinase-like proteins in inflammation, tissue remodeling, and injury. *Annu. Rev. Physiol.* **73**, 479–501 (2011).
174. Bargagli, E., Maggiorelli, C. & Rottoli, P. Human chitotriosidase: A potential new marker of sarcoidosis severity. *Respiration* **76**, 234–238 (2008).
175. Kzhyshkowska, J., Yin, S., Liu, T., Riabov, V. & Mitrofanova, I. Role of chitinase-like proteins in cancer. *Biol. Chem.* **397**, 231–247 (2016).
176. Høgdall, E. V. S. *et al.* YKL-40 tissue expression and plasma levels in patients with ovarian cancer. *BMC Cancer* **9**, 1–10 (2009).
177. Comabella, M. *et al.* Cerebrospinal fluid chitinase 3-like 1 levels are associated with conversion to multiple sclerosis. *Brain* **133**, 1082–1093 (2010).
178. Bouwens, E. *et al.* Circulating Biomarkers of Cell Adhesion Predict Clinical Outcome in Patients with Chronic Heart Failure. *J. Clin. Med.* **9**, 195 (2020).
179. Rathcke, C. N. & Vestergaard, H. YKL-40 - an emerging biomarker in cardiovascular disease and diabetes. *Cardiovasc. Diabetol.* **8**, 1–7 (2009).
180. Garg, U., Smith, L. D. & Yu, C. Lysosomal storage disorders: Sphingolipidoses. *Biomarkers Inborn Errors Metab.* 211–233 (2017) doi:10.1016/B978-0-12-802896-4.00017-1.
181. Ober, C. & Chupp, G. L. The chitinase and chitinase-like proteins: A review of genetic and functional studies in asthma and immune-mediated diseases. *Curr. Opin. Allergy Clin. Immunol.* **9**, 401–408 (2009).
182. Gudima, A. Analysis of reactions of macrophages to titanium and biodegradable coating materials. (2017).
183. Liu, Y., Xu, Z. & Li, X. Cytotoxicity of titanium dioxide nanoparticles in rat neuroglia cells. *Brain Inj.* **27**, 934–939 (2013).
184. Kumar, S., Meena, R. & Paulraj, R. Role of Macrophage (M1 and M2) in Titanium-Dioxide Nanoparticle-Induced Oxidative Stress and Inflammatory Response in Rat. *Appl. Biochem. Biotechnol.* **180**, 1257–1275 (2016).
185. Mirza, S. *et al.* Type 2-diabetes is associated with elevated levels of TNF-alpha, IL-6 and adiponectin and low levels of leptin in a population of Mexican Americans: A cross-sectional study. *Cytokine* **57**, 136–142 (2012).
186. Luo, W., Zhang, L., Sheng, L., Zhang, Z. & Yang, Z. Increased levels of YKL-40 in patients with diabetes mellitus: a systematic review and meta-analysis. *Diabetol. Metab. Syndr.* **13**, 1–9 (2021).
187. Celik, C. *et al.* Elevated circulating levels of YKL-40 are a marker of abnormal glucose tolerance in women with polycystic ovary syndrome. *Clin. Endocrinol. (Oxf)*. **77**, 893–897 (2012).
188. Kelstrup, L. *et al.* Levels of the inflammation marker YKL-40 in young adults exposed to intrauterine hyperglycemia. *Diabetes Res. Clin. Pract.* **114**, 50–54 (2016).
189. Zurawska-Płaksej, E., Kratz, E. M., Ferens-Sieczkowska, M., Knapik-Kordecka,

- M. & Piwowar, A. Changes in glycosylation of human blood plasma chitotriosidase in patients with type 2 diabetes. *Glycoconj. J.* **33**, 29–39 (2016).
190. Gewert, K., Svensson, U., Andersson, K., Holst, E. & Sundler, R. Dexamethasone differentially regulates cytokine transcription and translation in macrophages responding to bacteria or okadaic acid. *Cell. Signal.* **11**, 665–670 (1999).
191. Ding AH, Porteu F, Sanchez E, N. C. Shared actions of endotoxin and taxol on TNF receptors and TNF release. *Science (80- )*. **248**, 1986–1988 (1990).
192. De la Oliva, N., Navarro, X. & del Valle, J. Dexamethasone Reduces the Foreign Body Reaction to Intraneural Electrode Implants in the Peripheral Nerve of the Rat. *Anat. Rec.* **301**, 1722–1733 (2018).
193. Bode, C., Kranz, H., Siepmann, F. & Siepmann, J. In-situ forming PLGA implants for intraocular dexamethasone delivery. *Int. J. Pharm.* **548**, 337–348 (2018).
194. Chen, Q. *et al.* TiO<sub>2</sub> nanoparticles cause mitochondrial dysfunction, activate inflammatory responses, and attenuate phagocytosis in macrophages: A proteomic and metabolomic insight. *Redox Biol.* **15**, 266–276 (2018).
195. Yu, K. N. *et al.* Titanium dioxide nanoparticles induce endoplasmic reticulum stress-mediated autophagic cell death via mitochondria-associated endoplasmic reticulum membrane disruption in normal lung cells. *PLoS One* **10**, 1–17 (2015).
196. Li, B. & Dewey, C. N. RSEM: Accurate transcript quantification from RNA-seq data with or without a reference genome. *Bioinforma. Impact Accurate Quantif. Proteomic Genet. Anal. Res.* 41–74 (2014) doi:10.1201/b16589.
197. Alinovi, R. *et al.* Oxidative and pro-inflammatory effects of cobalt and titanium oxide nanoparticles on aortic and venous endothelial cells. *Toxicol. Vitro.* **29**, 426–437 (2015).
198. Mu, W. *et al.* Effect of Long-Term Intake of Dietary Titanium Dioxide Nanoparticles on Intestine Inflammation in Mice. *J. Agric. Food Chem.* **67**, 9382–9389 (2019).
199. Han, S. G., Newsome, B. & Hennig, B. Titanium dioxide nanoparticles increase inflammatory responses in vascular endothelial cells. *Toxicology* **306**, 1–8 (2013).
200. Rihane, N. *et al.* Microglial cells (BV-2) internalize titanium dioxide (TiO<sub>2</sub>) nanoparticles: toxicity and cellular responses. *Environ. Sci. Pollut. Res.* **23**, 9690–9699 (2016).
201. Hong, F. *et al.* Nanosized titanium dioxide resulted in the activation of TGF- $\beta$ /Smads/p38MAPK pathway in renal inflammation and fibration of mice. *J. Biomed. Mater. Res. - Part A* **104**, 1452–1461 (2016).
202. Revathi, A., Borrás, A. D., Muñoz, A. I., Richard, C. & Manivasagam, G. *Degradation mechanisms and future challenges of titanium and its alloys for dental implant applications in oral environment. Materials Science and Engineering C* vol. 76 (Elsevier B.V, 2017).
203. Mombelli, A., Hashim, D. & Cionca, N. What is the impact of titanium particles and biocorrosion on implant survival and complications? A critical review. *Clin. Oral Implants Res.* **29**, 37–53 (2018).
204. Rolfe, B. *et al.* The Fibrotic Response to Implanted Biomaterials: Implications for Tissue Engineering. *Regen. Med. Tissue Eng. - Cells Biomater.* (2011) doi:10.5772/21790.
205. Braga, T. T., Agudelo, J. S. H. & Camara, N. O. S. Macrophages during the fibrotic process: M2 as friend and foe. *Front. Immunol.* **6**, 1–8 (2015).
206. Dai, X., Liu, R., Li, N. & Yi, J. Titanium dioxide nanoparticles induce in vitro autophagy. *Hum. Exp. Toxicol.* **38**, 56–64 (2019).

207. Ribeiro, A. R. *et al.* Trojan-Like Internalization of Anatase Titanium Dioxide Nanoparticles by Human Osteoblast Cells. *Sci. Rep.* **6**, 1–11 (2016).
208. Shavandi, Z., Ghazanfari, T. & Moghaddam, K. N. In vitro toxicity of silver nanoparticles on murine peritoneal macrophages. *Immunopharmacol. Immunotoxicol.* **33**, 135–140 (2011).
209. Adamcakova-Dodd, A. *et al.* Toxicity assessment of zinc oxide nanoparticles using sub-acute and sub-chronic murine inhalation models. *Part. Fibre Toxicol.* **11**, 1–15 (2014).
210. Shao, R. *et al.* YKL-40, a secreted glycoprotein, promotes tumor angiogenesis. *Oncogene* **28**, 4456–4468 (2009).
211. Johansen, J. S., Williamson, M. K., Rice, J. S. & Price, P. A. Identification of proteins secreted by human osteoblastic cells in culture. *J. Bone Miner. Res.* **7**, 501–512 (1992).
212. Larionova, I. V., Sevastyanova, T. N., Rakina, A. A., Cherdyntseva, N. V. & Kzhyshkowska, J. G. Chitinase-like proteins as promising markers in cancer patients. *Sib. J. Oncol.* **17**, (2018).
213. Smith, G. C. *et al.* Soft tissue response to titanium dioxide nanotube modified implants. *Acta Biomater.* **7**, 3209–3215 (2011).
214. Hogdall, E. V. S. *et al.* Stability of YKL-40 concentration in blood samples. *Scand. J. Clin. Lab. Invest.* **60**, 247–252 (2000).
215. Richter, B. *et al.* YKL-40 and mast cells are associated with detrusor fibrosis in patients diagnosed with bladder pain syndrome/interstitial cystitis according to the 2008 criteria of the European Society for the Study of Interstitial Cystitis. *Histopathology* **57**, 371–383 (2010).
216. Johansen, J. S. *et al.* Serum YKL-40 levels in healthy children and adults. Comparison with serum and synovial fluid levels of YKL-40 in patients with osteoarthritis or trauma of the knee joint. *Br. J. Rheumatol.* **35**, 553–559 (1996).
217. Johansen, J. S. *et al.* Serum YKL-40 is increased in patients with hepatic fibrosis. *J. Hepatol.* **32**, 911–920 (2000).
218. Huang, K. T. *et al.* Titanium nanoparticle inhalation induces renal fibrosis in mice via an oxidative stress upregulated transforming growth factor- $\beta$  pathway. *Chem. Res. Toxicol.* **28**, 354–364 (2015).
219. Mackel, J. J. *et al.* Inflammation during fungal-associated allergic airway inflammation. (2021).
220. Hollak, C. E. M., Van Weely, S., Van Oers, M. H. J. & Aerts, J. M. F. G. Marked elevation of plasma chitotriosidase activity. A novel hallmark of Gaucher disease. *J. Clin. Invest.* **93**, 1288–1292 (1994).
221. Kolatat, K. *et al.* Adverse local tissue reaction (ALTR) associated with corrosion products in metal-on-metal and dual modular neck total hip replacements is associated with upregulation of interferon gamma-mediated chemokine signaling. *J. Orthop. Res.* **33**, 1487–1497 (2015).
222. Bordon, Y. Trans- Golgi network breaks away to activate NLRP3. *Nat. Rev. Immunol.* **19**, 68–69 (2019).
223. Ma, X. *et al.* Evaluation of Turning-Sized Gold Nanoparticles on Cellular Adhesion by Golgi Disruption in Vitro and in Vivo. *Nano Lett.* (2019) doi:10.1021/acs.nanolett.9b02826.
224. Chang, D., Sharma, L. & Dela Cruz, C. S. Chitotriosidase: A marker and modulator of lung disease. *Eur. Respir. Rev.* **29**, 1–12 (2020).
225. Lee, C. M. *et al.* Chitinase 1 regulates pulmonary fibrosis by modulating TGF- $\beta$ /SMAD7 pathway via TGFBRAP1 and FOXO3. *Life Sci. Alliance* **2**, 1–14 (2019).



226. Shinchu, H. *et al.* Gold Nanoparticles Coimmobilized with Small Molecule Toll-Like Receptor 7 Ligand and  $\alpha$ -Mannose as Adjuvants. *Bioconjug. Chem.* **30**, 2811–2821 (2019).
227. Chen, P., Kanehira, K. & Taniguchi, A. Role of toll-like receptors 3, 4 and 7 in cellular uptake and response to titanium dioxide nanoparticles. *Sci. Technol. Adv. Mater.* **14**, (2013).
228. Schraufstatter, I. U., Zhao, M., Khaldoyanidi, S. K. & Discipio, R. G. The chemokine CCL18 causes maturation of cultured monocytes to macrophages in the M2 spectrum. *Immunology* **135**, 287–298 (2012).
229. Tasaki, Y. *et al.* Chemokine PARC gene (SCYA18) generated by fusion of two MIP-1 $\alpha$ /LD78 $\alpha$ - like genes. *Genomics* **55**, 353–357 (1999).
230. Guan, P. *et al.* Genomic organization and biological characterization of the novel human CC chemokine DC-CK-1/PARC/MIP-4/SCYA18. *Genomics* **56**, 296–302 (1999).
231. Boot, R. G. *et al.* Marked elevation of the chemokine CCL18/PARC in Gaucher disease: A novel surrogate marker for assessing therapeutic intervention. *Blood* **103**, 33–39 (2004).
232. Boot, R. G. *et al.* Plasma chitotriosidase and CCL18 as surrogate markers for granulomatous macrophages in sarcoidosis. *Clin. Chim. Acta* **411**, 31–36 (2010).
233. Adema, G. J. *et al.* A dendritic-cell-derived C-C chemokine that preferentially attracts naive T cells. *Nature* **387**, 713–717 (1997).
234. Politz, O., Kodelja, V., Guillot, P., Orfanos, C. E. & Goerdt, S. Pseudoexons and regulatory elements in the genomic sequence of the  $\beta$ -chemokine, alternative macrophage activation-associated CC-chemokine (AMAC)-1. *Cytokine* **12**, 120–126 (2000).
235. Kodelja, V. *et al.* Alternative macrophage activation-associated CC-chemokine-1, a novel structural homologue of macrophage inflammatory protein-1 $\alpha$  with a Th2- associated expression pattern. *J. Immunol.* **160**, 1411–1418 (1998).
236. Schutyser, E. *et al.* Selective induction of CCL18/PARC by staphylococcal enterotoxins in mononuclear cells and enhanced levels in septic and rheumatoid arthritis. *Eur. J. Immunol.* **31**, 3755–3762 (2001).
237. Gavala, M. L. *et al.* Segmental allergen challenge enhances chitinase activity and levels of CCL18 in mild atopic asthma. *Clin. Exp. Allergy* **43**, 187–197 (2013).
238. Schutyser, E. *et al.* Identification of biologically active chemokine isoforms from ascitic fluid and elevated levels of CCL18/pulmonary and activation-regulated chemokine in ovarian carcinoma. *J. Biol. Chem.* **277**, 24584–24593 (2002).
239. Struyf, S. *et al.* PARC/CCL18 Is a Plasma CC Chemokine with Increased Levels in Childhood Acute Lymphoblastic Leukemia. *Am. J. Pathol.* **163**, 2065–2075 (2003).
240. Leung, S. Y. *et al.* Expression profiling identifies chemokine (C-C motif) ligand 18 as an independent prognostic indicator in gastric cancer. *Gastroenterology* **127**, 457–469 (2004).
241. Chen, J. *et al.* CCL18 from Tumor-Associated Macrophages Promotes Breast Cancer Metastasis via PITPNM3. *Cancer Cell.* **19**, 541–555 (2011).
242. Marchand, F. *et al.* Dental implants and diabetes: Conditions for success. *Diabetes Metab.* **38**, 14–19 (2012).
243. Ajami, E. *et al.* Bone healing and the effect of implant surface topography on osteoconduction in hyperglycemia. *Acta Biomater.* **10**, 394–405 (2014).
244. Moganti, K. Effect of hyperglycemia on the activation and epigenetic

- programming of primary human macrophages (Doctoral dissertation). (2017).
245. Omidian, M. *et al.* Effects of vitamin D supplementation on circulatory YKL-40 and MCP-1 biomarkers associated with vascular diabetic complications: A randomized, placebo-controlled, double-blind clinical trial. *Diabetes Metab. Syndr. Clin. Res. Rev.* **13**, 2873–2877 (2019).
  246. Zurawska-Płaksej, E., Ługowska, A., Hetmańczyk, K., Knapik-Kordecka, M. & Piwowar, A. Neutrophils as a source of chitinases and chitinase-like proteins in type 2 diabetes. *PLoS One* **10**, 1–11 (2015).
  247. Zhang, J., Liu, J. & Qin, X. Advances in early biomarkers of diabetic nephropathy. *Rev. Assoc. Med. Bras.* **64**, 85–92 (2018).
  248. Erbel, C. *et al.* Differential regulation of aldose reductase expression during macrophage polarization depends on hyperglycemia. *Innate Immun.* **22**, 230–237 (2016).
  249. Barnes. Anti-inflammatory actions of glucocorticoids. *J. Biogeogr.* **17**, 315 (1998).
  250. Kunz, L. I. Z. *et al.* Regulation of YKL-40 expression by corticosteroids: Effect on pro-inflammatory macrophages in vitro and its modulation in COPD in vivo. *Respir. Res.* **16**, 1–10 (2015).
  251. Shen, K. *et al.* The sustained release of dexamethasone from TiO<sub>2</sub> nanotubes reinforced by chitosan to enhance osteoblast function and anti-inflammation activity. *Mater. Sci. Eng. C* **116**, 111241 (2020).
  252. Horner, H. C., Munck, A. & Lienhard, G. E. Dexamethasone causes translocation of glucose transporters from the plasma membrane to an intracellular site in human fibroblasts. *J. Biol. Chem.* **262**, 17696–17702 (1987).
  253. He, Y. Y., Huang, J. L., Block, M. L., Hong, J. S. & Chignell, C. F. Role of phagocyte oxidase in UVA-induced oxidative stress and apoptosis in keratinocytes. *J. Invest. Dermatol.* **125**, 560–566 (2005).
  254. Dandona, P. *et al.* Effect of dexamethasone on reactive oxygen species generation by leukocytes and plasma interleukin-10 concentrations: A pharmacodynamic study. *Clin. Pharmacol. Ther.* **66**, 58–65 (1999).
  255. Huo, Y., Rangarajan, P., Ling, E. A. & Dheen, S. T. Dexamethasone inhibits the Nox-dependent ROS production via suppression of MKP-1-dependent MAPK pathways in activated microglia. *BMC Neurosci.* **12**, (2011).
  256. Ai, F., Zhao, G., Lv, W., Liu, B. & Lin, J. Dexamethasone induces aberrant macrophage immune function and apoptosis. *Oncol. Rep.* **43**, 427–436 (2020).
  257. Singh, D. K., Winocour, P. & Farrington, K. Oxidative stress in early diabetic nephropathy: Fueling the fire. *Nat. Rev. Endocrinol.* **7**, 176–184 (2011).
  258. Volpe, C. M. O., Villar-Delfino, P. H., Dos Anjos, P. M. F. & Nogueira-Machado, J. A. Cellular death, reactive oxygen species (ROS) and diabetic complications review-Article. *Cell Death Dis.* **9**, (2018).
  259. Nishanth, R. P., Jyotsna, R. G., Schlager, J. J., Hussain, S. M. & Reddanna, P. Inflammatory responses of RAW 264.7 macrophages upon exposure to nanoparticles: Role of ROS-NFκB signaling pathway. *Nanotoxicology* **5**, 502–516 (2011).
  260. Wang, M., Lai, X., Shao, L. & Li, L. Evaluation of immunoresponses and cytotoxicity from skin exposure to metallic nanoparticles. *International Journal of Nanomedicine* vol. 13 4445–4459 (2018).
  261. Ryan, G. R. *et al.* Rescue of the colony-stimulating factor 1 (CSF-1)-nullizygous mouse (Csf1<sup>op</sup>/Csf1<sup>op</sup>) phenotype with a CSF-1 transgene and identification of sites of local CSF-1 synthesis. *Blood* **98**, 74–84 (2001).
  262. Metzemaekers, M., Vanheule, V., Janssens, R., Struyf, S. & Proost, P. Overview of the mechanisms that may contribute to the non-redundant activities of

- interferon-inducible CXC chemokine receptor 3 ligands. *Front. Immunol.* **8**, (2018).
263. House, I. G. *et al.* Macrophage-derived CXCL9 and CXCL10 are required for antitumor immune responses following immune checkpoint blockade. *Clin. Cancer Res.* **26**, 487–504 (2020).
264. Hartgers, F. C. *et al.* DC-STAMP, a novel multimembrane-spanning molecule preferentially expressed by dendritic cells. *Eur. J. Immunol.* **30**, 3585–3590 (2000).
265. Eleveld-Trancikova, D. *et al.* The dendritic cell-derived protein DC-STAMP is highly conserved and localizes to the endoplasmic reticulum. *J. Leukoc. Biol.* **77**, 337–343 (2005).
266. Eleveld-Trancikova, D. *et al.* DC-STAMP interacts with ER-resident transcription factor LUMAN which becomes activated during DC maturation. *Mol. Immunol.* **47**, 1963–1973 (2010).
267. Eger, M. *et al.* Mechanism and Prevention of Titanium Particle-Induced Inflammation and Osteolysis. *Front. Immunol.* **9**, 2963 (2018).
268. Genova, R. M., Meyer, K. J., Anderson, M. G., Harper, M. M. & Pieper, A. A. Neprilysin inhibition promotes corneal wound healing. *Sci. Rep.* **8**, 1–11 (2018).
269. Iwata, N. *et al.* Metabolic regulation of brain A $\beta$  by neprilysin. *Science (80-. )*. **292**, 1550–1552 (2001).
270. El-Amouri, S. S. *et al.* Neprilysin protects neurons against A $\beta$  peptide toxicity. *Brain Res.* **1152**, 191–200 (2007).
271. Cherian, M. G., Jayasurya, A. & Bay, B. H. Metallothioneins in human tumors and potential roles in carcinogenesis. *Mutat. Res. - Fundam. Mol. Mech. Mutagen.* **533**, 201–209 (2003).
272. Theocharis, S. E., Margeli, A. P. & Koutselinis, A. Metallothionein: A multifunctional protein from toxicity to cancer. *Int. J. Biol. Markers* **18**, 162–169 (2003).
273. Liu, Z. *et al.* Metallothionein 1 family profiling identifies MT1X as a tumor suppressor involved in the progression and metastatic capacity of hepatocellular carcinoma. *Mol. Carcinog.* **57**, 1435–1444 (2018).
274. Kanda M, Nomoto S, Okamura Y, Nishikawa Y, Sugimoto H, Kanazumi N, Takeda S, N. A. Detection of metallothionein 1G as a methylated tumor suppressor gene in human hepatocellular carcinoma using a novel method of double combination array analysis. *Int. J. Oncol.* **35**, 477–483 (2009).
275. Joshi, B., Ordonez-Ercan, D., Dasgupta, P. & Chellappan, S. Induction of human metallothionein 1G promoter by VEGF and heavy metals: Differential involvement of E2F and metal transcription factors. *Oncogene* **24**, 2204–2217 (2005).
276. Çeşmeli, S. & Biray Avci, C. Application of titanium dioxide (TiO<sub>2</sub>) nanoparticles in cancer therapies. *J. Drug Target.* **27**, 762–766 (2019).
277. Ding, Z., Mizeracki, A. M., Hu, C. & Mehta, J. L. LOX-1 deletion and macrophage trafficking in atherosclerosis. *Biochem. Biophys. Res. Commun.* **440**, 210–214 (2013).
278. Hofnagel, O. *et al.* Proinflammatory cytokines regulate LOX-1 expression in vascular smooth muscle cells. *Arterioscler. Thromb. Vasc. Biol.* **24**, 1789–1795 (2004).
279. Balzan, S. & Lubrano, V. LOX-1 receptor: A potential link in atherosclerosis and cancer. *Life Sci.* **198**, 79–86 (2018).
280. Pirillo, A., Norata, G. D. & Catapano, A. L. LOX-1 , OxLDL , and Atherosclerosis. **2013**, (2013).

281. Chang, S. F., Chang, P. Y., Chou, Y. C. & Lu, S. C. Electronegative LDL Induces M1 Polarization of Human Macrophages Through a LOX-1-Dependent Pathway. *Inflammation* **43**, 1524–1535 (2020).
282. Luo, B. *et al.* LOX-1-Targeted Iron Oxide Nanoparticles Detect Early Diabetic Nephropathy in db/db Mice. *Mol. Imaging Biol.* **17**, 652–660 (2015).
283. Budai, L. *et al.* Investigation of genetic variants of  $\alpha$ -1 acid glycoprotein by ultra-performance liquid chromatography-mass spectrometry. *Anal. Bioanal. Chem.* **393**, 991–998 (2009).
284. Nakamura, K., Ito, I., Kobayashi, M., Herndon, D. N. & Suzuki, F. Orosomucoid 1 drives opportunistic infections through the polarization of monocytes to the M2b phenotype. *Cytokine* **73**, 8–15 (2015).
285. Bonate, P. L. Pathophysiology and Pharmacokinetics Following Burn Injury. *Clin. Pharmacokinet.* **18**, 118–130 (1990).
286. Bloedow, D. C., Hansbrough, J. F., Hardin, T. & Simons, M. Postburn serum drug binding and serum protein concentrations. *J. Clin. Pharmacol.* **26**, 147–151 (1986).
287. Ongay, S., Martín-Álvarez, P. J., Neusu, C. & de Frutos, M. Statistical evaluation of CZE-UV and CZE-ESI-MS data of intact  $\alpha$ -1-acid glycoprotein isoforms for their use as potential biomarkers in bladder cancer. *Electrophoresis* **31**, 3314–3325 (2010).
288. Kundin, W. D., Mechali, P., Hollinshead, A. C., Miller, H. & Bensimon, H. Cancer serum index: A useful nonspecific test as a parameter in multimodality screening and assessment of patients with cancer of the prostate. *Prostate* **2**, 207–217 (1981).
289. Wang, L. *et al.* Manipulation of macrophage polarization by peptide-coated gold nanoparticles and its protective effects on acute lung injury. *J. Nanobiotechnology* **18**, 1–16 (2020).
290. Xu, W. C. *et al.* Nanotubular TiO<sub>2</sub> regulates macrophage M2 polarization and increases macrophage secretion of vegf to accelerate endothelialization via the ERK1/2 and PI3K/AKT pathways. *Int. J. Nanomedicine* **14**, 441–455 (2019).
291. Chin, P. Y. Y., Cheok, Q., Glowacz, A. & Caesarendra, W. A review of in-vivo and in-vitro real-time corrosion monitoring systems of biodegradable metal implants. *Appl. Sci.* **10**, (2020).

## 7 CURRICULUM VITAE

### PERSONAL:

**Name:** Tatyana Sevastyanova  
**Date of birth:** 09.09.1988  
**Nationality:** Russian  
**Place of Birth:** Korolev, Moscow area  
**Email:** Tatyana.Sevastyanova@medma.uni-heidelberg.de

### EDUCATION AND PROFESSIONAL EXPERIENCE:

- 08.2017 - present** PhD student in the Lab of Prof. Julia Kzhyshkowska at the Institute for Transfusion Medicine and Immunology, Medical Faculty Mannheim, University of Heidelberg.  
PhD thesis title: "Analysis of macrophage responses to titanium nanoparticles in hyperglycemic conditions."
- 01.2016 - 07.2017** Practical student at the Lab. of Prof. J. Kzhyshkowska, Institute for Transfusion Medicine and Immunology, Medical Faculty Mannheim, University of Heidelberg.
- 06.2015 - 01.2016** Organisational manager in the Medical Center of Gazprom Space Systems, Moscow, Russia.
- 09.2011 - 04.2015** Master Thesis in Pharmacology. University of Rochester - Medical Center, USA. Laboratory of Prof. P. J. Kammermeier. Title: "Functional interaction between metabotropic glutamate receptors 1 and 5".
- 09.2007 - 06.2011** Bachelor studies in Biochemistry, Rochester Institute of Technology, USA.
- 09.2003 - 06.2007** Repton School, UK.

### TECHNICAL AND ANALYTICAL SKILLS:

**Biotechnology:** Whole-cell patch clamp (electrophysiology), microinjections, tissue culture techniques, confocal microscopy, flow cytometry (FACS), primary macrophage cultures, agarose gel electrophoresis, bacterial transformation, transfection, fluorescence microscopy, microbiological identification and plating, quantitative PCR, real-time PCR, animal microsurgery, yeast-two hybrid screen, calcium imaging with fura, enzyme linked immunosorbent assay (ELISA), cDNA synthesis, cell viability assays, protein and nucleic acid extraction and quantification and western blot.

- Chemistry:** Chemical safety, titrations, calibration of a buret, use of chemical balances and calibration, chromatography methods, fractional distillation, reflux, quantitative chemical analysis
- Computer:** Mac OS X, Microsoft Office, Matlab, Igor (Data analysis for voltage-clamp recordings), Prism-Graphpad, Lightcycler (RT-PCR analysis), Tecan (luminescence analysis), LaTeX, FlowJo\_V10.

#### **PUBLICATIONS:**

1. Yin S., Wang N., Riabov V., Mossel D.M., Larionova I., Schledzewski K., Trofimova O., Sevastyanova T., Zajakina A., Schmittermaier C., Gratchev A., Flatley A., Kremmer E., Zavyalova M., Cherdyntseva N., Simon-Keller K., Marx A., Klüter H., Goerdts S., Kzhyshkowska J. SICLP inhibits the growth of mouse mammary adenocarcinoma by preventing recruitment of tumor-associated macrophages. 2019; *IJC*, 146(5), 1396-1408.
2. Rendra E., Riabov V., Mossel D.M., Sevastyanova T., Harmsen M., Kzhyshkowska J. Reactive Oxygen Species (ROS) in Macrophage Activation and Function in Diabetes. 2019; *Immunobiology*, 224(2), 242-253.
3. I.V. Larionova, T.N. Sevastyanova, A.A. Rakina, N.V. Cherdyntseva, J. G. Kzhyshkowska.. Chitinase-like proteins as promising markers in cancer patients. 2018; *Siberian oncology journal*, 17(4), 99-105.
4. Sevastyanova, T. N., Kammermeier, P. J. Cooperative signaling between homodimers of metabotropic glutamate receptors 1 and 5. 2014; *Molecular pharmacology*, 86(5), 492-504.

#### **PRESENTATIONS:**

1. Sevastyanova T., Mossel M., Ryabov V., Vrana N.E., Klüter H., Kzhyshkowska J. Hyperglycemia modulates inflammatory responses to metal nanoparticles in human macrophages. Congress of the European Macrophage and Dendritic cell Society (EMDS) meeting, Verona, Italy; DZD Diabetes Research School (2018).
2. Sevastyanova T., Gudima A., Ryabov V., Vrana N.E., Klüter H., Kzhyshkowska J. Hyperglycemia enhances inflammatory responses to titanium implanted material in human macrophages. 4th Heidelberg International Symposium on Diabetic Complications, Heidelberg, Germany (2017).
3. Sevastyanova T., Gudima A., Ryabov V., Vrana N.E., Klüter H., Kzhyshkowska J. Hyperglycemia stimulates YKL40 and suppresses of CCL18 production in human primary macrophages exposed to polished titanium disks and TiO<sub>2</sub> nanoparticles. EMDS Meeting, Madrid, Spain (2017).
4. Sevastyanova, T. N., Kammermeier, P. J: Group I metabotropic glutamate receptors function in mutually dependent manner when co-expressed in neurons. Annual Pharmacology Meeting, Buffalo, NY, USA (2014).
5. Sevastyanova, T. N., Kammermeier, P. J: Metabotropic glutamate receptors 1 and 5 Function in mutually dependent manner upon their coupling. Society for Neuroscience 2013 Annual Meeting, San Diego, CA, USA (2013).
6. Sevastyanova, T. N., Kammermeier, P. J: A novel metabotropic glutamate receptor 1/5 functional interaction. 4th GPCR Colloquium, Boston, MA, USA (2013).
7. Sevastyanova, T. N., Kammermeier, P. J: Metabotropic glutamate receptors 1 and 5 function in mutually dependent manner when co-expressed in neurons. Graduate Student Society Meeting, Rochester, NY, USA (2012).
8. Sevastyanova T., Cohen D., Bidlack J. Novel compounds MCL-717 and MCL-720 are high affinity full agonists at the Mu opioid receptor. UR Summer scholar symposium, Rochester, NY, USA (2010).

## 8 ACKNOWLEDGEMENTS

It is my pleasure to thank those who supported me throughout the research and completion of my thesis. Foremost, I would like to express my special thanks of gratitude to my supervisor, Prof. Dr. Julia Kzhyshkowska for granting me the opportunity to do my Ph.D. at the University of Heidelberg and for her guidance and supervision through the entire period. Moreover, I am sincerely thankful to Christina Schmuttermaier for her initial training, advice and assistance with experiments, emotional support and companionship throughout my years in the Ph.D. program.

I would like to acknowledge Prof. Dr. Harald Klüter, director of the Institute of Transfusion Medicine and Immunology, Medical Faculty Mannheim, University of Heidelberg, for providing me with the facilities and research infrastructure to complete this thesis.

I am very grateful to group members of AG Prof. Dr. Julia Kzhyshkowska who supported me and I had the pleasure of working together with: Dr. Vladimir Riabov, Dr. Aleksandru Gudima, Dr. Julia Michel, Dr. Kondiah Moganti, Dr. Tengfei Liu, Dr. Marije Mossel, Isabel Porth, Dr. Shuiping Yin, Dr. Dandan Xu, Dr. Zhen Jiao, Ernesto Badillo, Leonie Schumacher and Lina Susana Silva-Bermudez. I especially thank Dr. Marije Mossel for providing me friendly advices and participating in the experiments. I also thank Dr. Vladimir Rybov for his scientific and technical guidance. I thank Zhen Jiao and Leonie Schumacher for their support in the experiments with confocal microscopy.

I am grateful to Dr. Carolina De La Torre from the Affymetrix Core Facility of Medical Research Center, Medical Faculty Mannheim, University of Heidelberg for assistance with hybridization of the gene expression microarrays and statistical analysis of the data. I acknowledge DFG GRK 1874: "DIAMICOM" program for organising the summer school to gain for theoretical and methodological knowledge. I acknowledge CoatDegraBac project for providing me the funding in the last year of my thesis completion. I thank Tomsk State University and Prof. Dr. Irina Kurzina for connecting me with Prof. Dr. Julia Kzhyshkowska.

Finally, my greetings go to my family for their constant support and encouragement. Special thanks go to my husband, Ernesto Badillo, and my father, Nikolai Nikolaevich Sevastianov.